UNIVERSITA' DEGLI STUDI DI PADOVA

DIPARTIMENTO DI INGEGNERIA INDUSTRIALE

CORSO DI LAUREA MAGISTRALE IN INGEGNERIA CHIMICA E DEI PROCESSI INDUSTRIALI

Tesi di Laurea Magistrale in
Ingegneria Chimica e dei Processi Industriali

Characterising powder flowability at high shear rates by the ball indentation method

Relatore: Prof. Andrea Claudio Santomaso

Correlatore: Dr. Colin Hare

Laureanda: MONICA TIRAPELLE

ANNO ACCADEMICO 2017-2018

To my dear parents.

Acknowledgement

It is gratefully acknowledge the supervision of Dr. Colin Hare that has followed me from the beginning of my experimental work and has given direction through the course of the project at the University of Surrey. His advises have always been useful and fundamental. I would like to convey an immeasurable amount of gratitude for the opportunity he gave me to attend a three days course about particle technology at the University of Leeds and to present a poster at the 40th IFPRI poster session in Edinburgh.

I would like to express my thanks also to my Italian supervisor, Professor Andrea Claudio Santomaso, who gave me assistance and support from Italy.

Last, but by no means least, I would like to thank my dearest parents for their unconditional love and support; and Mattia, for his enthusiasm, patience and encouragement.

Sommario

In numerose operazioni industriali che trattano solidi particolati è richiesta la caratterizzazione della scorrevolezza delle polveri. Tuttavia le tecniche tradizionali, tra cui la cella di taglio, non permettono di caratterizzare polveri sottoposte ad elevate velocità di deformazione, condizione che invece si verifica, ad esempio, in miscelatori industriali, trasportatori a coclea, o durante il riempimento di uno stampo. Per questo motivo, la tecnica di indentazione con sfera, solitamente utilizzata nella misura della durezza di materiali metallici (plastici), è stata qui studiata come nuova tecnica per descrivere il flusso di materiali granulari sottoposti ad elevate velocità di taglio. Per tale scopo, è stata valutata la resistenza al flusso di quattro diversi materiali in un ampio intervallo di velocità di deformazione, e in diverse condizioni operative. Si è inoltre aspirato a trovare una correlazione con il metodo dinamico del reometro per polveri FT4. I risultati ottenuti dimostrano che la durezza misurata è indipendente dalla velocità di taglio nel regime di flusso quasi statico, dove è pressoché costante. Nel regime di flusso intermedio invece, la resistenza al flusso può essere correlata con la velocità di deformazione; inoltre qui il comportamento reologico della polvere è assimilabile a quello di un liquido Newtoniano. Questi risultati sono in accordo con le simulazioni riportate in letteratura e con quanto ottenuto da Tardos *et al.* (2003), *Powder Technology*, **131**, 23-39. Nonostante ciò, il metodo presenta alcune limitazioni. La prima riguarda la variabilità del metodo con i materiali studiati: per alcune polveri non si può definire un intervallo di durezza stabile e, perciò, non è possibile conoscere in anticipo quanto a fondo penetrerà l'indentatore e se la resistenza al flusso misurata sarà nell'intervallo di durezza costante. Per finire, possono essere soggette a indentazione, solo polveri con un certo grado di coesione.

Abstract

Characterising powder flowability is often required in industrial operation of particulate solids. However, traditional powder flow measurement techniques, such as shear test, are not able to characterize powder at high shear rates, such as in industrial mixers, screw conveyors and die filling. Here, the Ball Indentation Method, which is usually used for measuring hardness of metallic structures, has been experimentally investigated as a new technique to describe powder flow at high shear rates. For this purpose, the flow resistance of four different powders has been evaluated for a range of shear rates and operation variables. Furthermore it has been tried to find a correlation with the variable flow rate method of the FT4 powder rheometer. The results indicate that the hardness is independent on the strain rate in quasi-static conditions, where it is almost constant. On the other hand, the flow resistance can be related to the strain rate in intermediate flow regime, where the rheological behaviour of the powders becomes liquid-like. The experimental results agree with the simulations reported in literature and correlate well with the trend established by Tardos *et al.* (2003), *Powder Technology*, **131**, 23-39, with the Couette device. However the method has some limitations. The first concerns the variability with materials, indeed for some powder a stable regime of hardness cannot be defined. Then it is not always possible to know in advance how far the indenter will penetrate, and whereas it will remain in the stable hardness range. Finally, only powder with a certain degree of cohesiveness can be subjected to penetration.

Contents

Introduction

Powder technology is one of the most ancient sciences. Indeed humankind has dealt with powder since the early days. One need only think to the threshing process for food preparation used in ancient Egypt, and some manufacturing technologies, as well as ceramic and glass production. Despite the fact that some consider powder technology to be the second oldest profession, it still is more an art than a science. The reason is that the particulate state of the matter is very difficult to characterize because it is influenced by a wide range of intrinsic properties and external environmental conditions. Furthermore, the previous history can significantly change the powder behaviour, as well as the vibration during transportation and the time of storage.

Because nowadays a huge number of industries, such as pharmaceutical, food, chemical and catalyst, are dealing with raw materials in solid form and are manufacturing solid products, developments in the prediction of both cohesive and free flowing powder behaviour, at different operative conditions, are required. In this way the powder handling and processing can be improved, and waste of time and money avoided. Reducing waste becomes particularly important in the case of particularly valuable materials like Active Pharmaceutical Ingredients (API).

Thus particle technology is an important field of investigation for many scientific and economic reasons, both for the national and international scientific landscape. This field of study includes different specific subjects such as the understanding of raindrops, oil emulsions, powders, slurries, and much else.

Unreliable powder flow is a major problem during processing of powders, and as such there are a number of methods available for powder flow characterisation. The shear cell is the most widely used method, particularly for powders subjected to moderate or high stresses, and under quasi-static conditions, with established methods for designing large bins and hoppers based on the measurement (A.W. Jenike, 1967). However, this method is not suitable for measuring the flowability of powder in dynamic systems, such as powder mixing.

Therefore this project was born with the purpose of investigating the flowability of different types of cohesive powders at high shear rates, which are characterised as the intermediate and dynamic flow regimes. The rheological behaviour of powder in these flow regimes can actually be investigated only with powder rheometers, which have been developed with the same principle of liquid rheometers, and with the Couette

device (G. I. Tardos *et al.,2003*); however rheometers are the only ones available commercially.

Here the powder flow behaviour at high shear rates is investigated with Ball Indentation Method, a technique that has been recently proposed for characterising loosely compacted cohesive powder (A. Hassanpour, M. Ghadiri, 2007). So the feasibility of the Ball Indentation technique, which directly measures hardness by dropping a ball onto a cylindrical bed of previously consolidated powder, has been explored. The impact of different spherical indenters on the flow properties of cohesive powders in different flow regimes is systematically investigated and the correlation between bulk cohesion and strain rate is evaluated. Finally the variation of hardness with strain rate is considered for several materials, and compared to flow energy measurements in the FT4 Powder Rheometer.

The thesis consists of four chapters. It starts with an overview on inter-particle bonds and mechanical properties of dry bulk solids. It places particular emphasis on powder flowability and on the methods used for powder flow characterisation. Successively the ball indentation method and FT4 powder rheometer, together with all the theoretical concepts behind and the working methods employed, have been described. This is followed by the particle characterisation of all the investigated materials and, finally, the results obtained with both the ball indentation method and the powder rheometer are presented.

In more detail, the first chapter treats what is called state of art. To understand particle technology is important knowing the bonds acting between and on individual particles. However, because here only dry systems have been considered, only the Van der Waals force, the Hamaker contribution and the electrostatic force are discussed. The second section of this chapter concerns the mechanical properties of bulk solids, with particular attention paid on the construction of the Yield locus and the Mohr's Circle. Then some of the methodologies used for powder flow characterisation are shown, among which there is a detailed literature review of the Ball Indentation Method and of the dynamic methodology of the FT4 powder rheometer.

In the second Chapter are reported the materials and the methods that have been used. At the beginning, the chapter focuses on the experimental setup of the Ball Indentation Method and on the methodology used to calculate the hardness. The procedure is here reported step by step. The second section concerns with the methodologies of the FT4 Powder Rheometer that have been used: indentation in quasi-static conditions, variable flow rate method at different tip speeds and rotational shear cell.

The third Chapter is about powder characterisation. So size, shape and morphology, as well as both a qualitative and quantitative evaluation of flowability, have been analysed for each investigated material. Moreover the flow behaviours of the materials are compared.

In the fourth and last chapter, all the results obtained both with the powder rheometer and the ball indentation technique are reported and commented upon. Here it is argued the feasibility of the Ball Indentation Method, considering the influence of different variables, and a comparison with the result obtained with the FT4 powder rheometer is made. Finally the evaluation of hardness in different flow regimes is reported and discussed in detail.

Chapter 1
Powder properties

Granular materials are complex systems, whose properties are only poorly understood. The reason is that the behaviour of a granular solid is influenced by a lot of properties, generally subdivided in three main groups: intrinsic physical properties, process conditions, and external environmental conditions. So factors like size, shape, roughness, porosity, bulk density and particles interactions, as well as stress, strain rate, storage time, temperature and humidity, may affect the powder performance. Besides, the same powder can manifest gas-like, liquid-like, and solid-like behaviour at different stress states.

In this chapter an overview of the most common inter-particle interactions acting between dry particles is reported. They are important because they lead to powder agglomeration and adhesion to process equipment. In the second section the importance of mechanical properties of powders under an applied load, which can have a profound effect on solid processing, is discussed. At the end of the chapter, the methods commonly used for characterizing the bulk flow behaviour of a powder are defined, with particular regard to the Ball Indentation Technique and the Variable Flow Rate method. The reason why the huge amount of methods available is because no one can be universally applied for measuring flowability of powder streams.

1.1. Interparticles bond and cohesion

Different types of interactions acting on, and between, individual particles exist. Their definition and prediction is particularly important in order to understand the particle behaviour. Indeed, when these forces became significant and overcome the gravity and the aerodynamic forces, they cause powder cohesion and agglomeration, as well as adherence to process equipment, which represents a hostile condition in most of particulate industrial processes.

The main forces acting between particles are the Van der Waals, the electrostatic, the magnetic and the mechanical forces. Furthermore, if moisture is added capillary forces are generated, mainly due to capillary pressure of liquid bridges in the contact zone of particles. However, in the following paragraphs the Van der Waals force, which is dominant in dry systems and when dealing with particles of small size; the

approximation done by Hamaker, which is useful for calculating the Van der Waals force in the case of stiff particles with smooth surface; and the electrostatic forces are briefly described.

1.1.1. Van der Waals forces

In 1873, Van der Waals noted the non-ideal behaviour of gases and attributed it to the existence of interactions between atoms and molecules. These interactions are due to interacting dipoles and, unlike chemical bounds such as the hydrogen or the ionic ones, are always present; also if they act on a short-range and their magnitude diminish with the distance.

The Van der Waals equations, that describes the gas behaviour taking into account the real gas volume and the inter-molecular attractions, is given by equation (1.1):

$$\left(P + \frac{a}{V_m^2}\right)(V_m - b) = RT, \tag{1.1}$$

where a represents the effect of dipoles, b the sterical effect, V_m the molar volume of the gas and R the universal gas constant. However, Van der Waals incorrectly treated the dipoles as static entities (R. Lee-Desautels, 2005).

In 1936, London understood the dynamic nature of dipoles and attributed the Van der Waals forces to the dispersion effect, which is the interaction between instantaneous dipoles at larger distance. The instantaneous change of dipole of one atom, due to orbiting electrons, creates an oscillating electric field that polarizes neighbour atoms. The attraction energy between two atoms, i and j, is given by equation (1.2):

$$E = -\frac{\lambda_{ij}}{H^6}, \tag{1.2}$$

where λ_{ij} is the London's constant of two atoms or molecules and H is their distance. This equation however is valid only for distances smaller than the wavelength of the major electronic absorption band for the gas. At larger separation the potential decays faster and the interaction energy becomes inversely proportional to H^7 (Lee-Desautels).

Van der Waals force operates both in vacuum and in a liquid environment, although it is substantially reduced in the latter case. Its estimation is not trivial and usually, for stiff particles with smooth surfaces, the Hamaker approximation is used.

1.1.2.Hamaker contribution

The Van der Waals forces exist not only between atoms and molecules, but it concern also with particles. Therefore Hamaker, in 1937, introduced a simple but accurate enough microscopic approach to Van der Waals force in which the concept of additivity has been used. This additive principle allows the force to be calculated based on the interaction between individual atoms making up the particles, and expression (1.3) represents the non-retarded attraction energy between two particles, 1 and 2:

$$E = \frac{-\int\int q_1 q_2 \lambda_{12} dV_1 dV_2}{H^6}, \tag{1.3}$$

where q_1 and q_2 are their atomic densities (atoms per cm^3) and V_1 and V_2 their volumes. This equation, together with the following one (given by 1.4), allows calculating the Van der Waals force:

$$F_{VDW} = \frac{\partial E}{\partial H}. \tag{1.4}$$

Hamaker solved this system of equations for bodies of regular geometries. For instance, the interaction acting between two spherical particles can be estimated using the following relation:

$$F_{VDW} = \frac{A\,x}{24\,H^2}, \tag{1.5}$$

where H is the distance, instead A and x are respectively the Hamaker constant, and the reduced diameter, calculated as reported below.

$$A = \pi^2 q_1 q_2 \lambda_{12}, \tag{1.6}$$

$$x = 2 * \frac{R_1 R_2}{R_1 + R_2}. \tag{1.7}$$

It should be noted that the inter-particle interactions most depend on superficial properties, rather than bulk properties; however the expressions above have been estimated assuming perfectly smooth surfaces.

In Figure 1.1 the values of the Van der Waals force for two identical spherical bodies under gravity have been reported as a function of the particle diameter. If the Van der Waals force is smaller than the gravitational force then adherence, which is defined as the ratio between the two forces, has a value less than unity, and powder results in free flowing behaviour. If the van der Waals force is greater than gravitational force, the powder behaves cohesively. Moreover, it appears clearly from the graph that the Van der Waals force becomes noticeable when particles are sufficiently close; and its magnitude reduces with increasing the particle diameter. Usually particles are considered to be cohesive when their diameter is smaller than about 100 μm; they agglomerate rather than flow because the van der Waals force easily exceeds gravity. However, because the flowability of a particulate system depends on many factors, this rough classification allows only a qualitative assessment of the adherence.

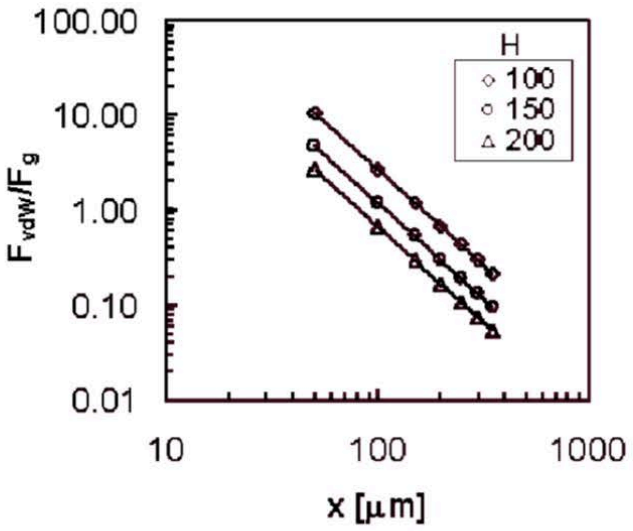

Figure 1.1. *Van der Waals force for two spherical bodies with same size at variable distance H under gravity (A. C. Santomaso, 2017).*

The assumption of Hamaker of a simple pairwise additivity ignores the influence of neighbour atoms that change the effective polarizability and introduce extra force terms. Besides, Hamaker theory cannot be readily extended to interactive bodies in a medium (J. N. Israelachvili, 2011).

In 1956, Lifshitz developed a macroscopic approach to the Van der Waals force where, differently from Hamaker's theory, he considered also the non-complete additivity of forces between individual atoms. He treated bodies as continuous media ignoring their atomic structure, thus forces have been derived in term of dielectric constants and refractive indices. However, the only thing that actually changes is the way the

Hamaker constant, *A*, is calculated. More details about the Lifshitz Theory of Van deer Waals Forces are reported in literature (J. N. Israelachvili, 2011).

1.1.3.Electrostatic forces

If two bodies with different electrical potentials come in contact, electrostatic forces originates. Due to impact or friction, charges can be transferred and can accumulate, especially if the materials are non-conductive, until the two partners become oppositely charged. This type of interaction acts on a long-range distance and so electrostatic force is classified as a non-contact force (A. C. Santomaso, 2017).

The expression that should be used for calculating the electrostatic force depends on both particle shape and relative distance. For instance, in the case of spherical particles having the same size, expressions (1.8) and (1.9) can be used respectively for particles that are close or distant enough.

$$F_{el} = \frac{\pi \sigma_1 \sigma_2}{\varepsilon} X^2 \,, \tag{1.8}$$

$$F_{el} = \frac{1}{4\pi\varepsilon} \frac{q_1 q_2}{L^2} \,, \tag{1.9}$$

where σ_i is the charge density of *i-th* particle, and $\varepsilon = \varepsilon_0 \varepsilon_r$ is the dielectric constant of the medium.

The resulting force acting between a spherical particle and the wall, which is represented as a flat surface, can instead be calculated using equation (1.10).

$$F_{el} = \frac{1}{4\pi\epsilon} \frac{\epsilon_w - \epsilon}{\epsilon_w + \epsilon} \frac{q^2}{(2L)^2} \,, \tag{1.10}$$

It should be noted that in humid environments this attraction reduces to zero. The liquid, which is conductive, covers the particle surface, the breakdown strength of air is reduced, and the maximum stable charge decreases. This leads to charge leakage and discharging (N. Harnby, 2001).

Furthermore, also electrostatic forces become stronger than gravitational one for smaller particles. So fine dry particles, if charged, are characterized by higher adhesion and cohesiveness. As the particle size increases these forces become less significant.

1.2. Mechanics of bulk solids

Unlike solids and fluids, powders are unique as a material form, and their behaviour depends on many factors such as their initial conditions (e.g. the powder stress state). For instance, a powder may behave like a continuum solid characterized by brittle fractures and plastic deformation if highly compacted. Instead the same powder can exhibits a liquid-like behaviour if subjected to high shear rates or high shear stresses; a common condition in industrial mixing processes (J. P. Seville, C.Y. Wu, 2016).

Although in some cases bulk solids behave like liquids, their mechanical properties are different and more complicated. As previously mentioned, the mechanic behaviour of powder depends on the stress state applied. Furthermore the existing interactions between particles influence the mechanics properties and the flow behaviour of granular materials. Figure 1.2 shows the shear stress variation for a powder in frictional flow regime and for a Newtonian liquid. For powders in quasi-static flow regime, where only frictional forces are present, the shear stress is fairly constant with the shear rate and the flow is assumed to be uninterrupted; so a continuum shear field exists. However, as discussed in paragraph §1.2.4, powder does not follow the same behaviour beyond the frictional flow regime. On the other hand for Newtonian liquids, a linear relationship between shear stress and shear rate exists, and the proportionality is called liquid viscosity.

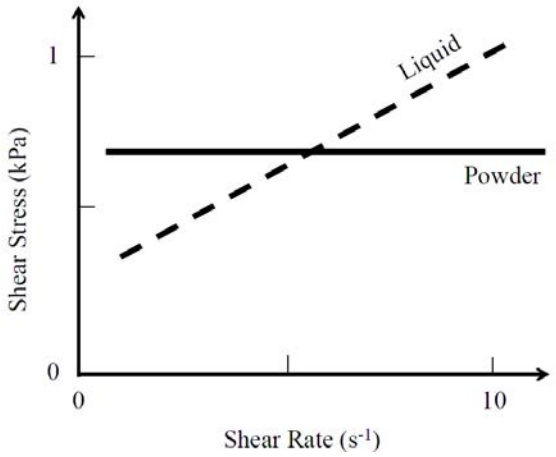

Figure 1.2. *Shear stress versus shear rate. Comparison between powders in frictional flow and liquids (J. P. Seville, C.Y. Wu, 2016).*

Figure 1.3 shows another relevant difference between liquids and powders. In the case of powders, the shear stress is influenced by the normal stress; so the initial powder compaction influences the powder flow behaviour (however their relation is not always

linear as represented). In the case of liquid, the shear stress is independent of the pressure applied and this is the reason why the liquid viscosity remains constant.

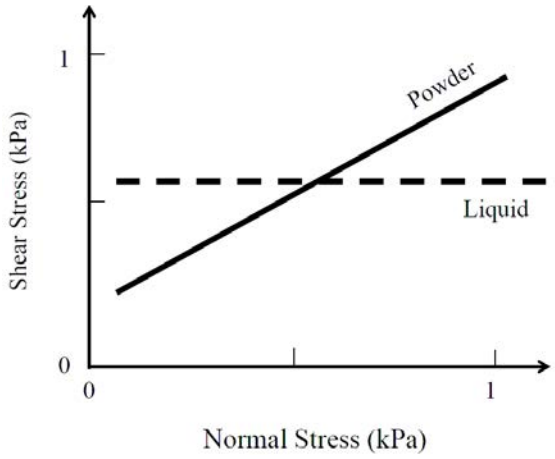

Figure 1.3. *Shear stress versus Normal stress. Comparison between powders and liquids (J. P. Seville, C.Y. Wu, 2016).*

It has been seen that powders, which are assembles of particles with different properties, are unique as material form and can behave differently under different conditions.

1.2.1. Mechanisms of deformation

Knowing the mechanical properties of a bulk material is of great importance for solid dosage form development and manufacturing, particularly in the case of tablet formulation.

In principle there are four essential deformation mechanisms that play an important role in powder flow and compaction. So, particulate materials can have the following different responses if subjected to loading: elastic deformation, plastic deformation, viscoelastic properties and failure (ductile or brittle) (G. E. Amidon et al., 2017).

Elastic deformation is completely reversible and characterizes the initial stage of powder deformation. The relationship between the applied stress, σ, and the strain, ε, is represented by the Hooke's law (as given in Eq. 1.11):

$$\sigma = E\,\varepsilon \ , \tag{1.11}$$

where E is the Young's modulus, also called elastic modulus, of the material and ε can be calculated as: $\varepsilon = (l - l_0)/l_0$. The reversibility of elastic deformations can be

understood considering that for small deformation, there is only a change in intermolecular spacing, whereas inter-particulate forces between atoms and molecules are not broken. Note that for a powder bed the elastic behaviour is almost always negligible.

When the elastic limit is exceeded, plastic deformation takes place. In this case, the resulting deformation is permanent and irreversible and, as Figure 1.4 shows, the stress-strain curve deviates from linearity. In this case an accurate model for plastic deformation predictions does not exist, also because it would vary significantly for different materials. The plastic properties of a material can be determined by indentation techniques, such as the Ball Indentation Method. Indeed, with indentation tests, it is possible to evaluate the Hardness, which is defined as the resistance of the powder to plastic, or permanent, deformation.

In addition to plastic deformation, when the powder starts to flow, there is a material failure, known as frictional failure or shear. To describe the powder flow properties, using plasticity, the well-known failure or yield hypothesis of Coulomb and Mohr is usually used (§1.2.2).

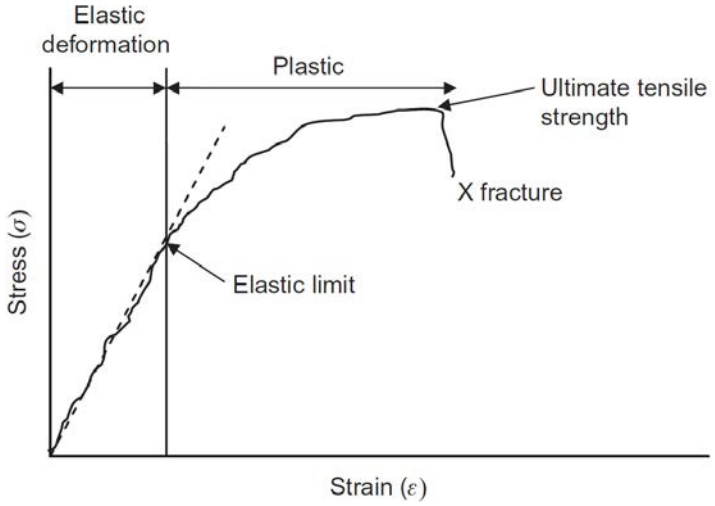

Figure 1.4. *Stress-strain curve (G. E. Amidon et al., 2017).*

Viscoelasticity is another mechanical property of the material, which reflects the time-dependent nature of the deformation. This usually happens when particles or molecules require time for rearranging under an applied stress. A typical example of time dependency is known as relaxation. Viscoelasticity cannot be ignored when dealing with pharmaceutical powders because their mechanical properties are usually affected by the deformation rate (G. E. Amidon et al., 2017).

1.2.2. Yield loci and Coulomb's law

In order to evaluate the flow properties of cohesive powders, it is important to know the conditions for frictional failure both internally and at the interface with the container wall (see Figure 1.5). For a powder to flow, the temporary internal connections between particles, and between particles and walls, must indeed break so relative displacement can take place. This failure condition, which is usually known as frictional failure or shear, can be analysed with Shear tester (§1.3.4). Repeating the test for decreasing values of normal-stresses, and representing the experimental failure points in a shear stress-normal stress diagram for biaxial stress state, allows the construction of the Yield Locus.

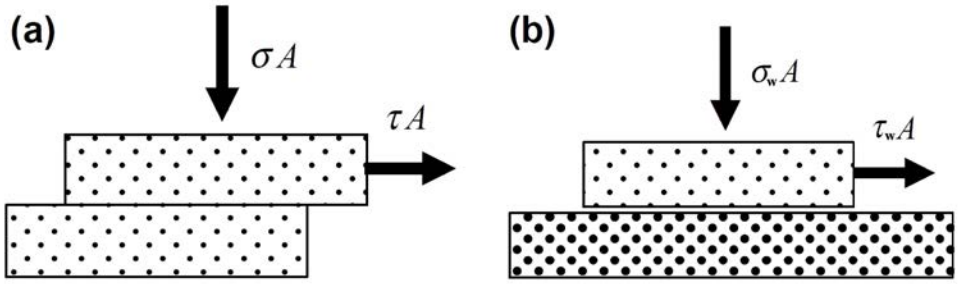

Figure 1.5. *Schematic illustration of (a) internal and (b) wall frictional failure. A is the area of the failure surface (J. P. Seville, C.Y. Wu, 2016).*

For describing the experimental Yield Locus mathematically more equations can be used, such as the Warren-Spring equation reported below (1.12):

$$\left(\frac{\tau}{C}\right)^n = \frac{\sigma + T}{T} \ , \tag{1.12}$$

where τ is the observed shear stress, σ is the normal stress of consolidation, n is defined as dimensionless curvature index ($1 \leq n \leq 2$), C and T are respectively the cohesive shear stress and the tensile strength of the compacted powder (M. Peleg *et al.*, 2010).

More often the Coulomb equation, which interpolate linearly the shear stress-normal stress points, is used. Its expression is reported below (1.13).

$$\tau = \mu\sigma + C \ , \tag{1.13}$$

Coulomb equation is considered to be a special case of the Warren-Spring equation obtained for $n = 1$ and introducing the coefficient of friction, μ, defined as the tangent of the angle δ. As long as Equation (1.13) represents the internal frictional failure, similarly Equation (1.14) describes the condition that must be satisfied for initialising failure at the wall, where μ_w is the wall frictional coefficient and C_w is the wall adhesive shear stress.

$$\tau = \mu_w \sigma + C_w \ . \tag{1.14}$$

It should be noted that both the equations above are referring to static friction, so to the friction that should be overcome in order to initiate the relative movement between particle-particle or particle-wall. However, the force required to maintaining continuous sliding (dynamic friction) is generally lower (J. P. Seville, C.Y. Wu, 2016).

In Figure 1.6 it is possible to see a schematic representation of a Yield Loci curve generated by the Warren-Spring equation. Figure 1.7 instead shows the linear Yield Loci Curve that is described by the Coulomb equation.

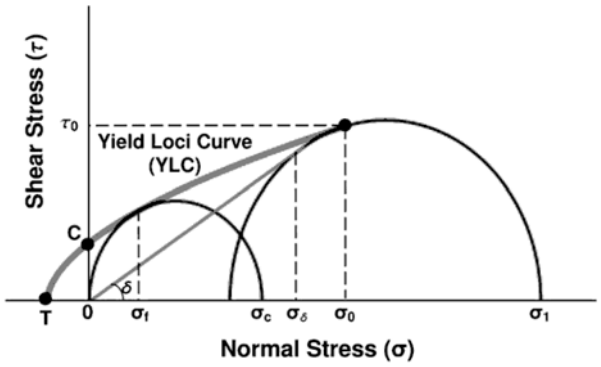

Figure 1.6. *Example of YLC described by the Warren-Spring equation (M. Peleg et al., 2010).*

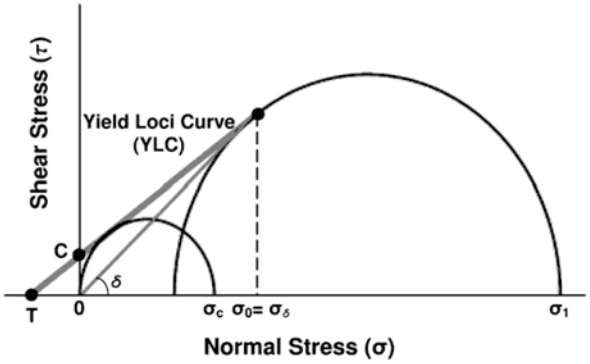

Figure 1.7. *Example of YLC described by the Coulomb equation (M. Peleg et al., 2010).*

1.2.3. Mohr circles and flow function

As previously discussed, in order to build the Yield Locus, which represents the incipient yield of a powder under a certain normal stress, the so called frictional failure or shear must be experimentally determined for decreasing values of normal stresses. The points obtained in this way are usually connected by a straight line thanks to the Coulomb equation, hence the linear Yield Loci results.

By constructing the two Mohr's semicircles tangential to the Yield Locus, both with their centre on the axis of the abscissa, but one passing through the origin (0,0) and the other passing through the pre-consolidation conditions, the Unconfined Yield Stress, σ_c, and the Major Consolidation Stress, σ_1, of a cohesive powder can be found (as reported in Figure 1.8). The former is given by the larger intersection of the smaller Mohr's circle with the axis $\tau = 0$. The bigger circle instead intersects the axis in σ_1 and σ_2, which are respectively the Major (the largest) and the Minor (the smallest) Consolidation stress.

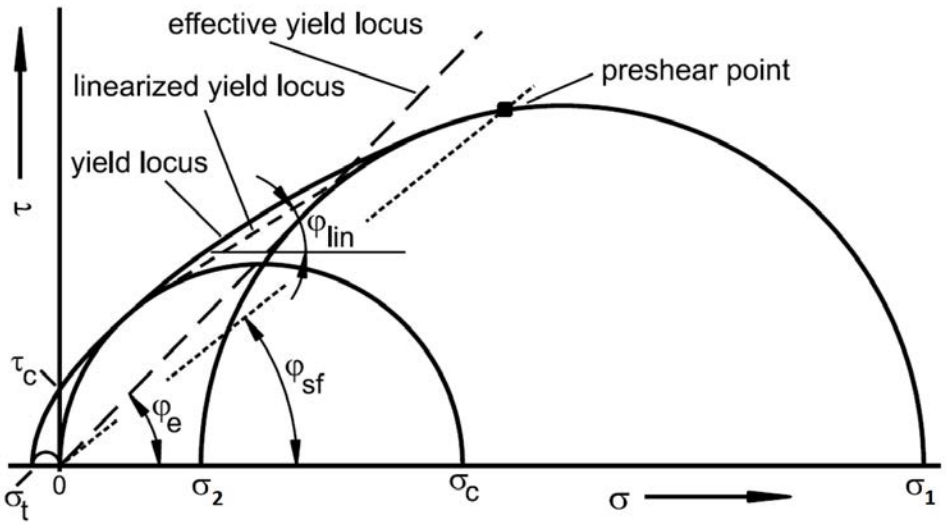

Figure 1.8. *Graphical representation of the parameters derivable from the Yield Locus and the Mohr's circles (Schulze D., 2007)*

From the yield locus, and building the Mohr's circles, it is possible to extract a lot of various important parameters concerning the flow properties of the investigated materials. These parameters are summarized in Table 1.1 and graphically represented in Figure 1.8.

Table 1.1. *Flow parameters coming from the Yield Locus and the Mohr's circles.*

Symbol	Flow parameters	Description
σ_1 or MPS	Major Principal Stress	Major intersection of the larger Mohr circle with the x axis
σ_2 or MCS	Minor Consolidation Stress	Minor intersection of the larger Mohr circle with the x axis
σ_c or UYS	Unconfined Yield Strength	Major intersection of the smaller Mohr circle with the x axis
φ_{lin} or AIF	Angle of internal friction	The angle obtained from the Yield Locus linearization.
φ_{sf} or AIF (S)	Angle of internal friction (steady state flow)	The angle defined by the line that runs through the origin and the pre-shear point
φ_e or AIF (E)	Effective angle of interval friction	The angle defined by tangent to the largest Mohr circle, passing from the origin
C or τ_c	Cohesion	The intersection of the Yield Locus with the y axis.

The ratio of the Major Principal Stress to the Unconfined Yield Strength at a defined normal load represents the Flow Function Coefficient, or Flow Factor, *ff* (Eq. 1.15), which was defined by Jenike.

$$ff = \frac{\sigma_1}{\sigma_c}. \tag{1.15}$$

According to the flowability scale published by Jenike (Table 1.2), the flow factor represents a useful and common way for characterising powder flowability.

Table 1.2. *Jenike classification of powder flowability.*

Flow factor (ff)	Flowability
$ff < 1$	No flow
$1 < ff < 2$	Very cohesive
$2 < ff < 4$	Cohesive
$4 < ff < 10$	Easy flowing
$ff > 10$	Free flowing

Because the flow factor is not expected to be constant for a material, and typically depends on the applied stress, or packing fraction, it should be evaluated at different normal loads. The flow function curve, which allows evaluating the flow performance of a powder under different set of conditions, is obtained by plotting the *ff* values obtained from the Yield Locus at different pre-consolidation values.

1.2.4.Flow fields

As seen in Figure 1.2, the behaviour of slowly flowing powders is different from that of liquids because they do not exhibit viscosity and the overwhelming interaction between particles is friction (G.I. Tardos *et al*., 2003). However, the rheological behaviour of powder changes for higher values of strain rate because shear stress becomes dependent on the strain rate. Thus, it is possible to identify different flow regimes whose classification is done based on the dimensionless shear rate, γ^*, or on the inertial number, *I*.

The classification of the flow regimes based on the dimensionless shear rate γ^*, has been proposed by Tardos G. I. *et al.* (2003). The dimensionless shear rate is defined as given by Equation (1.16),

$$\gamma^* = \gamma\sqrt{\frac{d_p}{g}}\ , \tag{1.16}$$

where d_p is the mean particle diameter, g is the gravitational force and γ is the shear rate. Specific to indentation, the latter is given by equation (1.17), where v_i and R_i are respectively the impact velocity and the indenter radius.

$$\gamma = \frac{v_i}{R_i}\ . \tag{1.17}$$

According to the classification of the flow regimes done by Tardos *et al*, at zero shear rates the powder is in static condition. The powder starts to deform only in the point defined by the yield condition. Then, for a narrow range of shear in between the static conditions and the following regime, the powder flow exhibits a stick slip-behaviour: the material flows and stops repeatedly.

After that, at low dimensionless shear rates ($\gamma^*<0.15$) the 'quasi-static' flow regime exists, where behaviour is dominated by frictional interactions and shear stress is independent of flow rate. In this regime, which is also called 'slow, frictional regime', the flow character is considered to be uninterrupted and the shear field is continuous. A set of differential equations derived by Schaeffer (D.G. Schaeffer, 1987) completely described this condition of flow.

For very high value of shear rates ($\gamma^*>3$) powders are in the 'rapid granular flow regime' (or 'dynamic flow regime'), where frictional forces between particles became negligible and the behaviour is dominated by rapid and short duration collisions.

In between the 'slow' and the 'rapid' flows, there is the intermediate regime where both collisional and frictional interactions between particles must be considered. However the boundaries between each regime are uncertain and not well defined due to the slight dependency on the inter-particle cohesion (G. I. Tardos *et al.*, 2003). A schematic representation of the flow regimes as a function of the dimensionless strain rate is reported below (Figure 1.9).

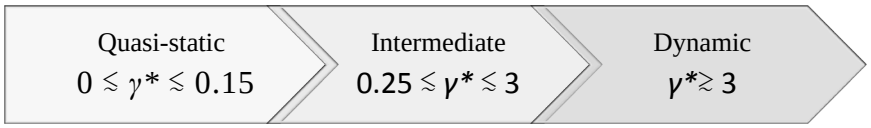

Figure 1.9. *Classification of powder flow regimes according to Tardos et al.*

If in the frictional-slow flow regime, the shear stress does not depend on the strain rate $\tau \neq f(\gamma)$, in dynamic flow regime the shear stress is a function of the square of the strain rate $\tau = \gamma^2$. In between the strain rate dependency has a power index less than 2 ($\tau = \gamma^n, n < 2$).

To classify flow regimes it can also be used the inertial number approach. *I*, is calculated as given by Eq. (1.18), where γ is the strain rate, ρ the particle density of the bed and σ_H is the hydrostatic stess.

$$I = \gamma\, d_p \sqrt{\rho/\sigma_H}\,. \tag{1.18}$$

In this case a dense flow regime is characterised by inertial numbers in between $10^{-3} < I \leq 10^{-1}$, instead $I > 10^{-1}$determines the collisional flow regime

The regime boundaries defined with the two approaches differ significantly, in particular the system enters the dense and collisional flow regimes at much lower impeller tip speeds if the classification is done with considering the inertial number (C. Hare and M. Ghadiri, 2017).

1.3. Powder flowability and measurement techniques

In this section it will be briefly described some of the techniques used for assessing the powder flowability, which can be defined as the capability of a powder or granular material to flow under a specific set of conditions. Evaluating the powder flowability is of great importance for reliable design of specific piece of equipment and proper operation of industrial processes. Predicting the flow performance of a powder is therefore needed for reliable design of equipment for storage, transportation or general handling of bulk solids.

The flowability cannot be defined as a single value for a given material since it is not an inherent bulk property. This means that it is highly dependent on a combination of physical properties, process conditions and environmental factors. For instance, the powder performance is strictly connected with the surface area per unit mass. So big particles spherical in shape, because their smaller surface area per unit of mass, flow better than microscopic irregular particles. Furthermore particles flow freely if their diameter is such that gravity prevails over the microscopic inter-particle interaction. Then, particles characterized by the same size and shape could behave differently if they differ in surface morphology or mechanical properties. Finally the flowability is influenced by external conditions as well as by the sample stress history.

Even though the flow characterization of powder represents a complex task, the widespread use of granular material has generated a huge variety of flowability measurement techniques, which can be distinct in qualitative and quantitative methods. The former are cheaper and faster, but the flow behaviour is assessing indirectly observing properties that are only supposed to be correlated with flowability. Furthermore they can be applied only for unconsolidated materials. On the other hand, quantitative methods allow directly evaluating the material during flow, and taking into account the initial loading force applied. However a single index cannot adequately characterise the flow performance of a powder under all conditions.

Some of the methods standardised by the European Pharmacopoeia, which is the reference book that provides standards for the European pharmaceutical industry, are reported below. The angle of repose, the compressibility index or Hausner ratio, and the flowrate thought an orifice are qualitative flowability measurements methods, shear cell instead represents a quantitative method. Furthermore also other methods, such as the unconfined yield stress, the indentation technique and the dynamic methodology of the powder rheometers are described.

1.3.1. Angle of repose

The angle of repose is one of the most common techniques used to characterize flow properties of bulk solids. It is defined as the angle formed by a pile of material of conical shape with the horizontal plane. Despite the angle of repose is not an intrinsic property of the material, it is well related with the inter-particle friction, or resistance to movement between particles.

A variety of different methods have been developed for determining the angle of repose, both in static and dynamic conditions. The basic methods in static condition are the poured and drained angle of repose (respectively represented in Figure 1.10, a and b). The former consists of pouring the material on a flat surface from a well-determined height, the latter instead consists of making a solid flowing through the central orifice of a container. In both cases the angle of repose can be determined looking at the pile of powder with the following simple geometrical relation (1.19):

$$\alpha_r = tan^{-1}\left(\frac{2 * height}{D_a - d}\right) , \tag{1.19}$$

where D_a represents the diameter of the conical pile of material, while d is the orifice diameter. Usually, for having consistent result, the height from which the powder flows is kept constant and the nature of the base is fixed and well known.

Alternatively the dynamic angle of repose, such as the rotating drum, can be carried out. After filling the powder in the drum, it rotates at a specific speed (Figure 1.10-c). Thanks to a high speed camera, the behaviour of the powder in motion can be captured and the angle of repose, which is in this case defined as the angle formed by the flowing powder with the horizon, can be evaluated.

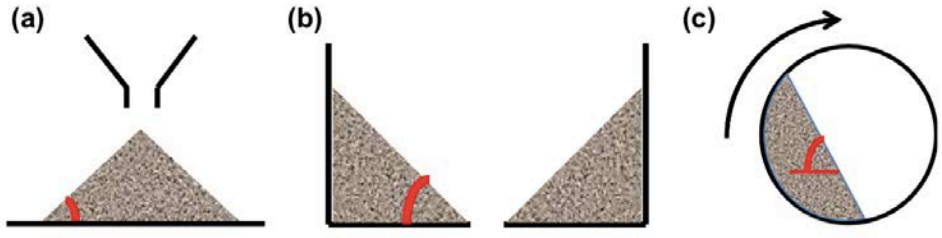

Figure 1.10. *(a) Poured angle of repose, (b) drained angle of repose, (c) dynamic angle of repose (J. P. Seville, C.Y. Wu, 2016).*

The methods discussed as far are fast, easy to perform and repeatable. Moreover they are very useful for evaluating the amount of material that can be stored in a silo. Despite this, the reproducibility becomes worst for cohesive materials since they exhibit very steep and irregular slopes due to the increase of friction and inter-particle interactions. Other constraints are the large amount of material required for performing the test, which is undesirable especially when dealing with API; and its high dependency on the test conditions, which affects the test robustness.

The scale of flowability generally used for evaluating the angle of repose has been classified by Carr in 1965. The flow properties and the corresponding angle of repose are reported in Table 1.3, together with the flowability scale of the compressibility index and the Hausner Ratio (§1.3.2). It should be noted that a granular material characterized by an angle of repose greater than 50 degree is hardly accepted in manufacturing processes due to its high cohesion and lack of flowability.

1.3.2. Compressibility index and Hausner Ratio

Although density is simply defined as the ratio between mass and volume, its determination is complicated when dealing with granular materials. This is because a defined amount of powder can fill different volumes if different is its packing state and the amount of air entrained in the bed. Besides how density changes after a normal load is influenced by a lot of factors like particle size, shape, cohesion and surface roughness.

Therefore several densities definitions have been introduced for bulk solids. Some of the most widely used are: the solid density, ρ_s; the bulk density, ρ_b; and the tapped density, ρ_t. The solid density, ρ_s, which is also called true or absolute density, is calculated excluding both the voids between particles, and the open and close voids in the particles themselves, so it does not depend on the powder packing state. The bulk density, ρ_b, which is calculated considering the total volume occupied including all the inter-particle voids, depends upon how the powder is handled and packed, and it is always less than the material's true density. Finally, the tapped density, ρ_t, is calculated similarly to the bulk density, but considering the volume occupied after tapping (J. P. Seville, C.Y. Wu, 2016).

The difference between densities before and after tapping is a useful parameter that can be used for evaluating powder flowability and packing state. For free-flowing materials, which easily minimise the void spaces when poured into a container, this change is

negligible; whereas in the case of more cohesive powders, which are loosely packed at low stresses but densify under higher stresses, the difference is higher.

Among the indicators proposed in literature to define flowability there are the compressibility index and the mathematically related Hausner ratio. They are both simple and fast, and therefore popular; however, due to their drawbacks, they cannot be used alone for evaluating the flow performance of a powder.

The compressibility index is a measure of how the density changes with the applied normal stresses and hence it quantifies how a powder is prone to consolidate. Instead the Hausner ratio is useful for determining the cohesion of a bulk solid. However these indices are equivalent because they are calculated using the same variables. The procedure is easy; it simply requires the measurement of the tapped density, ρ_t, and the bulk (poured) density, ρ_b. It is clear that, in order to have consistent and reproducible results, the material should be tapped until no further change in volume may be possible.

The equations used for calculating the Compressibility Index and the Hausner Ratio are given respectively by equations (1.20) and (1.21). Note that in both cases two equivalent expressions have been reported: one where the tapped density, ρ_t, and the bulk (poured) density, ρ_b, are used; another one where the variables are the initial unsettled volume, V_o, and the tapped volume, V_f. This is possible because volume and density are correlated through the mass of powder that remains constant before and after tapping.

$$CI\ [\%] = 100 * \frac{\rho_t - \rho_b}{\rho_t} = 100 * \frac{V_o - V_f}{V_o}, \tag{1.20}$$

$$HR\ [-] = \frac{\rho_t}{\rho_b} = \frac{V_o}{V_f}\ . \tag{1.21}$$

These indices allow only to roughly classifying the powder. If tapped and bulk densities do not deviate, the material can flow freely. On the other hand, very cohesive powders are characterized by a major change in volume after tapping. In fact, the applied normal stresses determine a reduction in the voidage between particles, which deploy themselves in a more ordinate manner. In Table 1.3 it is shown the empirical relation that correlate both the indexes with the powder flow characteristics. In the same table is reported also the flowability scale for the angle of repose (§1.3.1) in order to allow a comparison between different indicators.

Table 1.3. *Flowability scale for angle of repose, compressibility index and Hausner ratio.*

Flow behaviour	α_r [°]	CI [%]	HR [-]
Excellent	25-30	1-10	1.00-1.11
Good	31-35	11-15	1.12-1.18
Fair	36-40	16-20	1.19-1.25
Passable	41-45	21-25	1.26-1.34
Poor	46-55	26-31	1.35-1.45
Very poor	56-65	32-37	1.46-1.59
Very very poor	> 66	> 38	> 1.60

Despite the ease and the speed of the procedure, both compressibility index and Hausner ratio own a lot of drawbacks. For instance the method is operator dependent because the filling method and the different compaction dynamic could lead to different results. Hence they should not be applied when an accurate prediction of the powder flow performance is required. Nevertheless, the European Pharmacopoeia recommends the following precautions in order to standardize the method: the use of a 250 mL volume cylindrical in shape, the use of 100 g of material for each test, at least three repetitions for each measurement.

1.3.3. Flow rate through an orifice

The flow rate through an orifice represents another qualitative method for assessing the flow behaviour of bulk solids. In particular, this has been proposed as a better measure of powder flowability because it correlates directly the flow of a powder through processing equipment (European Pharmacopoeia, 2007).

By definition it represents the amount of material flowing through an orifice in a well define amount of time. Usually the orifice is in the flat bottom surface of a cylindrical container, but it could be also the orifice of funnels or hoppers. The flow rate can be determined both in mass or volumetric base. However, although the former is easier to evaluate, the volumetric flow rate is usually preferable since the die fill is volumetric.

The procedure is very simple to perform, but more methods are reported in literature. The variability is due to the relative dimensions of: orifice, container, particles and height of the powder bed. In particular, for reliable results, it is recommended the use of a container with a diameter at least twice the opening diameter, which in turn should not be smaller than six times the diameter of the largest particles. Besides the height of the

powder bed should not be smaller than twice the container diameter because for smaller values, the powder flow rate increases with the container emptying and the results could be not representative anymore.

The main advantage of the method is that it allows implementing both discrete and continuous measurements. Monitoring the flow continuously allows observing, simply thanks to an electronic balance, if the material has some pulsating flow patterns. However in between the drawbacks there are the wide range of method variability, as well as the large amount of material required, which could become a problem particularly for valuable powders. Besides, materials that behave cohesively tend to form arches on the hopper avoiding the flow; the flowrate could change as the container empties; and finally a scale or an empirical relation between the flow rate and the powder flow properties does not exist. This means that a comparison with the other flow indicators is not possible.

1.3.4. Shear cell

More robust flow results can be achieved with a shear cell. This is because, differently from the qualitative techniques discussed above, shear cell is a quantitative method: it allows directly evaluating the material behaviour during flow and to take into account the initial applied stress. The main purpose of performing a shear cell measurement is to evaluate the flowability of a powder for: comparison with the flowability of other substances, design process equipment such as hoppers and bins, prediction the flow performance of a material during industrial operations like tablet pressing, capsule and inhalers filling. Moreover, shear cell allows also evaluating the influence of time on powder flowability, which could in fact lead to an increase of cohesion between particles.

Although there are many variants of shear cells, each one described in detail in literature, the most important are the Jenike's and the Schulze's shear testers. The former is a translational shear tester, and is the first one design for measuring the flow function of powders. However it is rarely used today because the long time required for performing a test, the big amount of material needed, the necessity of using fresh powder for each applied stress, and the operator-dependency of the results. Figure 1.11 is a schematic representation of the Jenike shear tester. After loading the lid with a normal force, F_N, the upper ring is displaced horizontally against the fixed bottom ring, so a deformation takes place in the bulk solid. Dividing the normal force and the shear

force by the cross-sectional area, *A,* it is possible to determine the normal stress and the shear stress (D. Schulze, 2006).

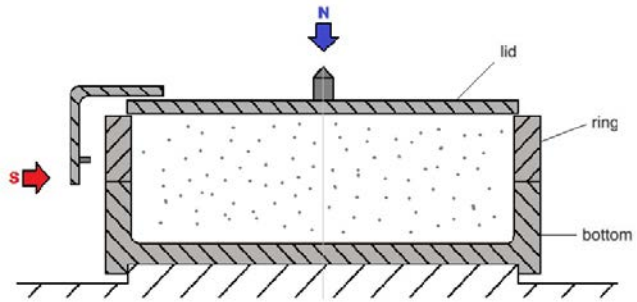

Figure 1.11. *Jenike shear tester.*

The Schulze shear tester (see Figure 1.12) is instead the most widespread, probably due to its commercial availability. It is a ring shear tester (rotational) introduced in the 1930s, advantageous for the small amount of material required with respect to other types of shear testers. In this case, after the appliances of a normal stress, the lid and the ring, which are both annular, rotate relative to each other creating a shear deformation within the bulk solid (D. Schulze, 2006). Between the rotational shear tester, there are also the cylindrical shear cell, whose principle is the exactly the same of the annular ones.

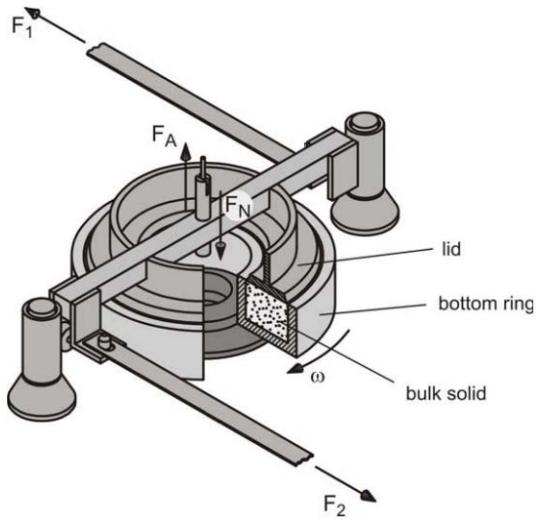

Figure 1.12. *Schulze ring shear tester type (D. Schulze, 2008).*

Unlike translational shear testers, rotational shear cells are less time consuming and lead to reproducible results. Then, since infinite strain can be achieved, all the shear point

can be obtained in a single sample. However, because of their geometry, in the case of rotational shear cells the powder bed cannot be uniformly sheared. Instead among rotational shear testers, the annular is advantageous over the cylindrical since the range of minimum to maximum radial distance is less. This means that there is less variability in shear rate across the bed.

Other types of shear cells exist, such as the plate-type shear cells and the tri-axial shear testers; however they are not described here because rarely used.

The main reasons why shear testers are so largely diffused for powder flow characterisation are: the reliability of the results, the high degree of experimental control and the large amount of obtainable information. With only one single test it is possible to obtain a wide range of parameters like flow factor, wall friction, internal friction, cohesion, as well as shear strength. Furthermore, it exist a mathematical methodology proposed by Jenike (A.W. Jenike, 1967) that allows to design the minimum orifice diameter and the angle of the hopper needed for guaranteeing mass flow, simply knowing some of the parameters given by the shear cells.

Nevertheless the shear testers could be too expensive for analysing pharmaceutical excipients. This is due to the large amount of material required for performing the test. Furthermore, this test is more time-consuming that the other qualitative methods described above. Other limitations concern with the operative restrictions of the method. Shear testers can only characterize material with consolidation states in a range of 10-100 kN/m^2 (A. C. Santomaso, 2017), so it cannot be used for estimating the behaviour of low consolidated powder, such as the powder filled in inhalers. Moreover it cannot be estimated the powder flow behaviour in dynamic conditions; hence it cannot be applied for describing dynamic operations like mixing. Finally, because the huge amount of existing shear cell configurations and test methods, it is always required a complete description of the system and the methodology used for performing the test.

Although the variety of methods, the same general procedure is carried out. After filling with care the particulate solid in the cell, the powder is firstly pre-consolidate to a selected normal stress, and then pre-sheared. This means that sample is sheared until the value of shear stress reaches a plateau, situation of steady state where density and shear rate remain constant. Subsequently it is applied a normal load smaller than the pre-consolidation one, and the powder is sheared further until a maximum of shear stress, which represents the shear strength of the powder bed under those conditions, is reached. The procedure just described is repeated more times for decreasing values of normal load, which are usually selected in between 20 and 80% the value of the initial

pre-consolidation load, in order to obtain more failure points. The procedure is graphically represented in Figure 1.13-a, where the shear strengths are reported as a function of times. After pre-shear under a normal stress, σ_{sf} , until achieving a stationary flow, the shear stress is reduced to zero and the normal stress is reduce to a value smaller than σ_{sf}, until incipient failure is registered. Then a second repetition is performed. The failure shear strengths, which have been obtained for different normal loads, can be plotted on a shear stress-normal stress diagram, together with the stationary flow point (Figure 1.13-b). The Yield Loci arises by interpolating these points (§1.2.2).

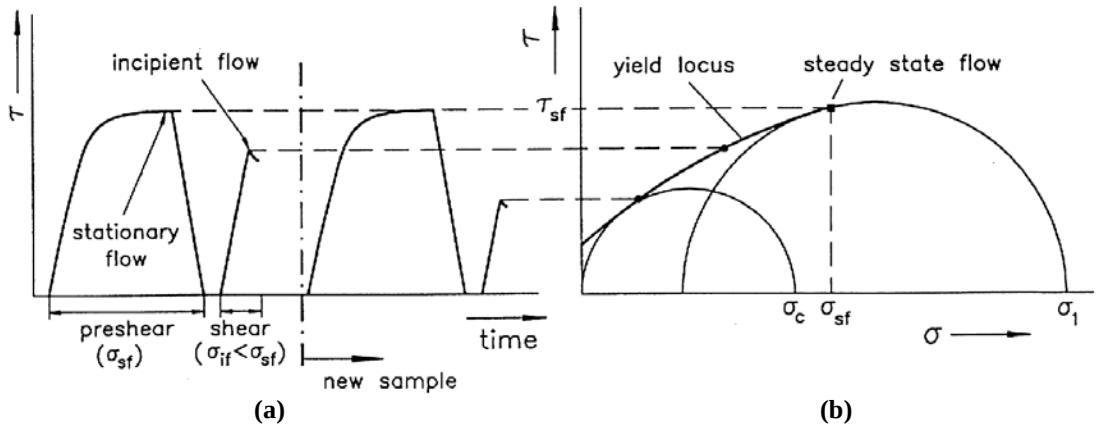

Figure 1.13. *(a) Example of Jenike's shear cell procedure. The failure points, reported on a (b) shear stress-normal stress diagram, allow the construction of the Yield Locus (J. Schwedes, 1999).*

The two Mohr circles tangent to the Yield Loci allows determining the Unconfined Yield Stress, σ_c, and the Major principal stress, σ_1, of the investigated material at that initial normal pre-consolidation stress. The procedure must be repeated more times, for different values of initial normal load, for obtaining more pairs σ_1 - σ_c, and so a complete material flow function. More theoretical details on Mohr's circle and Flow function have been reported in paragraph §1.2.3.

1.3.5. Uniaxial tester

Although it is not mentioned in the European Pharmacopoeia, another simple technique used to measure powder flowability is the uniaxial tester, which consists of observing the failure point of an unconfined powder bed previously consolidated.

As schematically represented in Figure 1.14, the powder is firstly filled into a hollow cylinder with frictionless walls and consolidated under a normal stress, σ_1, which is

called the consolidation stress or Major Principal Stress. After consolidation, the normal load is reduced to zero and the cylindrical wall is removed. Consecutively an increasing normal load is applied to the unconfined bed of powder until the failure of the specimen is reached, which means that a plastic deformation occurs. The stress at failure represents the Unconfined Yield Strength, σ_c, and generally, a higher initial pre-compression determines a higher Unconfined Yield Strength.

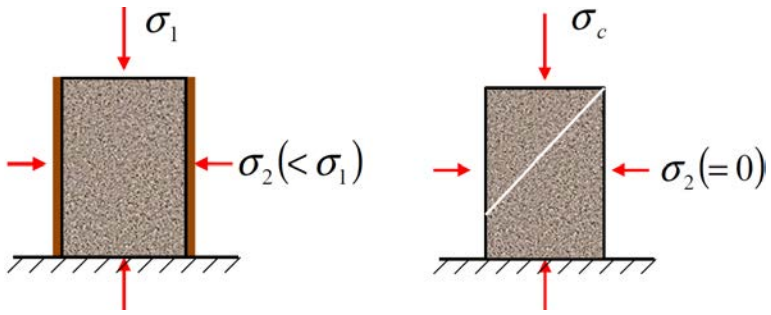

Figure 1.14. *Uniaxial tester (J. P. Seville, C.Y. Wu, 2016).*

Despite the shorter time required and the simplicity of the method, the uniaxial tester does not provide other information outside of the Unconfined Yield Strength. Furthermore, because the steady state is not reached during consolidation, the Mohr's circles obtained with this procedure are smaller than the ones achieved with shear testers, so σ_c is under-estimated. Finally, the bulk solid is strongly dependent on the sample stress history.

1.3.6. Ball Indentation Method

Ball indentation technique is a very common method used to evaluate hardness and tensile properties of continuum-solids, particularly for evaluating the integrity of metallic structures (Y. Tirupataiah, G. Sundararajan, 1989).

The same method can also be carried out on compacted powder bed for evaluating the cohesive bulk powder failure. In this case the spherical indenter is dropped onto a cylindrical bed of previously consolidated material. The method, introduced by Hassanpour and Ghadiri (2007), was born by the desire to investigate a methodology suitable for evaluating powder flowability also at low compaction level, in quasi-static flow condition and small scale. The hardness of the compacted bulk solid, which can be defined as the resistance of a material to plastic deformation, is determined as given by Equation 1.22:

$$H = \frac{F_{max}}{A} \ , \tag{1.22}$$

where F_{max} represents the maximum indentation load and A the projected area of the impression. In turn A, can be obtained from the following geometrical relations (1.23),

$$A = \pi \, D_i h_{c,max} - \pi \, h_{c,max}^2 \ . \tag{1.23}$$

where D_i is the diameter of the indenter and $h_{c,max}$ is the penetration depth, which is estimated considering the tangent to the unloading curve. A typical experimental loading and unloading curve is reported in Fig. 1.15. Instead in Fig. 1.16, the indentation profile and the parameters involved in the hardness calculations are shown.

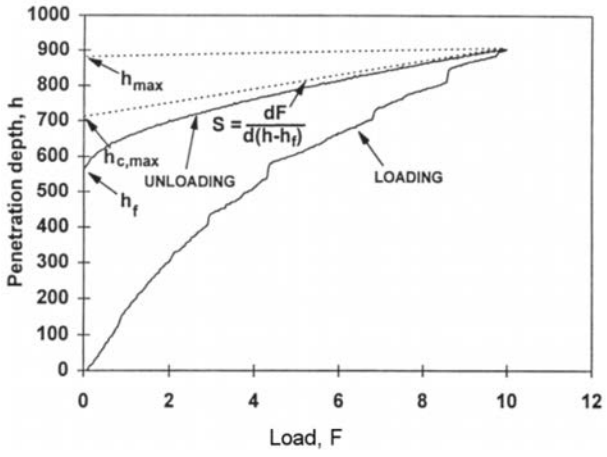

Figure 1.15. *Typical loading and unloading curve (Hassanpour and Ghadiri, 2007).*

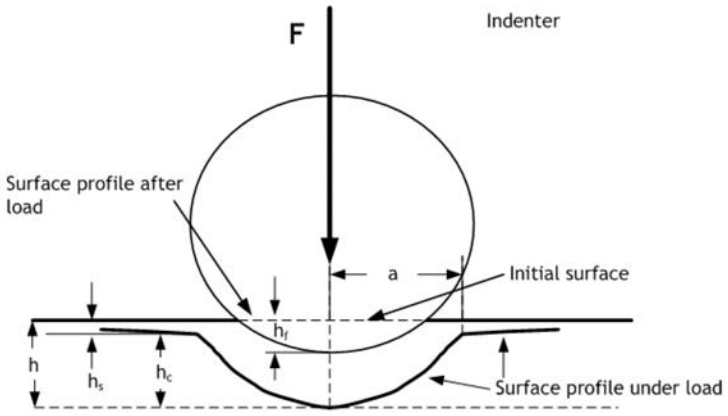

Figure 1.16. *Penetration profile and variables involved (Hassanpour and Ghadiri, 2007).*

In their work, Hassanpour and Ghadiri (2007) demonstrated that, also for powder like for continuum solids, the hardness, *H*, is related to the Unconfined Yield Strength, σ_c, through the so-called constraint factor, *C*, as reported in correlation (1.24). But, if for continuum solid *C* is usually equals to 3, for powders its value depends on single particle properties such as particle shape, roughness and friction coefficient. In any case the hardness is larger than the Unconfined Yield Strength and, both the indentation Hardness and Unconfined Yield Stress increase with pre-consolidation pressure.

$$C = \frac{H}{\sigma_c} \ , \tag{1.24}$$

Ball Indentation technique is suitable also for evaluating hardness in dynamic regime, when the flow is characterized by rapid and short collision between particles rather than friction (Phasa *et al.*, 2015). In the case of dynamic indentation, hardness, H_d, is calculated as the ratio between the kinetic energy of the indenter and the volume of the crater, as given by equation (1.25) proposed by Tirupataiah and Sundararajan.

$$H_d = \frac{M\, v_i^2}{2\, U} \ , \tag{1.25}$$

where *M* is the mass of the indenter, v_i is its impact velocity, and *U* represents the volume of the crated formed by the impact of the ball on the flat surface of a target material.

Despite Ball Indentation Method does not provide directly the value of the shear stress under a controlled normal stress, it represents a quick and simple way to evaluate the resistance of the powder bed to plastic deformation, and hence a measure of powder flowability. Furthermore, it is possible to investigate the flow behaviour also in the intermediate and dynamic flow regimes, conditions that nowadays can be evaluated only by other few techniques provided by powder rheometers and the Couette device.

In the last decade, the operational window of the ball indentation method has been intensively studied. For instance, in 2013, *Pasha et al.* simulated indentation within the quasi-static regime and found that the dimensionless penetration depth, h_d, namely the ratio between the penetration depth h and the radius of the indenter R_i, has to be at least 0.1. Smaller value of penetration depth could not be representative because the ball would interact with only few particles. Besides it may happen that oscillations appears for $h_d < 0.4$ because of the not fully initialized plastic flow in the powder bed. The

upper limit of the depth of penetration is instead due to the presence of the die wall. Usually, within this range, hardness stabilizes and get independent by the height of penetration. In term of indenter size, it has to be large enough to avoid localised consolidation in the powder bed; however if its diameter is too large (comparable in size to the die), the hardness is going to be affected by the wall.

Additionally, in 2015, Pasha *et al.* investigated the sensitivity of the stresses in assemblies of cohesive particles with spherical shape, always using the Distinct Element Method. Their study shows that the hardness, the deviatoric and the hydrostatic stresses within a powder bed, whose flat surface is subjected to spherical indentation, become strain rate dependent for strain rate greater than unity. This means that by increasing the strain rate, a liquid-like viscous character is manifested by the bulk powder. Hence, their simulations confirmed the possibility of capturing the dynamic of cohesive flow powder with the Ball Indentation Method.

Succesively Zafar *et al.* (2017) investigated in more detail the operational windows of the method in terms of sample size, indenter properties and dimensionless penetration depth. For instance it has been shown that, for having reliable results, the indenter size has to be at least 16 times the mean particle diameter, but it should not be more than 0.65 times the diameter of the powder bed. In the case of multiple indentations, a minimum separation distance of 1.5 times the indenter diameter has to be respected. Finally, he demonstrated that al low pre-consolidation values, the hardness measurements are independent from the Young's modulus of the indenter.

1.3.7.Powder rheometers

The powder rheometers, which have been designed on the model of the liquid rheometer but for characterizing the rheology of granular materials, enable different measurement applicable both to quality control and research. They allow determining different powder properties and handling parameters, in particular evaluating deviation in powder flow. Thus, powder rheometers represent another way for carrying out powder flow measurements; and the only commercially available instrumentation that allows investigating also the dynamic regime of flow.

The existing powder rheometers are: the Antoon Paar's, the Stable Micro System's and the Freeman's. Thanks to their design and the provided tools, different types of measurement can be carried out such as the shear cell test. However, the typical test used for evaluating the flow behaviour of a powder in dynamic condition, which means

when in motion, consists on measuring the total energy required to physically displace the sample by a helical blade. Indeed, while the blade moves through the powder bed with a specific tip speed, both the rotational and the vertical resistances to flow are measured.

1.3.7.1.The dynamic methodology of the FT4 powder rheometer

The FT4 powder rheometer from Freeman technology (see Figure 1.17) is a modern instrumentation capable to measure a wide range of shear, bulk and dynamic flow properties, considering different initial state of powder conditions: when it is consolidated, conditioned, aerated or even fluidised. Furthermore, it can be used to investigate the effect of a lot of external variables on powder flow characteristics such as humidity, electrostatic charges and time of storage.

Figure 1.17. *The FT4 apparatus (www.freemantech.co.uk).*

Among the FT4 available tests, the dynamic methodology (e.g. Basic Flow energy and Variable Flow Rate method) is suitable for a quantitative evaluation of the powder flowability. Indeed it measures the resistance of the powder to flow when in motion, which means the energy required to make the powder flow. Standard procedures of the FT4 dynamic test are the Basic Flow Energy and the Varible Flow Rate methods.

The Basic Flowability Energy, *BFE*, which is define as the work done by the blade that rotates downwards and counter clockwise from the top to the bottom of a precise volume of powder and that establish a well define flow pattern in the powder bed (as shown in Figure 1.18), is a flowability measurement of loosely compacted powder and can be used for evaluating the powder cohesiveness. However, the Basic Flowability Energy does not really simulate the powder flow during industrial processes because it does not take into account changes in process conditions.

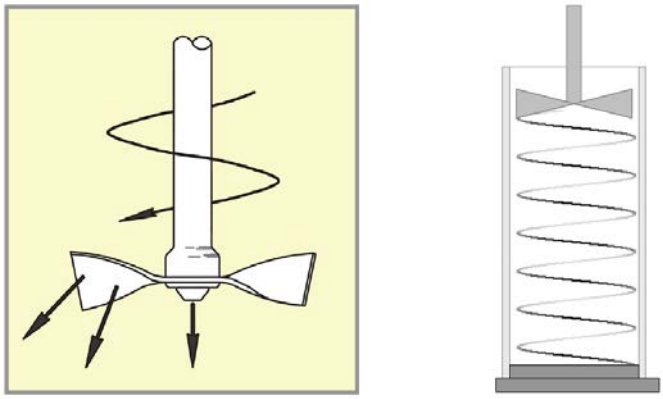

Figure 1.18. *Downward traverse of the blade through the powder bed (Freeman Tech., W7030, 2013).*

The Variable Flow Rate (VFR) method, which is the exact same protocol as the BFE test only with the tip speed during the downward traverse varied, allows estimating the total energy required to make the powder flows as a function of the impeller speed. Hence, a flow rate sensitivity analysis can be done. The sequence of this method consists on subjecting the powder to the action of a precision blade that rotates at different tip speeds. In particular for subsequent tests, the blade moves downwards and upwards at the following decreasing velocities: 100, 70, 40 and 10 mm/s. Note that in between tests, the conditioning cycle is performed in order to remove any stress history and establish a uniform and reproducible state. While the blade moves through the sample, both the rotational and vertical resistance to flow are measured and the rheological powder properties can be evaluated.

The powder's resistance to being made to flow in a dynamic state, which represents the difficulty of particles to interact or flow relative to one another and gives an indication of the powder rheology, is calculated as the area under the Energy Gradient curve, which represents the energy measured for each millimetre of blade travel. Alternatively, the total energy consumed during the downward traverse, E_{flow}, can be quantified

knowing the torque, *T*, and the normal force acting on the base, F_{base}, as a function of the height as given by Equation 1.26.

$$E_{flow} = \int_0^H \left(\frac{T}{R \tan(\alpha)} + F_{base} \right) dH \ , \tag{1.26}$$

where α is the helix angle, which is equal to 5º, and *R* is the impeller radius. However, this integral cannot be solved simply considering the total height travelled by the blade because the values of torque and force are constantly changing along the powder bed. It is therefore necessary to solve the integral for each small distance travelled.

Furthermore, the flow rate sensitivity of a powder can be evaluated using the Flow Rate Index, *FRI*, which is the ratio between the total flow energies calculated when the blade tip speed is reduced by a factor of 10 (Eq. 1.27). The flow rate sensitivity scale is reported in Table 1.4.

$$FRI = \frac{E_{tot,10mm/s}}{E_{tot,100mm/s}}, \tag{1.27}$$

Table 1.4. *Flow rate sensitivity scale (Freeman Technology, W7012,2007).*

FRI	**Flow Rate sensitivity**
FRI > 3	High
1 < FRI < 3	Average
FRI ≅ 1	Insensitive
FRI < 1	Pseudoplastic or Newtonian

In general, cohesive powders are sensitive to flow rate changes, so the energy required to move the blade through the sample is higher at lower speed (FRI > 1). This is due to many factors like the amount of air entrained, the particle interlocking and the extension of the air filled zone behind the blade. So, because at slower speed the particle interlocking is higher and the amount of air entertained is lower, more voids can escape from the sample and the resistance of powder to make it flow becomes higher. Free flowing powders instead behave differently; they are generally insensitive to changes in flow rates because the contact between particles remains always the same, independently from the shear rate (Freeman Technology, W7012, 2007).

Chapter 2
Materials and Methods

Due to the huge number of variables, powder characterisation and processing are complex issues in particle technology. And because granular solids cannot be described uniquely with individual techniques, it is always recommended the use of a multivariable approach. This is the reason why here flowability is investigated using different qualitative and quantitative methods. Furthermore, to investigate the powder flow at high shear rates, both the ball Indentation Method and the Variable Flow Rate technique of the FT4 powder rheometer are performed.

In this chapter it is described the experimental setup and the methodology of the Ball Indentation Method, which is used for evaluating the powder hardness for a range of indenter sizes, materials, impact velocities, as well as for different initial states of powder compaction. The second part of the chapter focuses on the FT4 powder rheometer, in particular on those methods that have been performed to purchase the aims of this thesis: indentation in quasi-static condition, variable flow rate method and rotational shear cell.

2.1. Ball Indentation Method

Unlike the most common test methods, ball indentation technique is suitable for measuring flow properties of bulk solids also at small compaction levels and in dynamic conditions. The experimental procedure used for assessing the hardness in intermediate and dynamic flow regimes is reported below.

2.1.1.Experimental setup and methodology

The experimental setup for the hardness measurements through the Ball Indentation Method is simple and inexpensive. It consists of an upright glass tube of about 40 mm internal diameter, a vacuum pump as release mechanism of the ball, some precise indenters, an instrument for compacting the power bed, a high speed camera and a software for post-processing analysis.

Figure 2.1. *Glass tube and 50 mm X 85 mL vessel.*

The glass tube is located just above the compacted powder sample (as shown in Figure 2.1), avoiding any contacts that could change, at least locally, the bulk properties of the investigated material. Because the indenter is located at the top of the tube before it is released, tubes of different height are used in order to investigate different impact velocities. Their heights and the corresponding velocities are reported in Table 2.1. Note that the instantaneous velocity, v_i, of the falling indenter that travels the distance h has been calculated considering no air resistances as given by $v_i = \sqrt{2\ g\ h}$. However this is only an initial estimation, useful for planning the tests. The real impact velocity is assessed for each performed test by post-process image analysis.

Table 2.1. *Used glass tubes and estimation of the corresponding impact velocities.*

Tube height [m]	0.05	0.10	0.20	0.50	0.80	10
Predicted v_i [m/s]	0.99	1.40	1.98	3.13	3.96	4.43

The release mechanism of the spherical indenter is done thanks to a vacuum pump in order to guarantee the repeatability of the test and the consistency of the results. In fact, the vacuum pump allows avoiding any possible rotations that the operator could impose on the spheres. By switching off the vacuum pump, the indenter is released inside the glass tube of the selected height. So the released indenter, which is accelerated under gravity, drops onto the compacted powder bed. As far as possible, it is important that the indenter falls in the centre of the cylindrical powder bed because, when its position gets too close to the wall, the hardness result could be not reliable anymore.

For performing the tests, indenters of different size, shape and density could be used. However here, only spherical indenters, which uniformly deform the bulk solid by shearing particle rather than consolidating, are investigated. They are made of four different materials: Nylon, Glass, Ceramic and Stainless Steel (represented in Figure 2.2-a, b, c, d), therefore the dependency of indenter density on the hardness measurements can be investigated. In Table 2.2 the densities of each material are reported.

Table 2.2. *Densities of the indenters.*

Material	**Density [kg/m^3]**
Nylon	1152.53 ± 17.97
Glass	2565.54 ± 34.61
Ceramic	3703.44 ± 170.36
Stainless Steel	7466.15 ± 357.81

Then, in order to investigate also the effect of the indenter size, and to achieve a wider range of strain rates, a range of different diameters is tested for each material type (see Figure 2.2-e, f, g, h). In conclusion, sixteen indenters of different size and density are used. In Table 2.3, all the indenters and their properties are summarized.

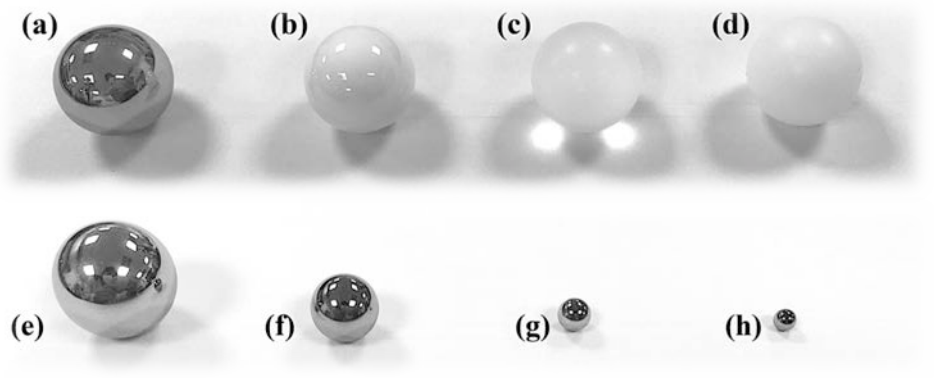

Figure 2.2. *Spherical indenters made of (a) stainless steel, (b) ceramic, (c) glass and (d) nylon. For each material the following size are available: (e) 15.87 mm, (f) 9.52 mm, (g) 4.77 mm and (h) 3.17 mm.*

The preparation of the compacted specimen is done with the FT4 powder rheometer. The powder is firstly conditioned in order to delete any previous history and make the sample reproducible. Then, with the vented piston supplied, a normal stress is applied. For compacting the powder, the vented piston moves downwards with a velocity of 0.05

mm/s. When the final wanted normal stress is reached, it is maintained for 1 minute in order to avoid any relaxation. The glass vessel that is used has a capability of 85 mL and an internal diameter of 50 mm. In this way it is possible to guarantee a bed height higher than the minimum required of 20 particles diameters, and to avoid the interference of the surrounding walls and the base of the die on the hardness measurements. The latter gets particularly important because the hardness measurements can be affected by the presence of the wall if the indenter size is comparable to the size of the die. In addition, to avoid any relaxation phenomena, the indentation is carried out on samples immediately after compaction.

Table 2.3. *Indenters physical properties.*

		Reported D [inch]	Measured D [mm]	Mass [g]	Volume [mm^3]
Nylon	N1	0.625	15.80	2.34	2065.24
	N2	0.375	9.48	0.51	446.09
	N3	0.188	4.68	0.06	53.67
	N4	0.125	3.07	0.02	15.20
Glass	G1	0.625	15.87	5.44	2092.81
	G2	0.375	9.52	1.15	451.29
	G3	0.188	4.77	0.14	56.83
	G4	0.125	3.17	0.04	16.68
Ceramic	C1	0.625	15.87	8.02	2092.81
	C2	0.375	9.52	1.76	451.76
	C3	0.188	4.76	0.20	56.47
	C4	0.125	3.17	0.06	16.68
S. Steel	SS1	0.625	15.80	16.04	2065.24
	SS2	0.375	9.45	3.45	441.87
	SS3	0.188	4.77	0.42	56.65
	SS4	0.125	3.18	0.12	16.84

After performing the indentation, it is necessary to evaluate both the impact velocity of the indenter, v_i, and the displaced volume, U, in order to calculate the hardness according to the relation proposed by Tirupataiah and Sundararajan (see Equation 1.25). So the unrelaxed volume, U, is calculated using the standard geometrical relation (2.1) for estimating the volume of a spherical cup:

$$U = \frac{\pi h}{6}\left[3\left(\frac{D_a}{2}\right)^2 + h^2\right]. \tag{2.1}$$

In turn h, which is the height of the penetration (see Figure 2.3), is calculated by Equation (2.2).

$$h = R_i - \sqrt{R_i^2 - \left(\frac{D_a}{2}\right)^2}\,. \tag{2.2}$$

Instead D_a, that is the diameter of the penetration, is determined by analysing the frames taken with the Phantom's high-speed camera, product by Vision Research (Figure 2.4).

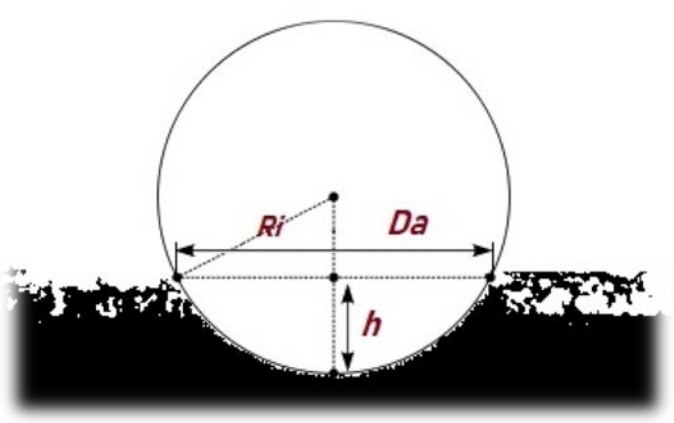

Figure 2.3. *Penetration profile of the spherical indenter into the powder bed.*

To improve pictures quality, the images acquisition is done with two powerful led lights directly pointing the sample, and behind the experimental setup a white background is installed. Without these precautions, pictures would be darker and images analysis would be difficult.

Figure 2.4. *Phantom's high-speed camera (http://www.phantomhighspeed.com).*

The captured frames are useful not only for measuring the diameter of the unrelaxed volume, and so the depth of the penetration, but also for determining the incident velocity of the ball on the powder bed. In order to have a very precise estimation of the impact velocity, a frame rate of 5000 fps has always been set. This means that the camera takes 5000 pictures per second, and that the time between two consecutive frames is 0.2 ms, small enough to guarantee accurate results.

2.1.2.Image analysis

In order to calculate precisely the instantaneous impact velocity of the spherical indenter on the powder and to estimate the volume of the crater imprinted on the bed by the indenter, the pictures taken with the high speed camera are analysed using ImageJ.

The procedure that is carried out for analysing the images is represented in Figure 2.5. After acquiring the image, the threshold has to be adjusted in order to obtain a high level of contrast between black and white. This allows distinguishing accurately the edge of the sphere. The diameter of the spherical indenter, which has a known length, is used as reference distance to set the scale and determine the length represented by each pixel.

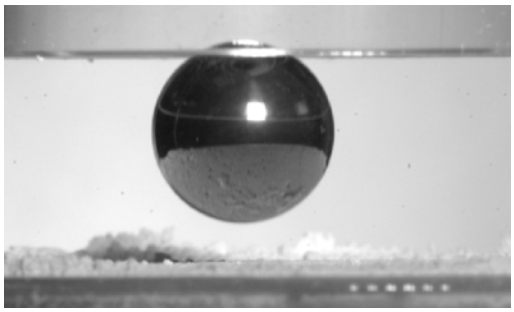

(a) Image acquisition

(b) Threshold adjusting

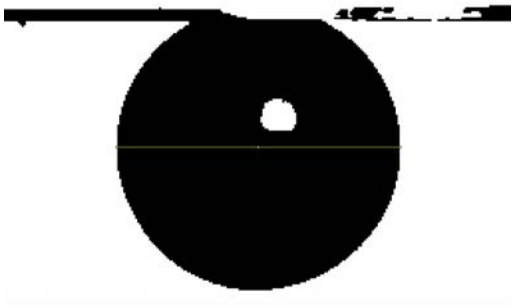

(c) Diameter drawing

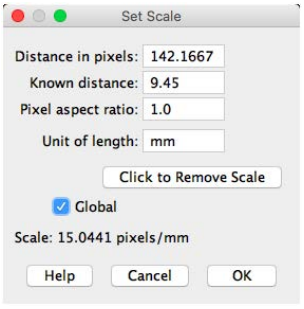

(d) Scale setting

Figure 2.5. *ImageJ procedure for the scale setting.*

At this point, the difference in height of more consecutive frames can be measured. Because the camera worked at a frame rate of 5000 fps, it passes 0.2 ms from one image to its following. The ratio between the distances travelled by the ball in two consecutive frames, divided by this interval of time, gives the velocity of the ball at that instant. To calculate the instantaneous impact velocity of the ball, it is enough analysing the difference in position of the indenter in a dozen consecutive frames before the ball touched the powder bed. In fact, because the indenter is accelerating under gravity, it would not make sense to determine the instantaneous velocity far away from the top surface of the powder sample. Note that usually the obtained values are coherent but sometimes some differences appear, hence it is needed to calculate the average.

With ImageJ it is also possible to estimate the so-called un-relaxed volume, by simply measuring the crater diameter or the height of the penetration. Here it is measured the diameter of the crater, D_a, instead of the penetration depth, h, because, since D_a is greater than h, the percentage error is lower and the accuracy is improved. Figure 2.6 shows an example of measurement of the crater diameter. Despite the powder is still splashing, the analysis is done once the ball is settled. Then, to be sure to measure correctly the value of D_a, although the powder heap formed around the indentation zone, the bed surface height beyond the edge of the heap is found by adjusting the image threshold.

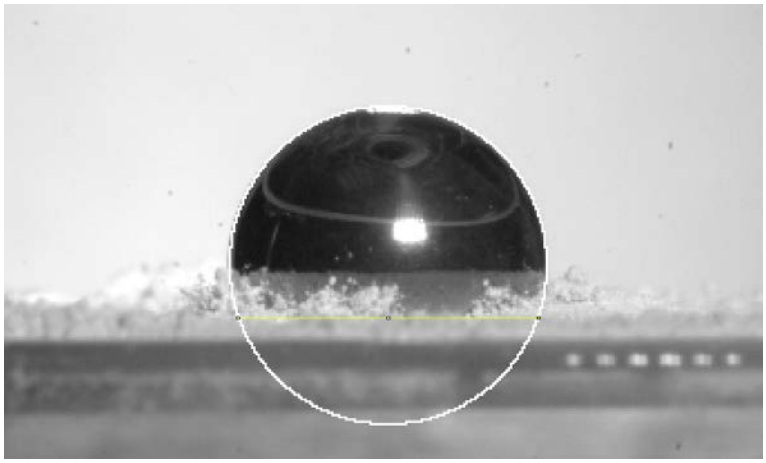

Figure 2.6. *Crater diameter measurement.*

However, from D_a, using Equation (2.2), the indentation depth h can easily be determined. Finally, from equations (2.1) and (1.25), respectively the un-relaxed volume, U, and the hardness, H_d, can be estimated.

2.1.3.Test planning

In order to have reliable results with the ball indentation method, it is necessary to identify for each material the range of dimensionless penetration depth, h/R_i, within which a relative constant value of hardness is obtained. Therefore a test plan is needed before performing indentation in order to assess which spherical indenters can be used on a determined compacted powder and which impact velocities are suitable.

The quasi-static indentation of the FT4 powder rheometer (§2.2.2.2) allows quantifying, at least for some values of dimensionless penetration depth, the hardness of a previously compacted powder bed that has been used for predicting the usable spherical indenters. Because generally hardness is constant around 0.5 dimensionless penetration depth, this is the value of hardness used to plan the tests.

Note that not all the feasible tests have been performed, but they have been selected in order to cover a wider range of dimensionless shear rate. Furthermore for each test, three measurements have been performed in order to calculating the standard deviation.

2.2. FT4 powder rheometer

The FT4 powder rheometer from Freeman technology is capable to measure a wide range of shear, bulk and dynamic flow properties, considering different initial state of powder conditions. Here the rotational shear cell, the compressibility test and hardness measurements in quasi-static condition are performed for characterising the powder; besides also the variable flow rate method is carried out for determining the powder properties during flow. Then the flowability evaluation achieved with the rheometer is compared to the variation of hardness with the strain rate achieved with the Ball Indentation technique. Note that before each test, the powder history is deleted with the FT4 conditioning method.

2.2.1.Conditioning

The way the powder is initially filled in the cup, vibrations of the sample, relaxation time, as well as excess of air, may have a huge effect on powder properties and could influence the measurements. To avoid this, and to ensure reproducibility samples and consistent results, the powder within the vessel is conditioned before each test cycle.

The FT4 conditioning is a simple and mechanical procedure that allows to delete the previous history of any specimen by removing any residual stress, and to standardize the initial packing state of the powder. It consists on subjecting the powder to the action of a dynamic blade. The helix, that has a 5 degrees angle and that moves clockwise, traverses downward and then upward the powder bed (see Figure 2.7). In this way each particle is disturbed and gently dropped for creating a homogeneously packed state. After conditioning, the results of each test can be considered independent of the initial stress level.

Figure 2.7. *Powder Conditioning with blade (www.freemantech.co.uk).*

Note that the blade direction during conditioning provides a slicing action to break up cohesive clusters, whilst during the flow energy test the blade direction is reversed so that it drives into the powder.

2.2.2.Bulk properties

The powder bulk properties, like packing state and bed voidage, does not measure directly the material flowability or shear. Nevertheless their evaluation is important because they can greatly affect the powder flow properties. Hence here powder compressibility and hardness are evaluated.

2.2.2.1.Density and compressibility

To obtain the compressibility profiles and the bulk density of the investigated materials, the standard compressibility test of the FT4 is applied at different state of initial compaction. The sample, filled in cylindrical split vessel, is firstly conditioned by the standard conditioning cycle (§2.2.1) in order to remove any residual stress. After that

the powder is split to ensure a well-known volume of material with a reproducible packing state and the instrument registers the mass of powder. The conditioned bulk density is computed as the ratio between the mass after splitting and the known volume of powder:

$$\rho_B = \frac{mass\ after\ splitting}{volume} \ . \tag{2.3}$$

At this point a vented piston, whose mesh allows the air to escape from the powder surface, consolidates the sample slowly, moving downwards at a fixed tip speed of 0.05 mm/s. Initially the normal force applied increases slowly from 0 to the 20 % of the final compression load. This cycle, which is called pre-compression cycle, is useful because it allows detecting the powder surface. After that powder is loaded until the final value of the desire compression. After each compression step, the normal stress is held constant for a fixed period of 60 seconds in order to guarantee powder stabilization and avoid any possible relaxation. The piston is then unloaded at the same speed as that of the loading, but in the opposite direction. The distance travelled by the vented piston during loading allows determining the final volume of the compacted powder. The change in volume as a function of the initial powder compaction is represented by the compressibility profile, which leads to a better knowledge of the powder flow behaviour. For instance, a little change in volume means an efficient packing state, characteristic of non-cohesive granular material. A bigger sensitivity to compression is instead due to the higher amount of air entrained, smaller particle dimensions, and likely to be cohesive materials. Furthermore, more cohesive the powder, bigger will be the travelled distance by the piston.

2.2.2.2.Hardness in quasi-static condition

As mentioned in the previous chapter, there is an operational window within which the ball indentation technique can be applied in order to have reliable hardness results. For instance hardness should be evaluated in the range of penetration depth where remains relatively constant. It has been therefore needed to plan the feasible test before starting, both for saving time and avoiding material wastage.

With the FT4 powder rheometer, using the supplied multi-punch indenter (Figure 2.8), it is evaluate the powder hardness at different value of pre-compression. The estimation of the hardness done in this way, although for quasi-static conditions, allows planning the spherical indentation tests.

Figure 2.8. *FT4 punch indenter.*

After conditioning and splitting, the powder is subjected to the action of the vented piston for compaction. Then the indenter, who has a spherical profile and a diameter of 4 mm, penetrates onto the flat and uniform top surface of the powder at a carriage speed of 0.05 mm/s. For any test cycle, 5 indentations are performed with the indenter rotate by 72 degree after each measurement (see Figure 2.9).

Figure 2.9. *Sample after indentation with the FT4 powder rheometer*.

The test is applied at the following different penetration values: 0.2, 0.4, 0.6, 0.8, 1.0, 1.4 and 1.8 mm, which means respectively 0.1, 0.2 0.3, 0.4, 0.5, 0.7 and 0.9 dimensionless penetration depth (because the indenter radius is 2 mm), for a given pre-compression load. Thus it is possible to investigate the hardness fluctuation along the entire range of penetration, and determine for each material the interval within which hardness remains relatively constant and represents the plastic yield stress. The same test is performed also at the fixed dimensionless penetration depth of 0.5 mm and on different pre-compacted powder in order to correlate the compressibility index with the initial state of powder compaction. For each test, three repetitions are performed in order to calculate the standard deviation.

It should be noted that the hardness, *H*, in quasi-static condition is calculated as the ratio between the maximum loading forces applied by the punch F_{max}, and the projected area of the penetration *A*, as proposed by Hassanpour and Ghadiri (1.22). Furthermore, because the elastic recovery was found to be negligible for all powders with respect to the plastic deformation, the final depth is not calculated considering the intersection of tangent to the unloading curve, which can be approximated as a vertical line, but the final height reached by the punch during loading. A demonstration of this is reported in Chapter 4.

2.2.3.Flow rate sensitivity

The FT4 powder rheometer is also used to evaluate the flow properties of the powders in terms of energy required to make them flow. Thus it is possible to quantitatively characterize powder rheology and cohesion, as well as determine the flow rate sensitivity.

2.2.3.1.Variable flow rate at different tip speed

To characterize the flow rate sensitivity of the powder, a modified version of the Variable Flow Rate method of the FT4 powder rheometer is carried out. The powder bed is firstly filled into a 160 mL vessel and subjected to a conditioning cycle. It is therefore possible to delete any previous stress history and establish a reproducible and uniform state. After conditioning, the test cycle takes place: the blade rotates at a given tip speed downwards and in counter clockwise from the top to the bottom of a precise volume of powder establishing a well define flow pattern. The sequence of conditioning and test cycle is repeated more times for decreasing values of tip speed: 300, 250, 200, 150, 100, 70, 40 and 10 mm/s. This allows evaluating the flow rate sensitivity of the powders in a wider range of tip speed with respect to the standard method.

For determining the role of consolidation in flow properties measurements, the test has been implemented not only on non-consolidated materials, but also on a previously compacted powder bed. Thus, after each conditioning test, the powder is compacted by the vented piston to a desire normal stress and, after that, the test cycle is carried out.

From the results the Basic Flow Energy, which is defined as the energy needed to displace the conditioned powder bed only during the downwards traverse of the blade, is evaluated. However, because the Basic Flow Energy does not take in account for

differences in mass, in order to make comparable the results, it is always calculated considering the same penetration depth of 20 mm

The energy is determined as the area beneath the energy gradient vs. height graph thanks to a Matlab program specially developed. The code, which is reported in Appendix 1, give as output a Matrix that contains, for the three repetitions done for each measurement, the total energy at different tip speeds. Reporting the total flow energy calculated in this way as a function of tip speed (see Figure 2.10) allows to identify the powder rheology and to assess the flow rate sensitivity.

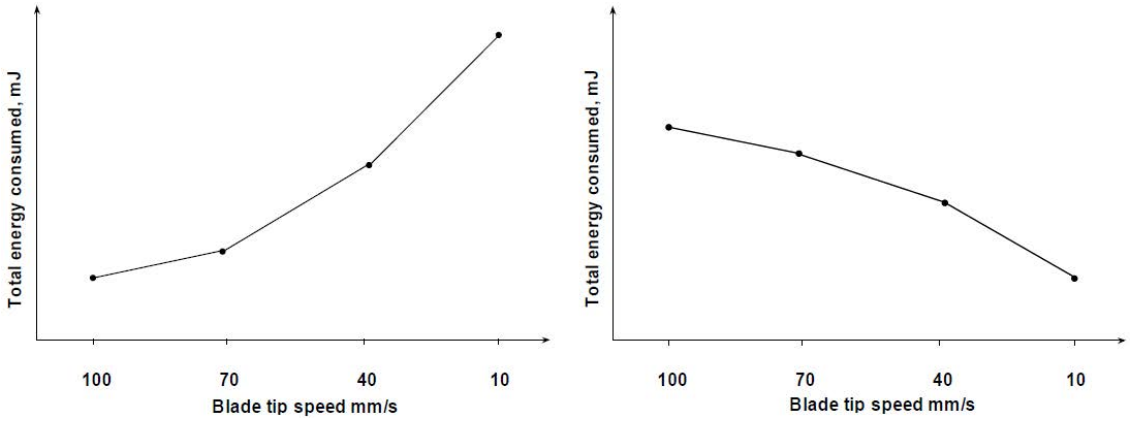

Figure 2.10. *Total flow energy versus tip speed. Example of cohesive powder with high flow rate sensitivity on the left, and Newtonian flowrate on the right (Image modify from Freeman Technology, W7012, 2007).*

Note that for cohesive powders, which have high flow rate sensitivity, the Basic Flow Energy increases for decreasing value of tip speed; whilst for liquid-like powders the energy decreases with the tip speed. In some cases powders could also be insensitive to flow rate, thus the energy is independent of the rotational velocity of the blade.

2.2.4.Rotational shear cell

The shear cell tests are carried out using the 48 mm rotational shear cell accessory of the FT4 powder rheometer. As shown in Figure 2.11, the rotational shear cell module consists of a shear head that induce both vertical and rotational stresses on the powder bed.

Such as all the other shear cells commercially available, the FT4 shear tester is a fairly static technique that measures the powder behaviour during its transition from no-flow to flow. Despite some discrepancies with respect to the result obtaining with other shear

tester, this technique has been acknowledged and published by the ASTM International Committee D18 on Soil and Rock.

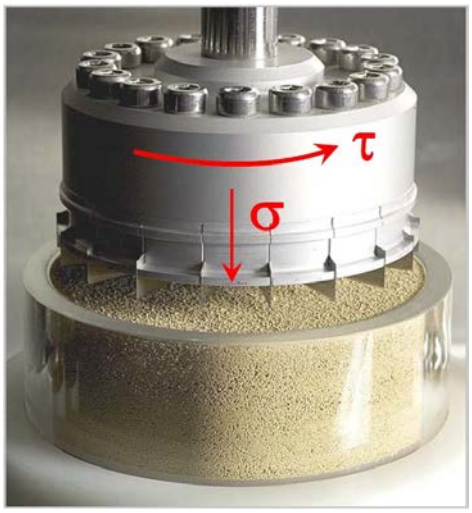

Figure 2.11. *Rotation Shear cell of the FT4 powder rheometer (Freeman Technology, W7018, 2010).*

The procedure is simple. The sample, after being filled into the vessel, is conditioned by the blade in order to remove any stress history and achieve a reproducible and homogeneous state. Successively, the powder is split and the blade is replaced with the vented piston, which slowly pre-compacts the powder under a certainly normal load. After the pre-consolidation step, the shear cell accessory is installed. It moves downwards until the required normal stress is established and then, stars rotating slowly until a critically consolidation state is reached. This stage, which is called pre-shear, leads to a steady state situation where the density remains constant and the shear rate approaches to zero. Subsequently, the normal load is lowered and the shear stress increases until the bed fails or shears. The shear stress that causes failure and creates flow is measured. In order to build the Yield locus characteristic of the material, the pre-shear/shear sequence has to be repeated more times. Here it has been measured a series of five yield points for a range of reducing normal stresses (see Figure 2.12).

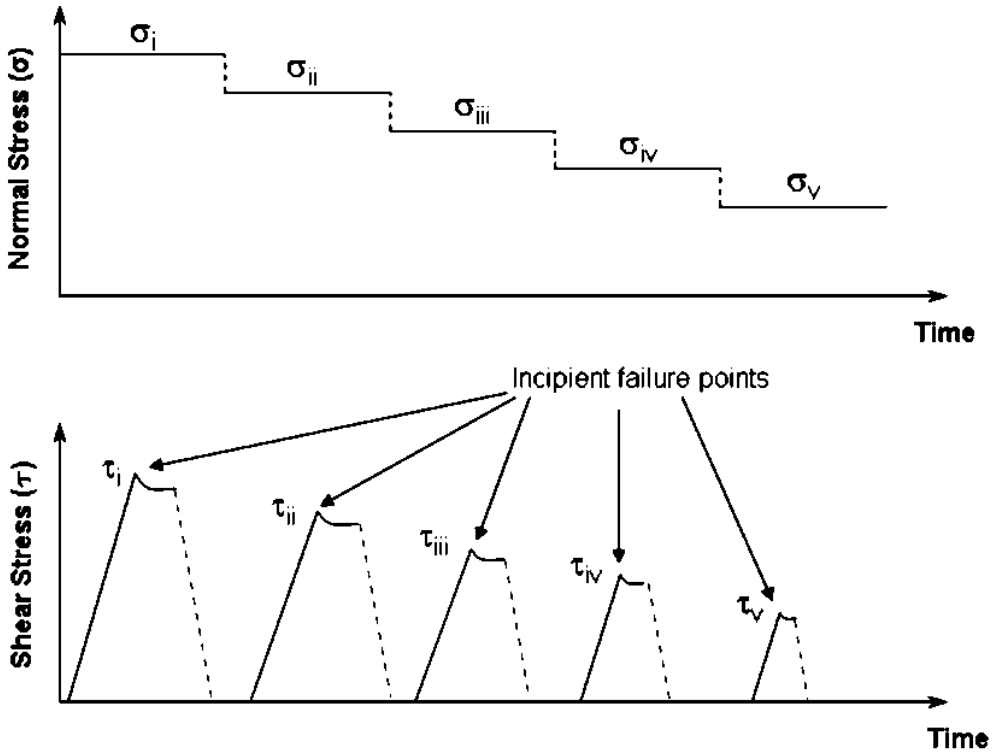

Figure 2.12. *Normal stress and shear stress as a function of time in a series of five yield points (Image modified from Freeman Technology, W7018, 2010).*

Note that it is recommended to apply normal load in between the 20 % and the 80 % of the pre-shear. What normal stresses are applied at each pre-shear stress are reported in Table 2.4.

Table 2.4. *Normal stresses applied at each pre-shear stress.*

Preshear	**Normal stresses [kPa]**				
[kPa]	σ_1	σ_2	σ_3	σ_4	σ_5
1	0.70	0.60	0.50	0.40	0.30
2	1.50	1.25	1.00	0.75	0.50
3	2.00	1.75	1.50	1.25	1.00
6	4.00	3.50	3.00	2.50	2.00
9	7.00	6.00	5.00	4.00	3.00
12	8.40	7.20	6.00	4.80	3.60
15	9.00	8.00	7.00	6.00	5.00

The construction of the Yield Locus is done in the FT4 powder rheometer using the Coulomb equation, which means that the shear stress-normal stress failure points are

interpolating linearly using Equation (1.13). However, for some materials appear that the linear extrapolation is not good enough.

Chapter 3
Powder characterization

Since the particulate state of the matter exhibits a range of size and shape, an important component of any study dealing with particles is to understand bulk properties, as well as shape, size distribution and flow behaviour of each investigated material.

Here four different powders are used as tested materials. They are two different grades of Titanium Dioxide (R-104 and DT-51), lactose monohydrate (GranuLac 140) and Waxy Corn Starch. The choice to use these fine powders is due to their high surface area-to-volume ratio and other bulk characteristics that make them suitable for achieving our purposes and very attractive for a lot of industries, such as foods, cosmetics, pharmaceuticals, plastics, paints, detergents, catalysts, coating, etc. However, they have different flowabilities: some of them exhibit a cohesive behaviour due to the presence of strong inter-particle forces, which exceed gravity, whilst the others can flow easily under certain conditions. Because their different behaviours, it is possible to investigate the BIM for a range of powder flow characteristics.

Two different instruments have been used to determine the particles size distribution, depending on the size range of the particles. The particle size characterisation of the two grades of Titanium Dioxide, which are the finer powders tested, has been performed using the Zetasizer Nano that allows analysing particles which dimensions between 0.3 nm and 10 μm. The dynamic image analysis, performed with QicPic, is instead used for characterising Lactose Monohydrate and Waxy Corn Starch.

In order to identify particles shape and surface roughness, the microscopic morphology of all powders is obtained through Scanning Electron Microscope (SEM). Furthermore, looking at the SEM micrographs, it is possible to evaluate the representativeness of the particle size distributions, the particles elongation, and the tendency to agglomerate. As expected, size and shape are strongly correlated with particle flow behaviour.

Finally, the flowability of the bulk solids is evaluated qualitatively, with the compressibility profile, and quantitatively, performing the shear tester of the FT4 powder rheometer at different values of pre-shear. This leads to the construction of their flow functions, which are reported at the end of this chapter. Note that the flowability evaluation by the ball indentation method, both in quasi-static conditions and at high strain rates, as well as the FT4 impeller test, are instead discussed in the fourth chapter.

3.1. Titanium dioxide

Nowadays Titanium Dioxide is the most popular particulate filler, representing the 70% of the total pigments production. It is used in a lot of application with which people are commonly familiar with, for instance in the production of capacitors, ceramics, coating, cosmetics, fibers, food, inks, pharmaceuticals, paper and, above all, in the polymer industries because of the whiteness, brightness and opacity that provides. The high demand is due to its physical properties, in detail it is made particularly efficient by its refractive index and reflective capability. It can be obtained from different minerals: rutile, anatase, brookite and ilmenite. Furthermore, depending on the colouring and opacity purposes, different commercial grades of TiO_2 can be used, and two production processes are available: the sulphate and chloride processes. The latter is the more common because of the higher purity, and the lower amount of waste and toxic materials produced (G. Wypych, 2016).

In this work it has been used two different polymorphs of Titanium dioxide: the rutile pigment Ti-Pure™ R-104 obtained from the chloride process, which is characterized by the higher refractive index than all the other commercial pigments and has a very small particles diameter; and the anatase TiO_2, which is nowadays more actively investigated for photo-catalysis and photo-electrochemical applications. To enable a better understanding of their behaviour, their particle characterisation is reported below.

3.1.1.Rutile pigment R104

The finest and most cohesive powder used here is the rutile Titanium Dioxide pigment, TiO_2 R-104, manufactured by Chemours.

3.1.1.1.Particle size distribution

Because the particle size of TiO_2 R-104 is about hundreds of nanometres, the suitable technique for performing the size analysis is the Laser diffraction. Here it is used the Zetasizer Nano, a Malvern instrument allows measuring particles in the range from 0.3 nm to 10 μm. The technique consists of subjecting a solution of a representative sample of powder to an incident laser. The pattern of scattered light intensity versus scattering angle leads to the construction of the particle size distribution.

For optimal results, the concentration of the solution has to be within the recommended range that is, for particle size in between 100 nm and 1 μm, and assuming a density of 1

g/cm^3, within 10^{-3} % and 10 % in mass (Malvern Instruments Ltd, 2013). Here a number of concentrations are prepared using Butanone as solvent (the refractive indices of solvent and solute are reported in Table 3.1). Moreover, in order to breakup agglomerates and having good quality results, the sample is sonicated for 10 minutes in an ultrasonic bath.

Table 3.1. *Refractive Indices of Butanone and TiO_2.*

	Refractive Index
Butanone	1.3788
Anatase TiO_2	2.493 - 2.554
Rutile TiO_2	2.616 - 2.903

The undersize cumulative distribution and the frequency distribution that are attained using a 0.16 mg/mL solution are reported in Figure 3.1. Instead Table 3.2 reports some representative diameters, all based on volume.

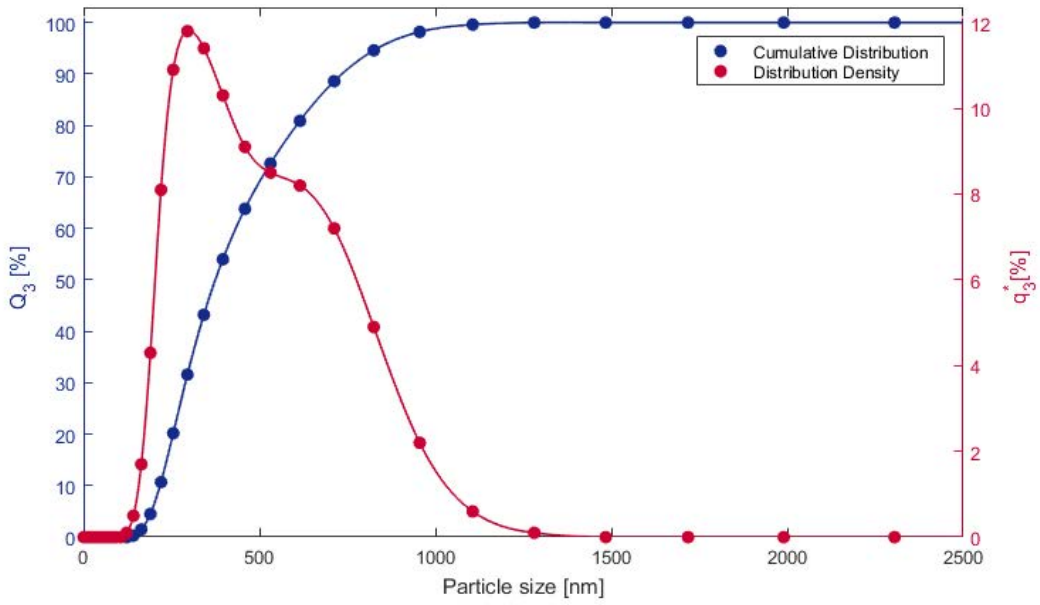

Figure 3.1. *Undersize cumulative distribution and distribution density of TiO_2 R-104 (volumetric base).*

Table 3.2. *Representative diameters of TiO_2 R-104.*

$d_{10,3}$	216.80 nm
$d_{50,3}$	376.06 nm
$d_{90,3}$	738.67 nm
$d_{99,3}$	1041.46 nm

The particle size distribution of Titanium Dioxide R-104 is narrow, irregular and slightly bi-modal. The first peak, at about 300 nm, is due to a huge number of smaller particles, whilst the presence of a smaller number of bigger particles determines the plateau around 600 μm and the right tail. From the particle distribution it can also be seen that he 50 % of particles have an equivalent diameter smaller than 0.38 μm, instead the 99% smaller than 1.04 μm.

3.1.1.2.Morphology

In this paragraph it is reported the microscopic morphology investigation of Titanium Dioxide R-104, done with SEM. After having dispersed the powder onto a metal surface, making sure to use a representative sample particles, and coated with a thin layer of gold from a vacuum evaporator, the backscattering measurement of an electrons beam has been performed. In Figure 3.2 some of the obtained images are reported.

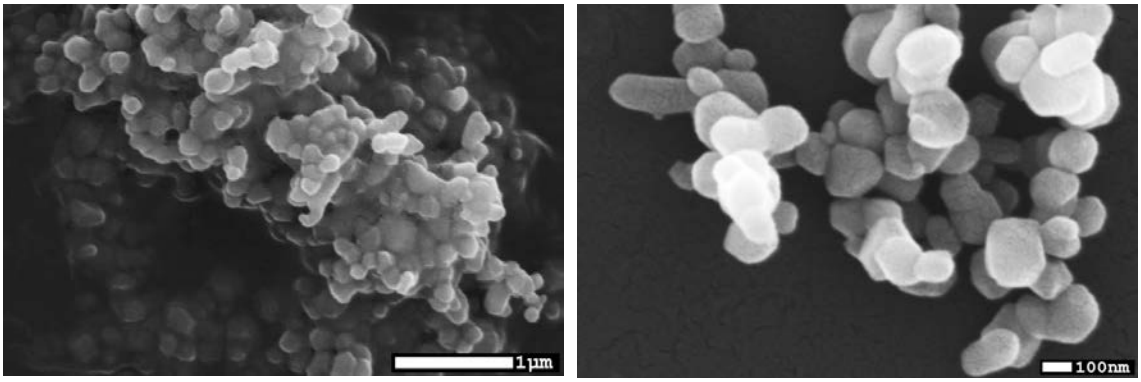

Figure 3.2. *SEM micrographs of TiO_2 R-104.*

From the SEM micrographs it appears clearly the tendency of titanium dioxide to agglomerate. It was not possible to see single dispersed particles, but only groups of particles stuck together due to the strong inter-particle forces. The particles have irregular shape, but approximately the same dimension. Furthermore, particles deviate from being spherical and are a bit elongated, meaning that their aspect ratio is larger than 1. In some cases particles have an almost hexagonal profile, with rounded edges, and smooth surfaces. The irregular shape, together with the small particle dimensions, leads to high cohesiveness.

3.1.1.3.Flow characteristics

Ti-Pure R-104 exhibits a very cohesive behaviour. This becomes immediately evident when the powder is handled. For instance, by simply tumbling the vessel, it is possible to recognize the typical flow behaviour of cohesive powders, its tendency to agglomerate and the formation of a dusty environment. This is due to the small size and the irregular shape that determine a very high surface over volume ratio, and hence strong attraction forces exceeding gravity. The cohesiveness of the material is characterised both through qualitative parameter of the FT4 compressibility test (results are reported in §3.4), and quantitatively thanks to shear cell measurements.

For TiO_2 R-104, the Yield loci are established for the following six pre-consolidation normal loads: 1, 2, 3, 6, 9 and 15 kPa, whose applied normal stresses are reported in Table 2.4. Despite for each pre-shear three repetitions are carried out, in Figure 3.3 the yield locus and the Mohr's circles of one repetition for each one are reported.

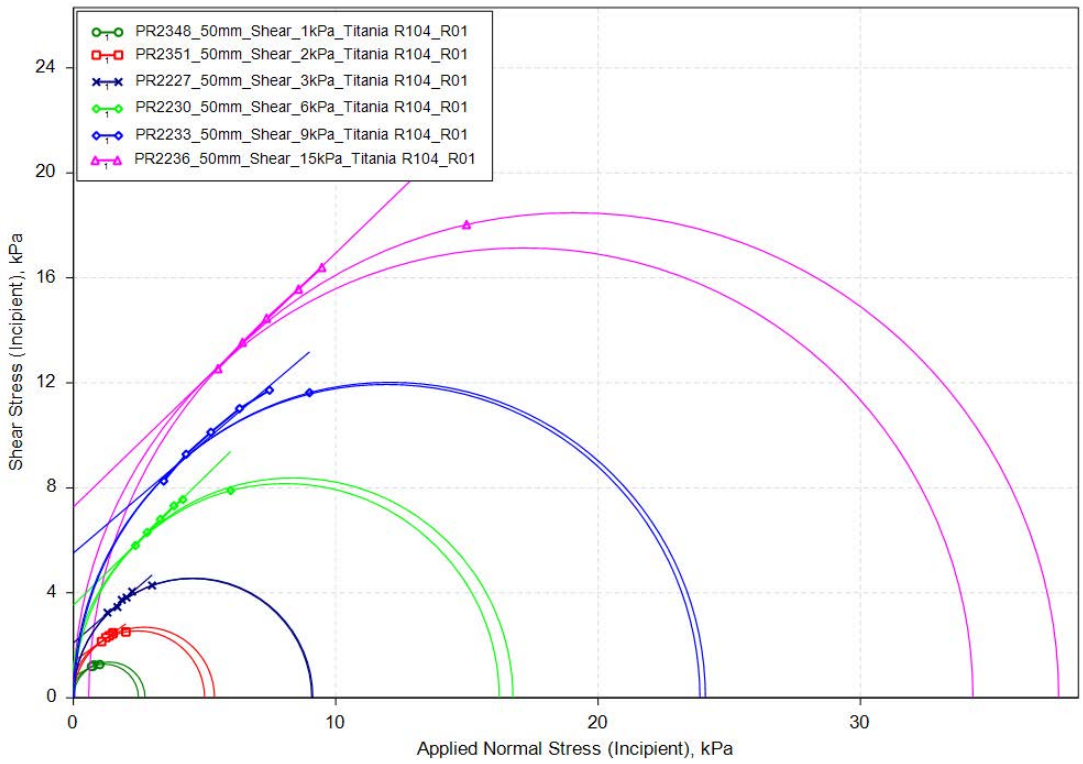

Figure 3.3. *Mohr's Circles and Yield Loci of TiO_2 R-104 at 1, 2, 3, 6, 9 and 15 kPa normal pre-shear.*

From Figure 3.3, it appears that the Yield Loci are very well approximated by a straight line (Coulomb's law) and the yield locus data points are close to the failure Mohr circle thus, the estimated Unconfined Yield Strengths are representative. Furthermore, because the flow factor of the material is 0.9 at 1 kPa pre-consolidation load, and 1.1 at

15 kPa pre-shear, the powder can be classified as '*not flowing*' or '*very cohesive*'. However the material flow function is reported and discussed in paragraph § 3.4.

To conclude, for all the discussed reasons, TiO_2 does not flow freely, but tends to bridge and rathole in industrial operations and equipment. Sometimes, to overcome this issue, a layer of organic or inorganic coating is applied on the particles surface. However, because its high cohesiveness, TiO_2R-104 is suitable for performing ball indentation.

3.1.2.Anatase polymorphism DT51

The second grade of Titanium Dioxide investigated here is CristalACTiV™ DT-51, a high surface area ultrafine TiO_2 powder sold by Cristal Global (www.crista.com).

3.1.2.1.Particle size distribution

The Zetasizer Nano from Malvern is used in order to analyze the particle size distribution of TiO_2 DT-51. As before, the analysis is done using Butanone as solvent and sonicated the solution for 10 minutes in an ultrasonic bath. In this way the agglomerates are broken and sedimentation is avoided. Figure 3.4. shows a good quality measurement obtained using a 0.29 mg/mL solution.

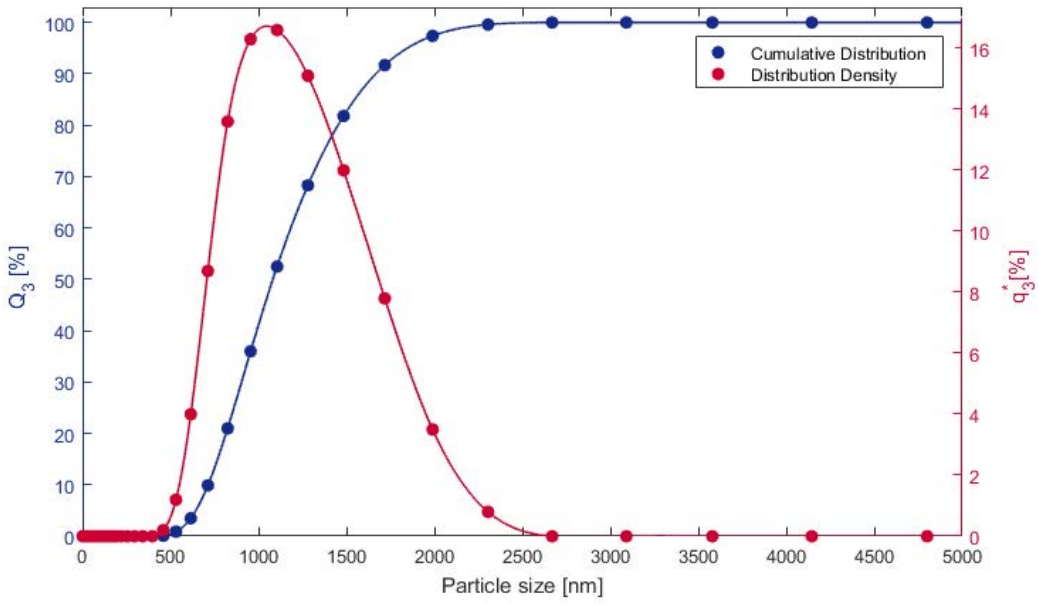

Figure 3.4. *Cumulative distribution and distribution density of TiO_2 DT-51.*

This grade of Titanium Dioxide is characterized by larger particles and more regular particle size distribution: it is perfectly mono-modal, mean and average diameters are

close to each other and, because the almost bell-shaped distribution, a normal distribution could be use to describe the particle size. Note that TiO_2 DT-51 median diameter, $d_{50,3}$, which is reported in Table 3.3 together with others representative diameters, is used as reference size in the calculation of the shear rates.

Table 3.3. *Representative diameters of TiO_2 DT-51.*

$d_{10,3}$	713.41 nm
$d_{50,3}$	1083.18 nm
$d_{90,3}$	1677.82 nm
$d_{99,3}$	2075.91 nm

To conclude, Titanium Dioxide DT-51 has particle dimensions larger than Titanium Dioxide R-104.

3.1.2.2.Morphology

The cohesiveness of Titanium Dioxide is due to its size, but also to its shape. Indeed it is characterized by irregular shaped particles that tend to agglomerate. In Figure 3.5 are reported a few SEM micrographs obtained after coating with a layer of gold some micrograms of powder.

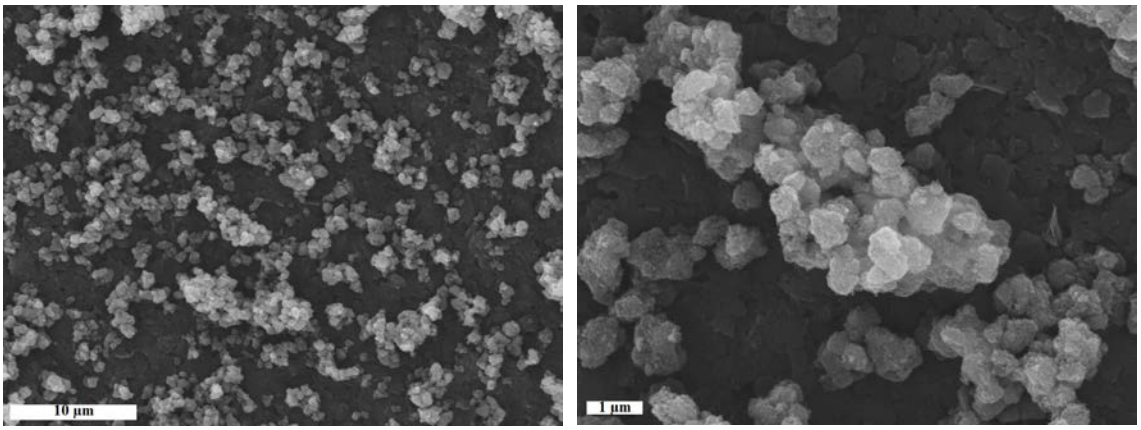

Figure 3.5. *SEM micrographs of Titanium Dioxide DT-51.*

Despite SEM analysis confirms the particle tendency to agglomerate, individual particles can be identified. They are irregular, a bit elongated and their surface is rough. Some particles are sharp-edged and roughly polyhedral shaped.

3.1.2.3.Flow characteristics

The cohesiveness of Titanium Dioxide DT-51, which can be simply recognized by tumbling the vessel, is also confirmed by shear cell measurements. In Figure 3.6 a family of Yield Loci, which is obtained applying the shear cell test of the FT4 at 1, 2, 3, 6, 9 and 12 kPa pre-shear, is reported.

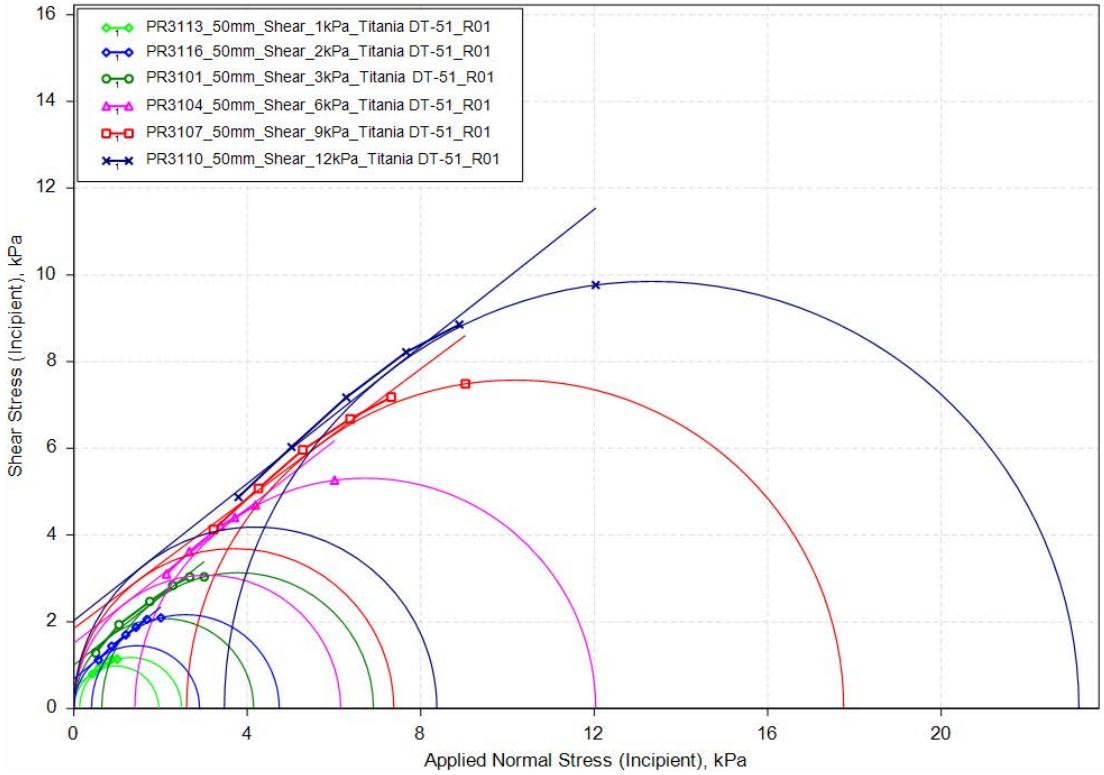

Figure 3.6. *Mohr's Circles and Yield Loci of TiO_2 DT-51 at 1, 2, 3, 6, 9 and 12 kPa normal pre-shear.*

Unlike Titanium Dioxide R-104, in this case the linear Coulomb approximation of the static Yield Loci are not accurate, and hence the results are affected. Indeed, particularly at low stresses, the Yield Locus tends to curve downwards and this leads to an overestimation of the tensile strengths. Although the cohesiveness of the powder, looking at the Mohr's circles, it appears that TiO_2 DT-51 is less cohesive than TiO_2 R-104. However a detailed comparison between the investigated materials is reported in paragraph § 3.4.

3.2. α–lactose monohydrate

One of the most commonly used excipient in the pharmaceutical industries is Lactose powder. This is due not only to its chemical and physical properties, but also to its bulk behaviour. Furthermore it is globally available, it has high storage stability and good blending properties. Different types of lactose powders, which differ mainly for the production method, exist. Then, depending on the type, it can be involved in a lot of processes like tableting, granulation and cups filling (Meggle, 2014).

In this study GranuLac 140 produced by Meggle has been analysed, a α–lactose monohydrate powder that comes from the milling process of recrystallized particles. This process leads to fine particles with disrupted shapes that behave cohesively, an advantage for both dry and wet granulation processes (Meggle, 2014). More details on the bulk properties of GranuLac 140 are reported in the following paragraphs.

3.2.1.Particle size distribution

The particle dimensions of GranuLac are greater than the ones of Titanium Dioxide, and big enough to be able to perform particle size characterization with dynamic image analysis. This technique consists of dispersing particles in a gas or liquid flow that passes through a source of light. The particle projections, which are captured by a digital detector, are analysed to obtain size and shape information. What dynamic image analysis measures is therefore the diameter based on the equivalent projected area. Especially if the particles are elongated, dynamic image analysis is more accurate than static methods because particle orientations are randomly captured. In static condition indeed, elongated particles usually lie on their maximum plane of stability and this leads to an over estimation of the particle size measurement.

The instrument for dynamic image analysis used is QicPic by Sympatec Gmbh. There are different types of configurations available on the market, however the one used here consists of: the QicPic image analysis sensor, which takes high-resolution pictures of the falling particles, backlit by a pulsed light source; a gravity disperser, which guarantee gentle dispersion of the particles accelerated under gravity and avoid collisions; and a dosing unit for separating the particles and reducing the agglomerates. The software evaluates in a very short time all the captured particles and calculates the diameters of the spheres with an equivalent projected area.

For evaluating the size distribution of GranuLac, no any dispersive agent is used. A small amount of a representative sample is simply filled into the funnel. In order to have

reliable results, three repetitions are carried out, each one with at least 300 000 particles, which is the minimum recommended. Because the repetitions have the same outcome, the quality of the measurement is considered satisfactory. Figure 3.7 shows the average of the three measurements, where the red and the blue lines represent the distribution density and the undersized cumulative distribution, respectively, both evaluated on a volumetric base. In this case particles are not completely mono-modal in size, and distribution cannot be considered a bell-shaped distribution. The long right tail and the positive skew indicate that there are a relatively small number of larger particles.

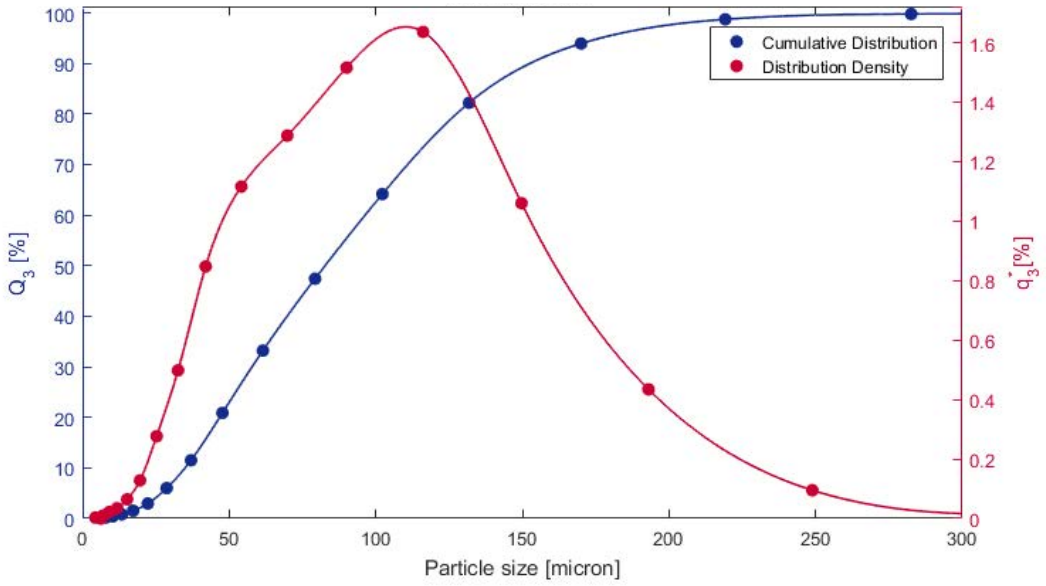

Figure 3.7. *Undersize cumulative distribution and distribution density of GranuLac (Volumetric base).*

In Table 3.4 are reported some representative diameters. The median diameter, $d_{50,3}$, indicates that half population has an equivalent diameter smaller than 82.80 µm. It should also be noted that the volumetric mean diameter is bigger than the median value because of the shape of the distribution.

Table 3.4. *Representative diameters of GranuLac.*

$d_{10,3}$	34.67 µm
$d_{50,3}$	82.80 µm
$d_{90,3}$	157.09 µm
$d_{99,3}$	233.87 µm
SMD	62.60 µm
VMD	90.37 µm

Among the investigated material, GranuLac is the one characterised by the largest particle dimension. It has been chosen because, due to its dimension, it allows investigating higher values of shear rates. Therefore with GranuLac, the intermediate flow regime as defined by Tardos *et al.* (2003), can be completely characterized.

3.2.2.Morphology

The milling process, at which α –lactose monohydrate particles are subjected in order to create GranuLac 140, influences the powder properties and its functional performance. Indeed, after milling, particles become angular-shaped and cannot be considered equidimensional. This is shown clearly in the SEM micrographs reported in Figure 3.8. The grains are rather irregular, the edges are sharp, and they differ for their dimensions. Besides particles do not tend to agglomerate; and smaller particles are dispersed on the surface of bigger grains. The surface is not smooth and the roughness rises with the decrease of the particle dimensions.

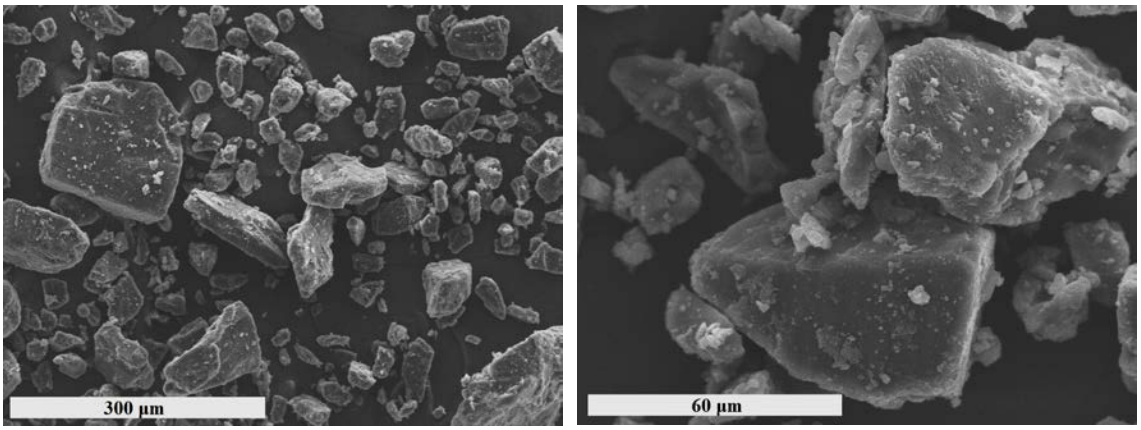

Figure 3.8. *SEM micrographs of GranuLac 140.*

Because the sharp-edges and the roughly polyhedral shape, GranuLac 140 can be classified as a powder with angular grains (Allen, 1990). However, for an accurate particle shape determination, some quantitative descriptors are evaluated. Aspect ratio and sphericity provided by the QicPic analyser are reported in Table 3.5.

Table 3.5. *Quantitative descriptors of shape.*

	Aspect Ratio	**Sphericity**
$x_{10,3}$	0.540	0.611
$x_{50,3}$	0.711	0.806
$x_{90,3}$	0.850	0.891

The aspect ratio, which is defined as the ratio between the smaller and the larger dimension of a bi-dimensional image, indicates that GranuLac is characterized by elongated particles: the 80 % in mass of particles have a width that lies in between the 0.54 and 0.85 times the length. The sphericity is another important shape factor that, according to Wadell, is defined as follow (Eq. 3.1):

$$Sphericity = \left(\frac{surface\ of\ the\ sphere}{surface\ of\ the\ particle}\right)_{same\ volume}. \quad (3.1)$$

Because the 80% of particles have a sphericity in between 0.611 and 0.891, it can be said that the grains deviates from being spherical, are quite irregular and the surface is rough.

3.2.3.Flow characteristics

Figures 3.9 and 3.10 show the Yield Loci and the Mohr's circles obtained performing the shear test at 3, 6, 9 and 12 and 15 kPa pre-shear respectively. Note that, despite not all repetitions are reported, the shear cell test is repeated three times for each pre-shear.

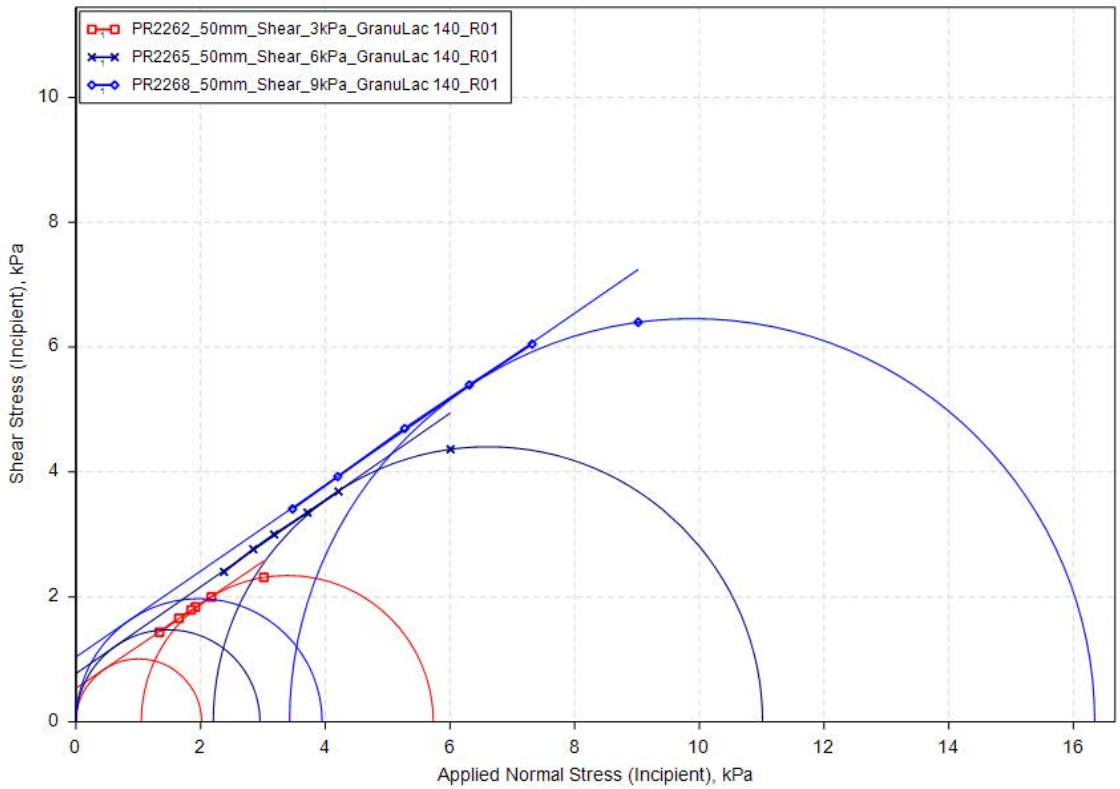

Figure 3.9. *Mohr's Circles and Yield Loci of GranuLac 140 at 3, 6 and 9 kPa normal pre-shear.*

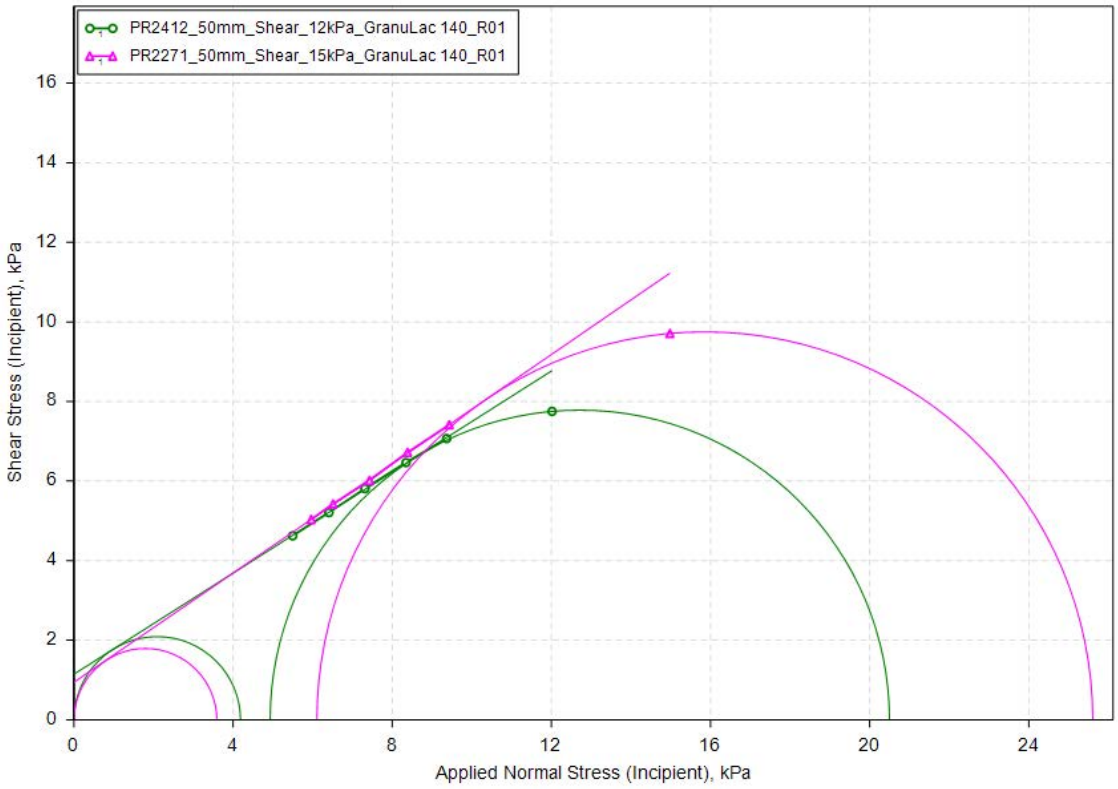

Figure 3.10. *Mohr's Circles and Yield Loci of GranuLac 140 at 12 and 15 kPa normal pre-shear.*

In this case the linear approximation of the Yield Loci seems to be accurate. From the extrapolation of the abscissa it appears that the cohesion, which is the shear stress when the normal stress is zero, does not vary too much with the initial pre-consolidation value. The material flow function, which is reported later on (see Figure 3.17), falls on the boundary between the cohesive and easy-flowing ranges.

In conclusion, with the rotational shear module of the FT4 powder rheometer, it is confirmed that, although GranuLac 140 is the most cohesive among the lactose monohydrate powders due to the milling process at which it is subjected, it can flow easily under certain normal loads.

3.3. Waxy Corn Starch

Starch is the second largest biomass produced on the Earth. It represents the major energy source for human and animal diets and an important raw material for industrial applications such as in corn syrup, paper, textile, food, and bioethanol industries (Y. Ai and Jl. Jane, 2016).

The 99 % of the commercial starch production is represented by corn, wheat, rice, cassava, and potato (FA. Manthey, 2016). About Corn Starch, its chemical composition and properties, are determined by the relative amount of amylose and amylopectin. Here it is used as investigated material Waxy Corn Starch, which is made of 100 % of amylopectin (P. Clifton and J. Keogh, 2016).

3.3.1.Particle size distribution

To perform the particle size distribution of Waxy Corn Starch, it is used the dynamic image analyser QicPic. The analysis is carried out in dry condition, using only gravity as dispersive force. Figure 3.11 shows the undersize cumulative distribution and the distribution density, both on volumetric base, as average of the three repetitions done. The right tail of the distribution density indicates that there are few big particles that influence the distribution, and determine the positive skew. Furthermore, due to the presence of the two peaks, the size cannot be defined as mono-modal. However, the principal peak is rather narrow.

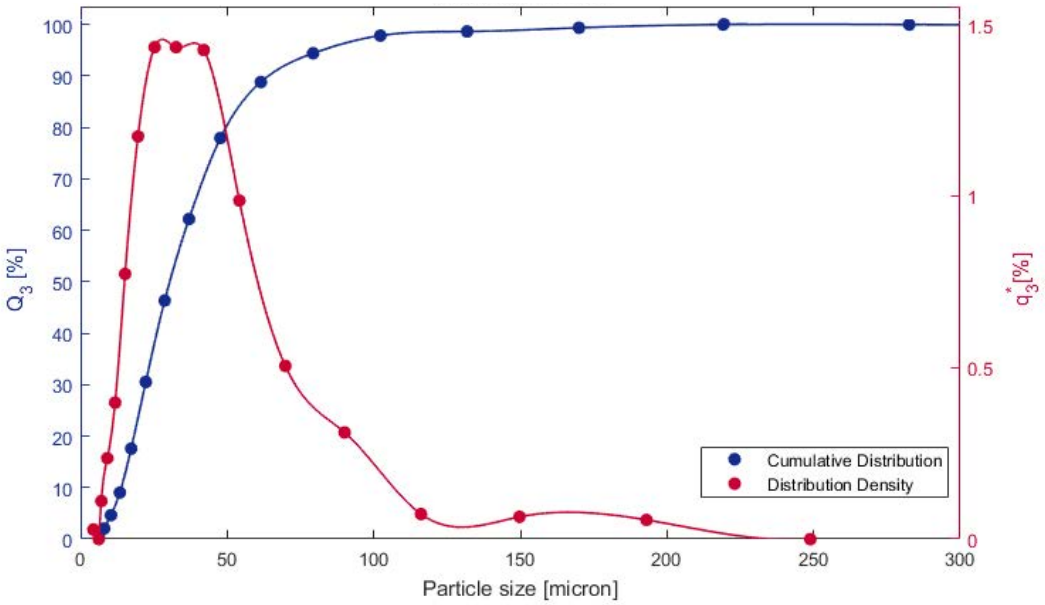

Figure 3.11. *Volumetric cumulative distribution and distribution density of Waxy Corn Starch.*

In Table 3.6 are summarized some of the more representative diameters. It appears that the 50 % of particles are smaller than 30.60 μm; and 80 % of the particles have a diameter in between 13.82 ($d_{10,3}$) and 65.2 μm ($d_{90,3}$). It is clear that the average diameter of Waxy Corn Starch is in between the diameter of GranuLac and the two

TiO_2 grades. However, more information about particle size, shape and surface roughness, are obtained from the Scanning Electron Microscope.

Table 3.6. *Representative diameters of Waxy Corn Starch.*

$d_{10,3}$	13.82 µm
$d_{50,3}$	30.60 µm
$d_{90,3}$	65.2 µm
$d_{99,3}$	150.00 µm
SMD	24.87 µm
VMD	36.89 µm

3.3.2.Morphology

In Figure 3.12 are reported two images of some Waxy Corn Starch granules viewed using Scanning Electron Microscope. It should be noted from SEM analysis that these particles have the more regular shape and are mostly equidimensional. However, they are generally polygonal and hence again far away from being spherical. Then, because granules of Waxy Corn Starch are well dispersed, they have no tendency to agglomerate or cake; the particle surfaces are rather smooth; and there are not nanoparticles on the surface of the bigger grains.

Note that, looking at the scale of the micrographs, particles seem to be smaller than how previously found by the dynamic Image analysis. The reasons could be that the dry analysis is not suitable for Waxy Corn Starch or, more likely, that a few bigger particles determine a shift of the median diameter calculated by QicPic.

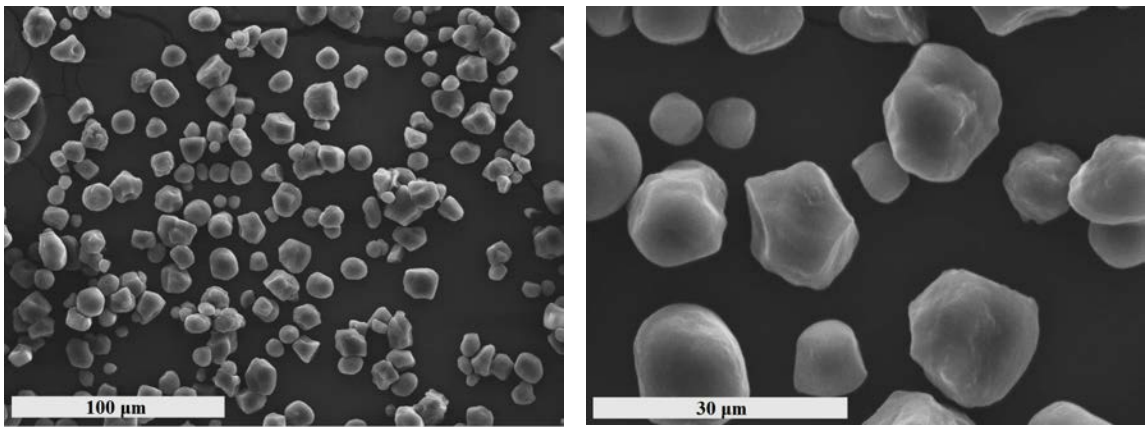

Figure 3.12. *SEM micrograph of Waxy Corn Starch.*

From the quantitative descriptors summarized in Table 3.7, it can be concluded that the width of the 50 % of particles is smaller than the 70% of the length. Furthermore it is confirmed that grains are far away from being spherical.

Table 3.7. *Quantitative descriptors of shape.*

	Aspect Ratio	**Sphericity**
$x_{10,3}$	0.509	0.548
$x_{50,3}$	0.704	0.773
$x_{90,3}$	0.845	0.898

Particle size and shape of Waxy Corn Starch influence the flow behaviour of the powder, which is discussed in detail below.

3.3.3.Flow characteristics

The flow characteristic of Waxy Corn Starch is strongly affected by the moisture content, which has been revealed to be, during its usage, equal to 7.16 (± 1.01) %. So, despite its dimensions are smaller than the ones of GranuLac, it flows easier.

Figures 3.13 and 3.14 show the Yield Loci and the Mohr's circles obtained performing the shear cell test at the following pre-shear: 3, 6, 9, 12 and 15 kPa.

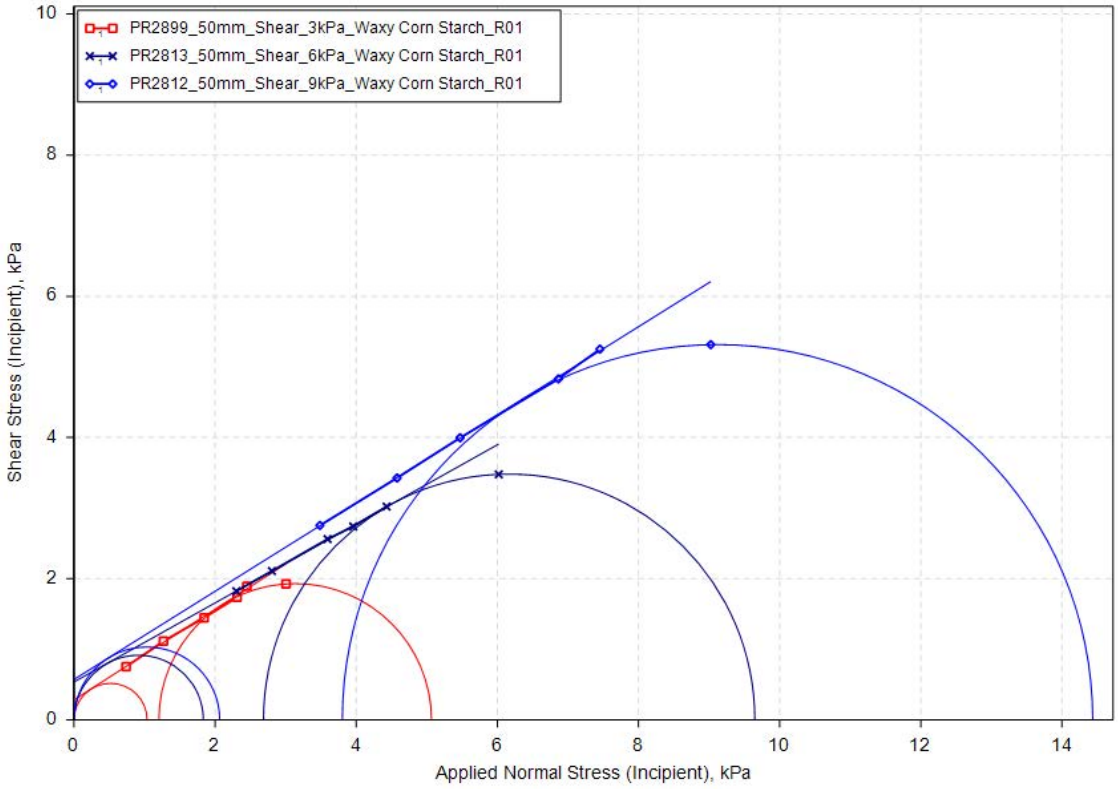

Figure 3.13. *Mohr's Circles and Yield Loci of Waxy Corn Starch (pre-shear: 3, 6 and 9 kPa).*

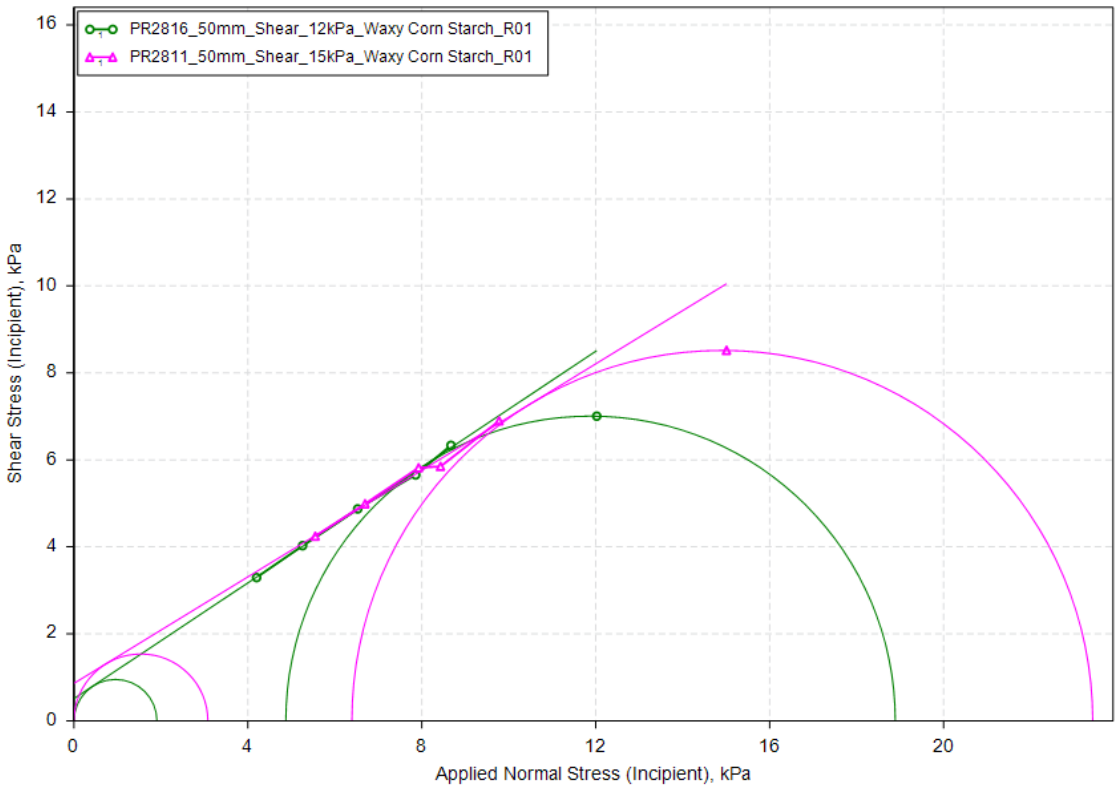

Figure 3.14. *Mohr's Circles and Yield Loci of Waxy Corn Starch (pre-shear: 12 and 15 kPa).*

One should note that in this case the linear extrapolation of the abscissa of the Yield Loci is accurate and, because the very small value of the yield loci intercepts, the material is rather free flowing. Besides, because the fluctuating profile of the shear stress versus time (Figure 3.15), Waxy Corn Starch results to have a very marked slip-stick behaviour.

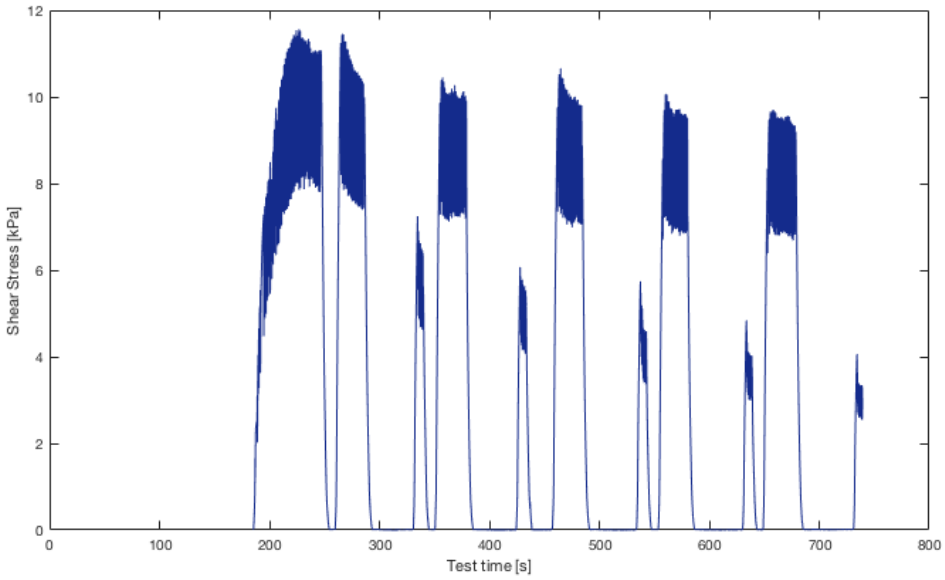

Figure 3.15. *Example of shear stress versus time profile obtained performing shear cell test on Waxy Corn Starch*.

Because its slip-stick behaviour, Waxy Corn Starch flows and stops repeatedly and, during the test, the compression load cannot be maintained constant for long time.

3.4. Comparative analysis

The FT4 powder rheometer is used to obtain the compressibility profile of the investigated materials. The percentage change in volume of the powders after compression plotted against the normal stress applied, is an indirect measure of the powder flowability and is represented in Figure 3.16. Although in all cases the compressibility percentage increases for higher values of consolidation stress, there is a pronounced difference between rather cohesive powders and more free flowing materials. Indeed, as expected, the two TiO_2 grades, which are poorly flowing bulk solids, are more compressible due to the larger amount of entrained air. The compressibility profile of Lactose Monohydrate indicates an average sensitivity to compression and it is in between the profiles of Titanium Dioxide and Waxy Corn

Starch. In turn the latter is the least compressible one, likely due to the regular shape of the particles that determines an ordered arrangement and a low degree of bed voidage, and hence a low tendency for further consolidation.

Also the ratio between the final and the initial density as a function of the powder compaction can be used as indicator of the likely fluidization characteristic of the powder. However, because this is mathematically equivalent at the percentage reduction in volume previously discussed, the patterns would be the same as in Figure 3.16. Note that in both cases the particle-particle friction is reflected in a moving mass of powder rather than in a static condition, and the friction between the powder and the wall could have a bit influenced the level of compaction.

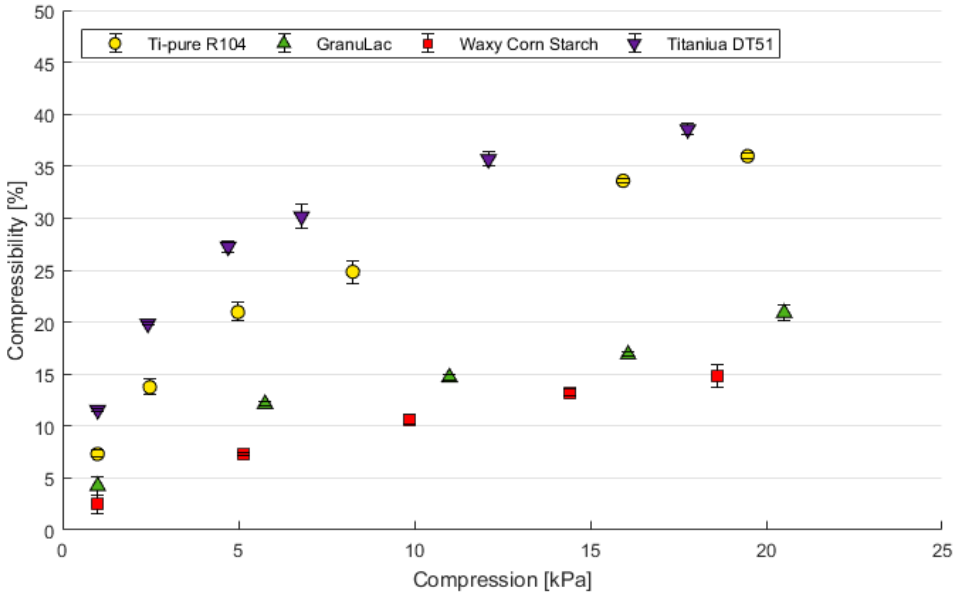

Figure 3.16. *Compressibility profiles against normal stress.*

The compressibility profile is a good indicator for quality control; however, sometimes a quantitative evaluation of powder flowability is required. As previously seen, in order to quantitatively characterize the powders, the rotational shear tester of the FT4 powder rheometer has been used. The test is applied for all materials tested at different pre-consolidation stresses; and three repetitions are performed for each measurement. In this way a family of Yield Loci is attained for each material and the flow factors can be calculated. In Figure 3.17, the flow functions, which relate the unconfined yield strength and the major principal stress during consolidation, are drawn. Instead some of the obtainable parameters, such as τ_c, σ_c, σ_1, are reported in Appendix 2.

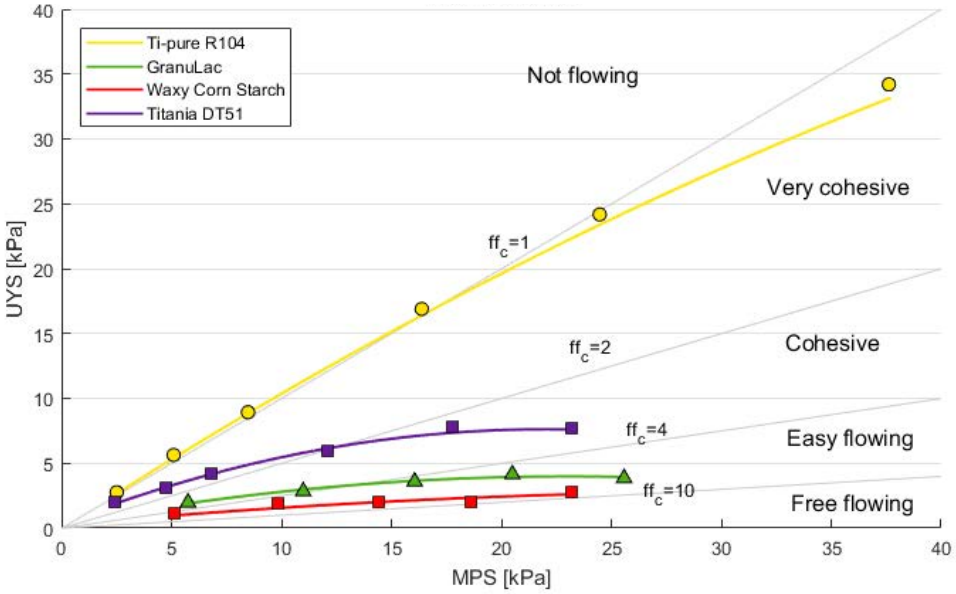

Figure 3.17. *Flow functions of the investigated materials.*

The flow function of Titanium Dioxide R-104 is about one at all applied stresses and denotes the extreme cohesive characteristic of this powder. For some major principal stress, it is even smaller than one and, according to the flowability scale published by Jenike (1964) (Table 1.2), the powder does not flow in that condition. The flow function of Titanium Dioxide DT-51 falls on the boundary between the very cohesive and the cohesive ranges. Instead, the two coarser powders, lactose monohydrate and waxy corn starch, belong mainly in the easy flowing region. Note that in all cases there is a slight tendency toward higher flow factors at high consolidation, meaning that better flowability is obtained at higher normal load.

Overall, there is good agreement between what gained from the compressibility profiles and the quantitative results obtained with the shear cell measurements. However, if in the former case TiO_2 DT-51 results to be the most compressible one, and hence the most cohesive, in the latter case it results that TiO_2 R-104 has the lowest flowability. In conclusion the compressibility profile is suitable for a preliminary and quick evaluation of the flow behaviour but, because it is not directly a flowability measurement, shear cell is needed to have more accurate results.

It is noteworthy saying that, due to the very different behaviours of the tested materials, the feasibility of the ball indentation method can be investigated in all the ranges of flowability.

Chapter 4
Experimental results and discussion

In this study the flow properties of a range of four powders have been examined also through hardness measurements and flow rate sensitivity. Here a comprehensive report of the results is presented.

This chapter is structured such that, first, it is reported the hardness measurements that have been obtained in quasi-static condition with the FT4 powder rheometer. Then, the flowability characterisation of the powders at high strain rates, done with the experimental setup of the Ball Indentation Method, is described. For the latter case, particular attention is paid to the hardness dependency on the dimensionless shear rate and, because the tested powders are characterized by different size and flowability, it has been possible to evaluate more flow regimes. The feasibility and the adequacy of the method itself are also considered.

Next, the flowability of each powder is evaluated considering the flow rate sensitivity both in free surface conditions and after compaction for impeller tip speed ranging from 10 to 300 mm/s. Lastly, it is attempted to identify similar behaviour with hardness results.

4.1. Hardness results

In this paragraphs the hardness results obtained with ball indentation are reported, both in quasi-static conditions and in intermediate regime of flow.

When the rheometer is used, the hardness, H, is given by the ratio of the maximum indentation load, F_{max}, to the projected area of the penetration, A. To calculate the area of the base of the spherical cap, A, it is required the knowledge of the final depth of the impression, h (see Equation 1.23). Here, it is assumed that no elastic recovery takes place during unloading, so h is considered to be the final penetration depth reached by the indenter during loading. Some typical experimental indentation loading/unloading cycles are reported in Figure 4.1. These examples demonstrate that the assumption is reliable for each tested material because the tangents of the unloading curves can be approximated rather accurately with vertical lines. Sometimes the intercept point of unloading cycle and penetration depth axis is smaller than the final depth reached

during loading; however the change in slope at the end of the unloading curves is only due to some particles that stick on the indenter. From Figure 4.1, it is also interesting to notice that, the more free flowing the materials, the higher the fluctuations of the loading curves (see Fig. 4.1-c and d); whilst for the two grades of TiO_2, which are very cohesive, the loading curves are roughly linear (see Fig. 4.1-a and b). The reason could be that in the case of more free flowing powders, particularly for higher penetration depths, the bed becomes compacted and particles are made flowing to each other rather than being sheared. It could also be due to the huge difference in particle dimensions between the two grades of Titanium Dioxide with respect to GranuLac and Waxy Corn Starch. So, whilst the formers result to be like continuous mediums, it is the granularity of the latters that determines the fluctuations.

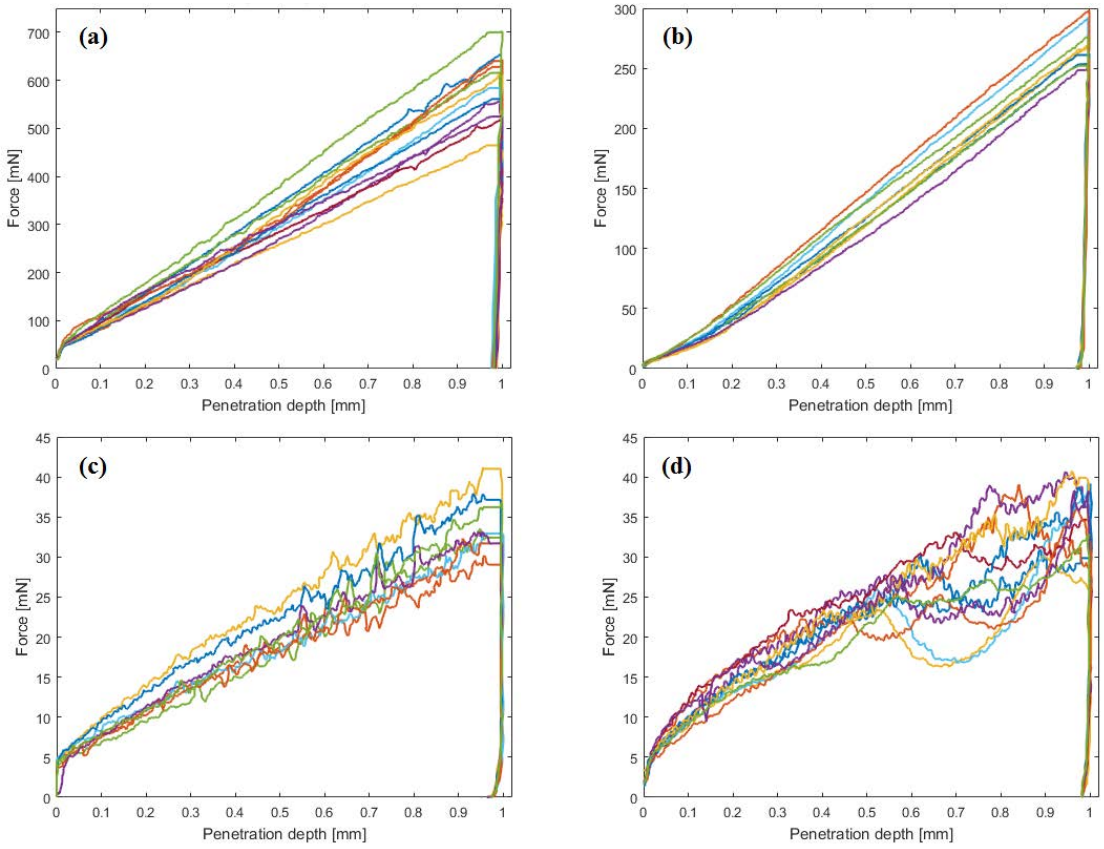

Figure 4.1. *Typical indentation loading/unloading circles on (a) TiO_2 R-104 samples consolidated to 20 kPa; (b) TiO_2 DT-51samples consolidated at 12.12 kPa; (c) GranuLac samples consolidated at 5.75 kPa; (d) Waxy Corn Starch samples consolidated at 14.89 kPa. The penetration depth is always equal to 1 mm, which means 0.5 dimensionless penetration depth.*

Unlike for the FT4 quasi-static hardness measurements, the force cannot be detected when performing dynamic Ball Indentation, so the loading/unloading curves are not available. Therefore the hardness is calculated as given by the relation proposed by

Tirupataiah and Sundararajan in 1990 (see Equation 1.25). In this case the parameters needed are: the mass of the indenter, its impact velocity, and the volume of the crated formed by the impact, *U*.

The hardness measurements obtained performing Ball Indentation Method are graphically reported using circles, upward-pointing triangles, squares and downward-pointing triangles that represent the data obtained using Nylon, Glass, Ceramic and Stainless Steel balls, respectively. The error bars in figures indicate the standard deviation always based on three experiments.

It is worth noting that all the experimental tests reported in this study have been carried out under ambient conditions of 20–25 °C temperature and the relative humidity of 45–60%. The powder moisture content has not been monitored, except for Waxy Corn Starch, which properties are more affected by different moistures.

4.1.1. Titanium Dioxide R-104

As planned, first the hardness measurements are done in quasi-static conditions with the FT4 powder rheometer. The hardness is calculated after compacting the powder at the major principal stresses, which have been obtained with shear cell tests, and considering a dimensionless penetration depth of 0.5. Thus, for TiO_2 R-104 the Hardness has been evaluated after compacting the powder at the following normal loads: 2.51, 5.10, 8.48 and 16.38 kPa. As Figure 4.2-a shows, the Hardness increases linearly with powder compaction due to the high packing state and the lower amount of air entrained in the powder bed.

Successively, the Hardness has been calculated considering penetration depths in between 0.1 and 0.9 and on 20 kPa previously compacted samples. As Figure 4.2-b illustrates, the Hardness is not constant for the entire range of penetration depth. In particular, despite it slightly changes for dimensionless penetration depth smaller then 0.5, it can be considered enough constant there. On the other hand, Hardness increases rapidly for higher values of penetration. This means that the Hardness can be used as a measure of the plastic deformation only for $h/R_i < 0.5$, whilst for higher value of dimensionless penetration depth hardness would be overestimated.

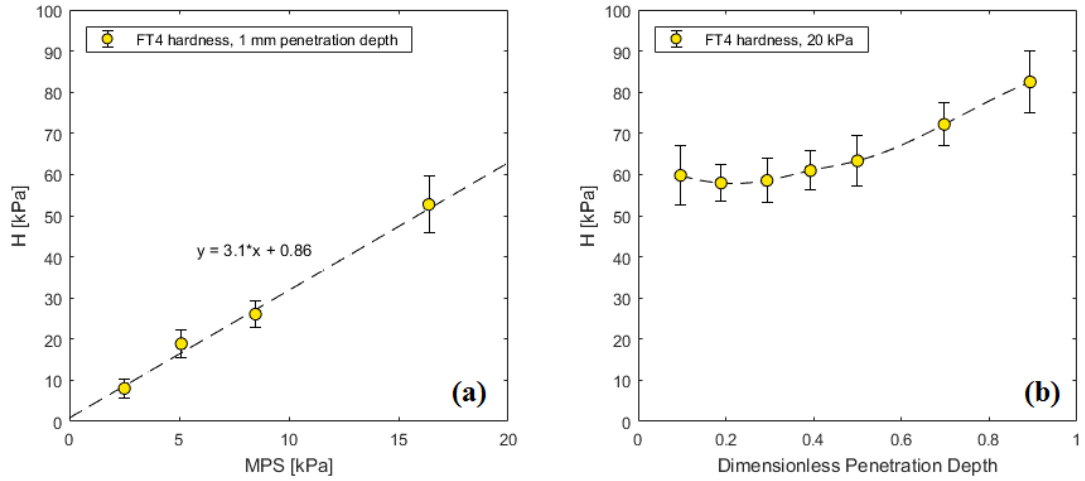

Figure 4.2. *Hardness measurements with the FT4 powder rheometer (a) considering 0.5 dimensionless penetration depth at different powder bed compactions and (b) for a range of dimensionless penetration depth when the powder is compacted at 20 kPa.*

The hardness results in Figure 4.2-a are used for defining the velocity range for all the indenter materials based on the assumption that hardness is independent of the velocity. For this determination, equations 2.2, 2.1 and 1.25 are used for finding D_a, U and v_i in the order they are presented. The minimum and maximum velocity applicable, considering 0.1 and 0.5 dimensionless penetration depth respectively, are reported in Table 4.1 together with the indenter drop heights that could be used, considering the following available tube lengths: 0.05, 0.1, 0.2, 0.5, 0.8 and 1.0 m.

Table 4.1. *Velocity range for all the indenter materials and height of the tubes suitable with TiO_2 R-104.*

		5 kPa	10 kPa	15 kPa	20 kPa
Nylon	$v_{i,min}$ [m/s]	0.46±0.01	0.59±0.01	0.76±0.01	0.87±0.01
	$v_{i,max}$ [m/s]	2.13±0.03	2.73±0.04	3.54±0.06	4.02±0.06
	H_{tube} [m]	0.05, 0.1, 0.2	0.05, 0.1, 0.2	0.05, 0.1, 0.2, 0.5	All except 1.0
Glass	$v_{i,min}$ [m/s]	0.31±.00	0.4±0.00	0.51±0.00	0.58±0.00
	$v_{i,max}$ [m/s]	1.44±0.01	1.84±0.01	2.39±0.02	2.71±0.02
	H_{tube} [m]	0.05, 0.1	0.05, 0.1	0.05, 0.1, 0.2	0.05, 0.1, 0.2
Ceramic	$v_{i,min}$ [m/s]	0.29±0.01	0.33±0.01	0.43±0.01	0.49±0.01
	$v_{i,max}$ [m/s]	1.20±0.03	1.53±0.04	1.99±0.05	2.26±0.06
	H_{tube} [m]	0.05	0.05, 0.1	0.05, 0.1, 0.2	0.05, 0.1, 0.2
S. steel	$v_{i,min}$ [m/s]	0.18±0.01	0.23±0.01	0.30±0.01	0.34±0.01
	$v_{i,max}$ [m/s]	0.84±0.02	1.08±0.03	1.40±0.04	1.59±0.04
	H_{tube} [m]	---	0.05	0.05, 0.1	0.05, 0.1

Despite the assumption done, the table represents a good starting point for determining which indenters can be used and at which drop heights, avoiding the use of balls that otherwise would penetrate too deep in the powder bed or would not penetrate far enough.

As previously discussed, the main purpose of this study is to investigate the hardness dependency on the dimensionless shear rate. The median diameter $d_{50,3}$, which is equal to 377 nm (see table 3.2), is used as reference size in the calculation of dimensionless shear rate, γ^*, in order to determining the regime of flow according to Tardos *et al.* (2003) (§ 1.2.4). Because γ^* is proportional to the square root of the particle diameter, due to the small particle dimensions of TiO_2 R-104, its rheological behaviour can be evaluated only at low dimensionless shear rate. So ball indentation method can be used to assess the flow behaviour of Titanium Dioxide R-104 in the slow, frictional regime, in the uncertain boundary, and only partially in the intermediate regime of flow.

More ball indentation measurements have been carried out. Firstly, to determine the feasibility of the method, all the indenters have been impacted in the same conditions. Then, in order to reach higher shear rates as well as to determine the influence of the initial state of powder bed compaction, other tests have been performed.

The bar chart reported in Figure 4.3 illustrates the hardness results obtained dropping all the sixteen available indenters on a powder bed compacted at 20 kPa, and considering an impact velocity of the balls equals to 1.99 (±0.04) m/s. It can be seen that the hardness remains relatively constant using Nylon, Glass and Ceramic indenters, whilst the hardness is higher using Stainless Steel balls. The reason is that Stainless Steel indenters penetrate deeper in the powder bed, at those depths where hardness is overestimated (see Fig. 4.2-b). Overall, it can be said that as far as the hardness is in the constant range of dimensionless penetration depth, the indenter material does not influence the result. Besides, hardness measurements are independent of indenter size, if the indentation zone is distant enough from the surrounding walls. Only the biggest Stainless Steel indenter over-estimates the hardness with respect to smaller spheres of the same materials, likely because there is not sufficient clearance between the edge of the indentation zone and the die wall. When too close to the wall of the vessel indeed, the particles-wall friction becomes higher than the internal angle of friction.

The data represented in Figure 4.3 have been obtained analysing, for each test type, the indentation profiles reported in Figure 4.4. Note that the pictures are set for material type (rows) and size (columns).

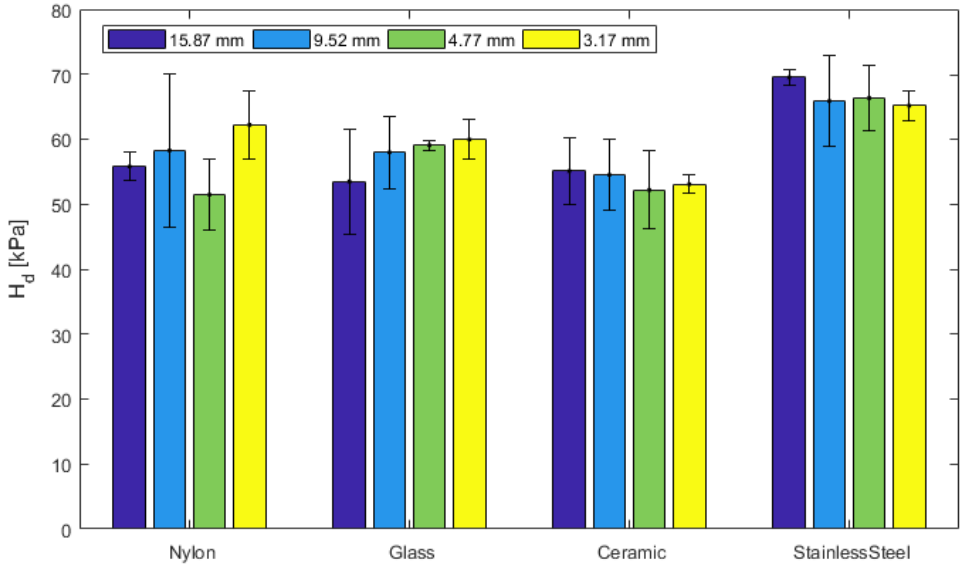

Figure 4.3. *Hardness measurements with the BIM. The hardness values are obtained dropping all the 16 available indenters into 20 kPa compacted powder beds at 1.99 m/s (±0.04).*

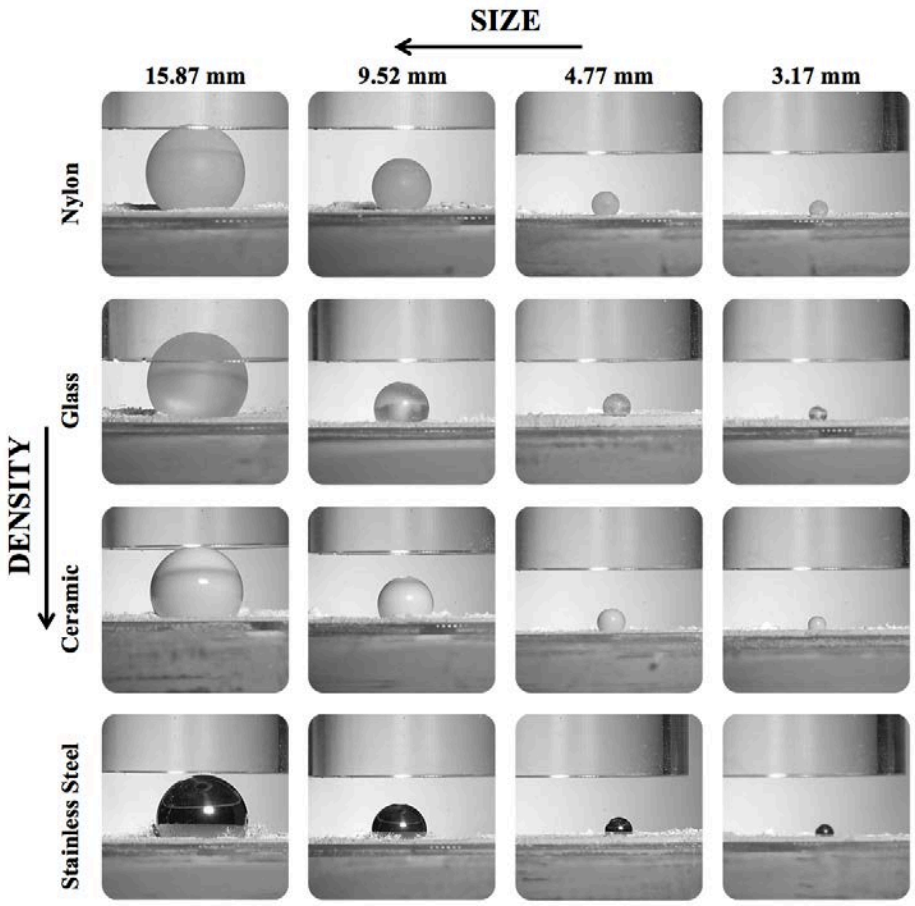

Figure 4.4. *Pictures of all the 16 available indenters dropped onto 20 kPa compacted powder beds at 1.99 m/s (±0.04). Along the rows, from the lighter to the heavier: Nylon, Glass, Ceramic and Stainless Steel respectively. Along the columns, in order: 15.87, 9.52, 4.77 and 3.17 mm.*

The same data as before are illustrated in Figures 4.5 and 4.6, where the hardness is represented as a function of dimensionless shear rate and penetration depth respectively. As expected, hardness is relatively independent of the strain rates using indenters of the same material, regardless of their size. Indeed, for $\gamma^*<0.15$, the friction between particles is predominant, and the shear field is continuous. It is noteworthy that the hardness does not increase for $\gamma^* \cong 0.20$, also if in the uncertain boundary between quasi-static and intermediate regime of flow. This could be because, in their theoretical explanation, Tardos *et al.* (2003) assumed perfectly spherical particles with mono-modal distribution, assumption that cannot be applied for TiO_2 R-104.

The overestimation of hardness using Stainless Steel balls is well explained by Figure 4.6, where it appears clearly that Stainless Steel indenters penetrate until dimensionless penetration depth larger than 0.5. The same graph reports also the FT4 hardness measurements, so differences amongst the quasi-static and the dynamic indentation can be explored. It results that, for TiO_2, the two techniques correlate well with each other.

In conclusion, as far as the height of the penetration is in the range of constant hardness and the indenter does not interact with the die wall, the measurement are reliable and the method is feasible: indenter type and size does not affect the results, FT4 and ball indentation measurements are well correlated and, keeping with the theoretical explanation, Hardness is insensitive to strain rate variations in the slow frictional regime.

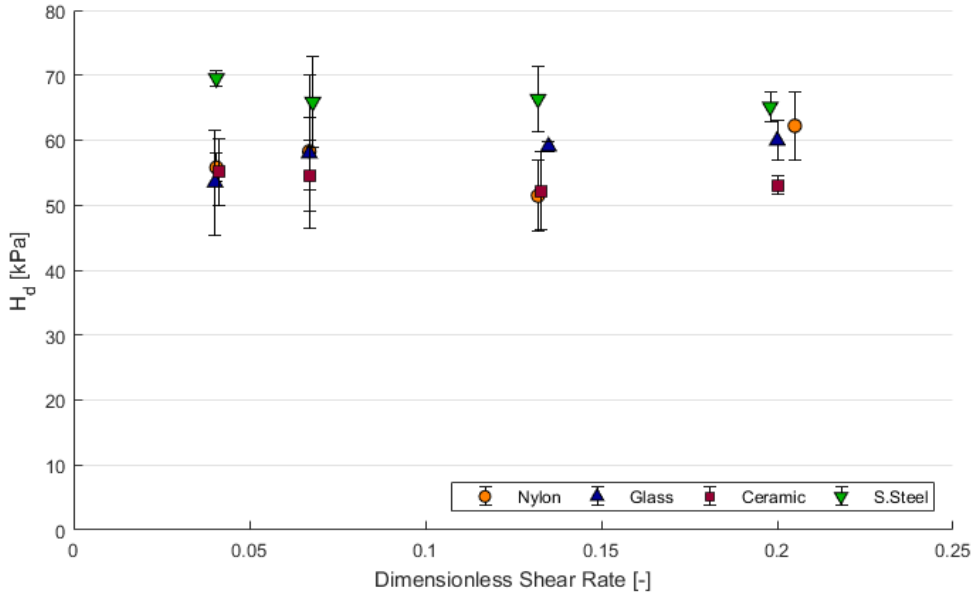

Figure 4.5. *Hardness versus dimensionless shear rates. The hardness values are obtained dropping all the 16 available indenters onto 20 kPa compacted powder beds at 1.99 m/s (±0.04).*

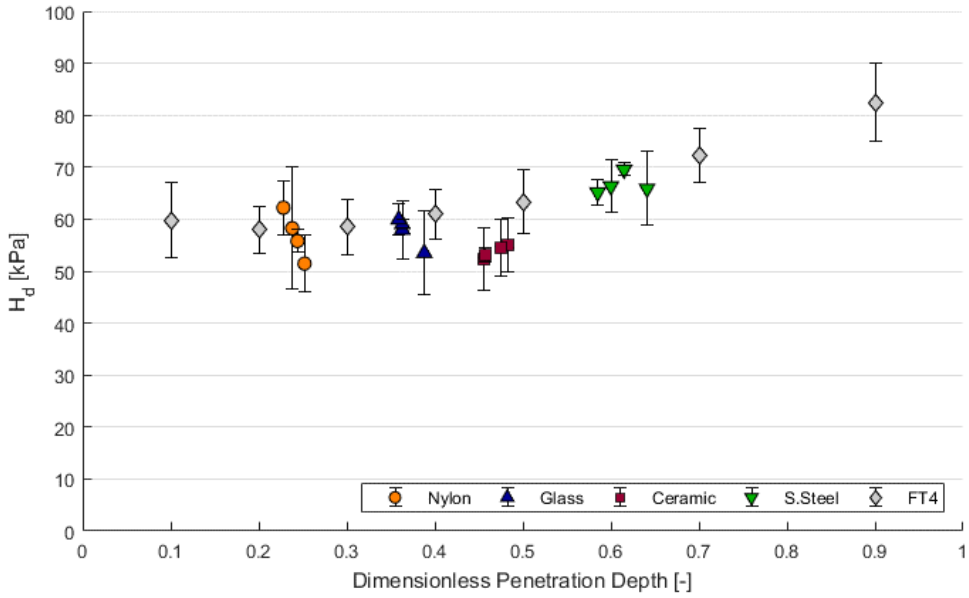

Figure 4.6. *Hardness versus dimensionless penetration depth. Comparison between the hardness obtained with the BIM (v_i=1.99 ± 0.04 m/s) and the FT4 indentation test. In all cases powder is compacted at 20 kPa.*

Ball indentation measurements have been carried out also for TiO_2 R-104 samples consolidated at 5 kPa. In this case any size Nylon and Ceramic indenters have been dropped from the top of 0.5 m and 0.1 m height tubes respectively. From 0.5 m height, indenters have impacted with a velocity of 3.11 (±0.05) m/s, and this leads to higher value of shear rates. Figure 4.7 shows the hardness results obtained in these conditions. If for $\gamma^*<0.15$, stresses are independent of strain rate; hardness slightly increases for $\gamma^*>0.2$. However, what happens in between is not clear, and the strain rate value for which hardness becomes strain rate dependent cannot be unambiguously determined. Note that the error bar is generally larger for Nylon balls because, due to the opacity of nylon, the backscattering of light is different, and the threshold cannot be well determined as in the case of other materials. Furthermore, smaller indenters (see measurement at $\gamma^* \cong 0.32$ for Nylon and at $\gamma^* \cong 0.14$ for Ceramic) usually lead to larger standard deviation: since the smaller dimensions, the percentage of error is bigger.

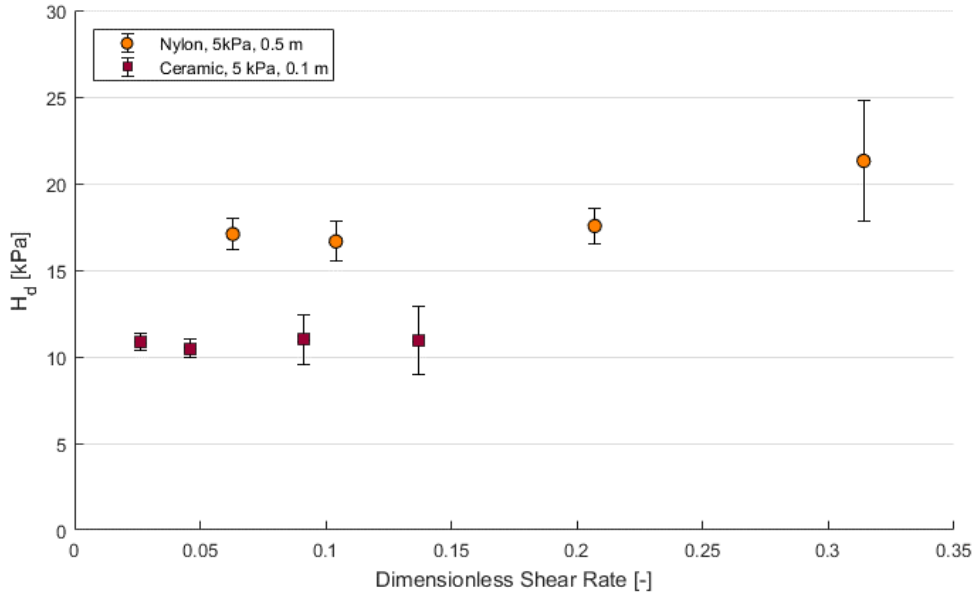

Figure 4.7. *Hardness measurements using all size Nylon and Ceramic indenters on 5 kPa pre-compacted powder beds. The impact velocity is respectively: 3.11 (±0.05) m/s for Nylon and 1.35 (±0.05) m/s for Ceramic spheres. The range of dimensionless penetration depth investigated results to be in between 0.64 (±0.05) and 0.81 (±0.03).*

Then, in order to investigate larger dimensionless shear rates, a wide range of indentation speeds have been experimented with the smaller Nylon indenter (d_i=3.17 mm) on a 10 kPa compacted powder bed. The impact velocities, v_i, measured by post processing image analysis are: 1.48 (±0.02) m/s, 2.07 (±0.00) m/s, 2.95 (±0.00) m/s, 3.55 (±0.00) m/s and 4.07 (±0.00) m/s.

The hardness values such obtained are shown in Figure 4.8, where it can be seen that the hardness growths rather linearly by increasing the strain rate. It is noteworthy that in this case it can be assessed not only the powder rheological behaviour in the uncertain boundary, but also in the earlier part of the intermediate regime, up to $\gamma^* \cong 0.45$.

Finally, for TiO_2, it has also been evaluated the hardness dependency on the initial powder bed compaction. Despite this is not the main focus of this study, Figure 4.9 is reported because it could be a cue for further studies and future works. Differently from what found in the quasi-static FT4 indentation experiments, hardness does not increases linearly with the bed compaction, but in a quadratic manner. Furthermore, the error bars increases in width with the compression.

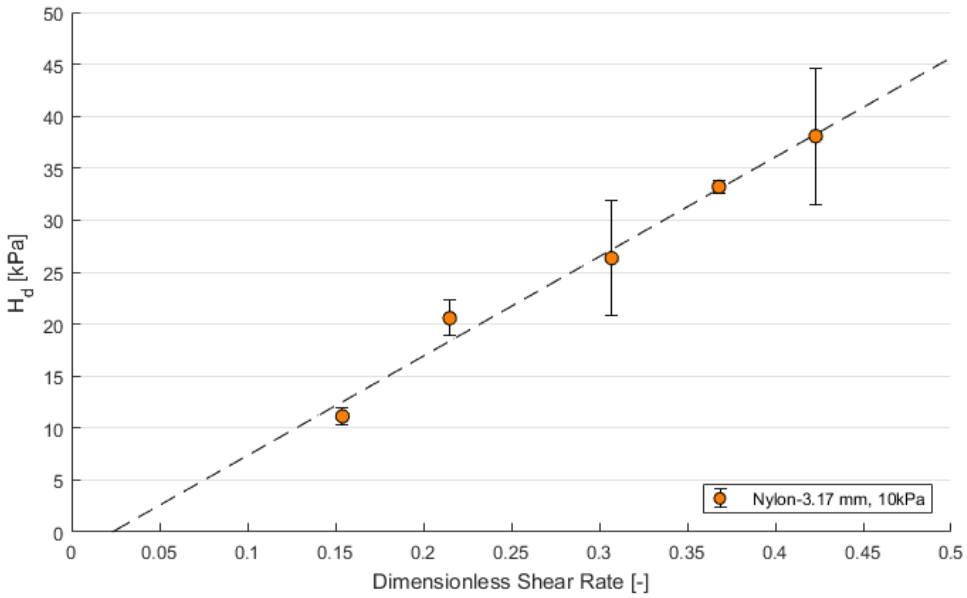

Figure 4.8. *Hardness versus dimensionless shear rate using the smaller nylon indenter on a 10 kPa compacted bed at different impact velocities. The range of dimensionless penetration depth investigated results to be in between 0.42 (±0.02) and 0.66 (±0.06).*

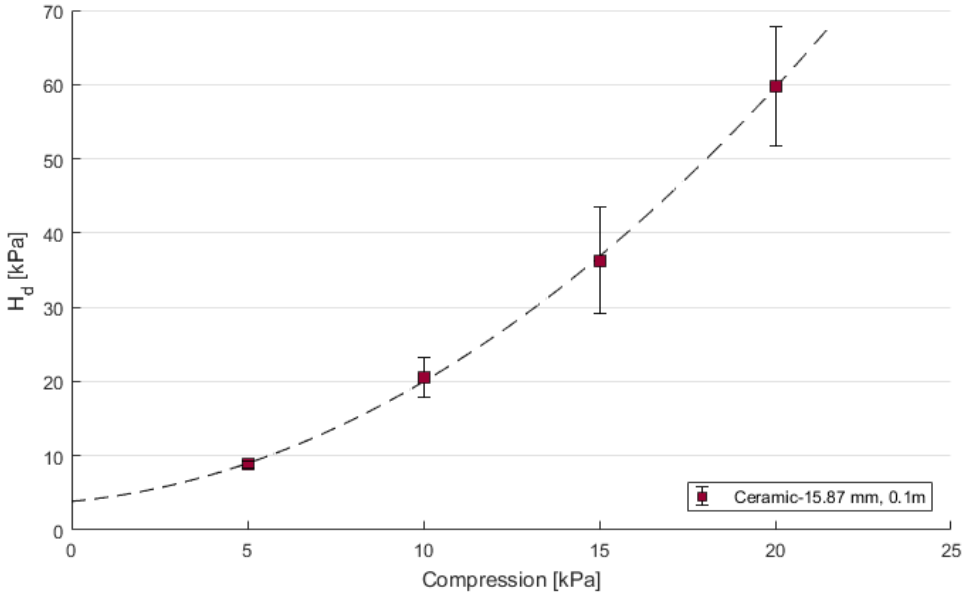

Figure 4.9. *Hardness versus normal load using the bigger Ceramic indenter (15.87 mm) at 1.41 m/s (±0.03) impact velocity.*

From the assessment of TiO_2 R-104 through the Ball Indentation Method, which has been performed in different conditions, the main outcome is that stresses become strain rate dependent at about $\gamma^* \cong 0.2$, although the boundary is not very well defined.

4.1.2.Titanium Dioxide DT-51

The same procedure as before has been applied on all the other tested materials. So also for Titanium Dioxide DT-51 it has been firstly applied the quasi-static indentation with the FT4 powder rheometer.

The quasi-static hardness, as a function of the applied normal stress, is represented in Figure 4.10-a. All the points have been obtained considering a dimensionless penetration depth of 0.5. It can be seen that the hardness increases with an increase in the pre-consolidation pressure rather linearly, and the error bars increases in width with the compression. These hardness values are the ones used to assess which indenter, and at which speed, can be used to perform indentation with the Ball Indentation Technique.

To investigate the effect of dimensionless penetration depth, quasi-static hardness measurements have been carried out on 12.12 kPa compacted powder beds. As Figure 4.10-b shows, in this case a range of dimensionless penetration depth, within which a relative constant value of hardness is obtained, cannot be identified. So, because hardness is affected by the height of the penetration, it should not be used as a measure of resistance to plastic deformation for this grade of Titanium Dioxide. The risk indeed is to underestimate or overestimate hardness for lower or higher penetration respectively.

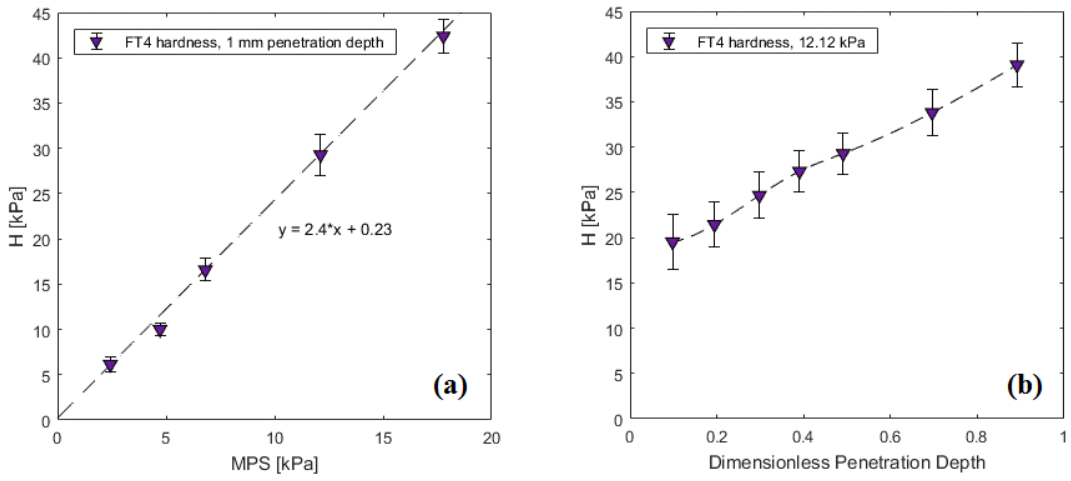

Figure 4.10. *Hardness measurements with the FT4 powder rheometer (a) considering 0.5 dimensionless penetration depth at different powder bed compactions and (b) for a range of dimensionless penetration depth when the powder is compacted at 12.12 kPa.*

Table 4.2 shows the velocity range for all the indenter material, which has been calculated considering 0.1 and 0.9 as the minimum and maximum dimensionless

penetration depth respectively. Furthermore it is reported the height of tubes that can be used in the BIM experimental setup.

Table 4.2. *Velocity range for all the indenter materials and height of the tubes suitable with TiO_2 DT-51.*

		4.72 kPa	**6.81 kPa**	**12.12 kPa**	**17.78 kPa**
Nylon	$v_{i,min}$ [m/s]	0.35±0.01	0.45±0.01	0.59±0.01	0.72±0.01
	$v_{i,max}$ [m/s]	2.69±0.04	3.42±0.05	4.54±0.07	5.49±0.09
	H_{tube} [m]	0.05, 0.1, 0.2	0.05, 0.1, 0.2, 0.5	all	all
Glass	$v_{i,min}$ [m/s]	0.24±0.00	0.30±0.00	0.40±0.00	0.48±0.00
	$v_{i,max}$ [m/s]	1.82±0.01	2.31±0.02	3.06±0.02	3.7±0.03
	H_{tube} [m]	0.05, 0.1	0.05, 0.1, 0.2	0.05, 0.1, 0.2, 0.5	0.05, 0.1, 0.2, 0.5
Ceramic	$v_{i,min}$ [m/s]	0.20±0.01	0.25±0.01	0.33±0.01	0.40±0.01
	$v_{i,max}$ [m/s]	1.51±0.04	1.92±0.05	2.55±0.07	3.08±0.08
	H_{tube} [m]	0.05, 0.1	0.05, 0.1	0.05, 0.1, 0.2	0.05, 0.1, 0.2
S. steel	$v_{i,min}$ [m/s]	0.14±0.00	0.18±0.00	0.23±0.01	0.28±0.01
	$v_{i,max}$ [m/s]	1.07±0.03	1.35±0.04	1.80±0.05	2.17±0.06
	H_{tube} [m]	0.05	0.05	0.05, 0.1	0.05, 0.1, 0.2

Despite particle dimensions of TiO_2 DT-51 are larger than dimensions of TiO_2 R-104, it is again not enough to investigate the dynamic regime of flow. However, it is possible to go further than before and investigating dimensionless shear rates until nearly $\gamma^* \cong 0.9$.

All the sixteen available indenters have been used to evaluate the powder flowability of TiO_2 DT-51 samples consolidated at 12.12 kPa. The indenters have been dropped from the top of the 0.10 m tube; hence their impact velocity has been measured to be around 1.40 m/s. The results obtained are represented in the bar chart (Figure 4.11), from which a conclusion cannot be drawn. It seems that there is no correlation between indenter size and material. However, to better understand what happens, the same data set is represented in Figures 4.12 and 4.13, as function of dimensionless shear rate and penetration depth, respectively.

Looking at the Figure 4.12 it can be seen that the hardness remains unchanged at low dimensionless penetration depth, but it increases for γ^* higher than approximately 0.2. So, for low values of dimensionless shear rate, which are characteristic of the slow frictional flow regime, the hardness is relatively independent of both indenter type and strain rate; whilst the hardness becomes shear rate dependent at higher value of γ^*,

namely in the transition between the quasi-static and the intermediate state, as well as in the lower intermediate regime of flow.

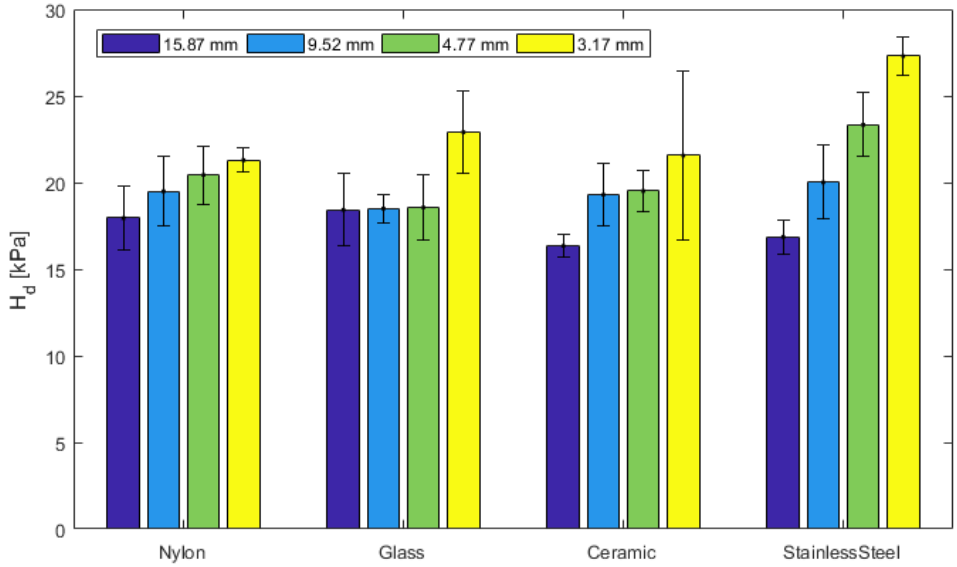

Figure 4.11. *Hardness measurements with the BIM. The hardness values are obtained dropping all the 16 available indenters onto 12.12 kPa compacted powder beds at 1.40 m/s (±0.02).*

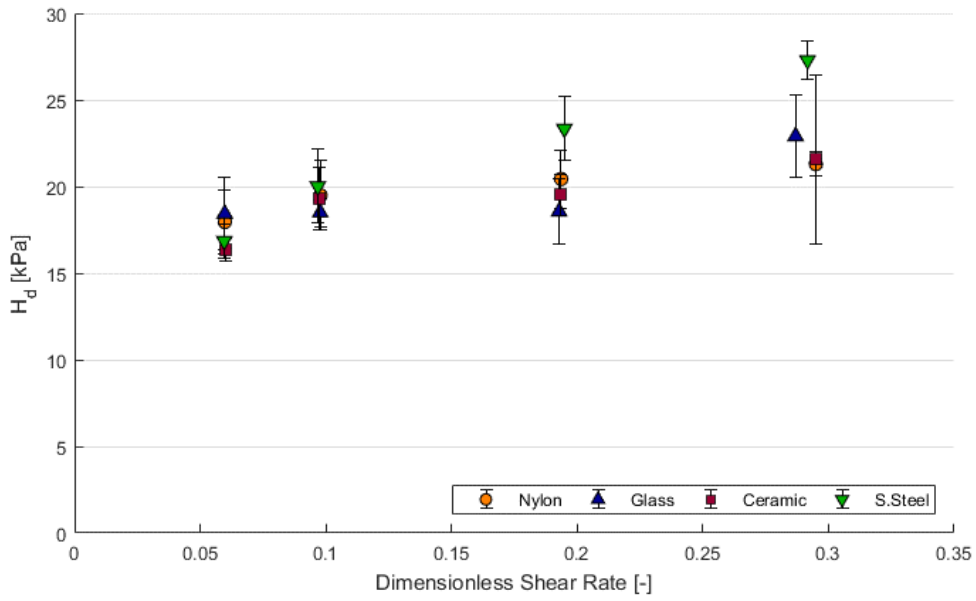

Figure 4.12. *Hardness versus dimensionless shear rates. The hardness values are obtained dropping all the 16 available indenters onto 12.12 kPa compacted powder beds at 1.40 m/s (±0.02).*

From Figure 4.12 it can be see that the hardness variation determined with Stainless Steel indenters is higher than in the other cases. This can be explained looking at Figure

4.13. There, it can be seen that Stainless Steel indenters allow investigating a wider range of dimensionless penetration depth, hence larger is the detected variation of hardness.

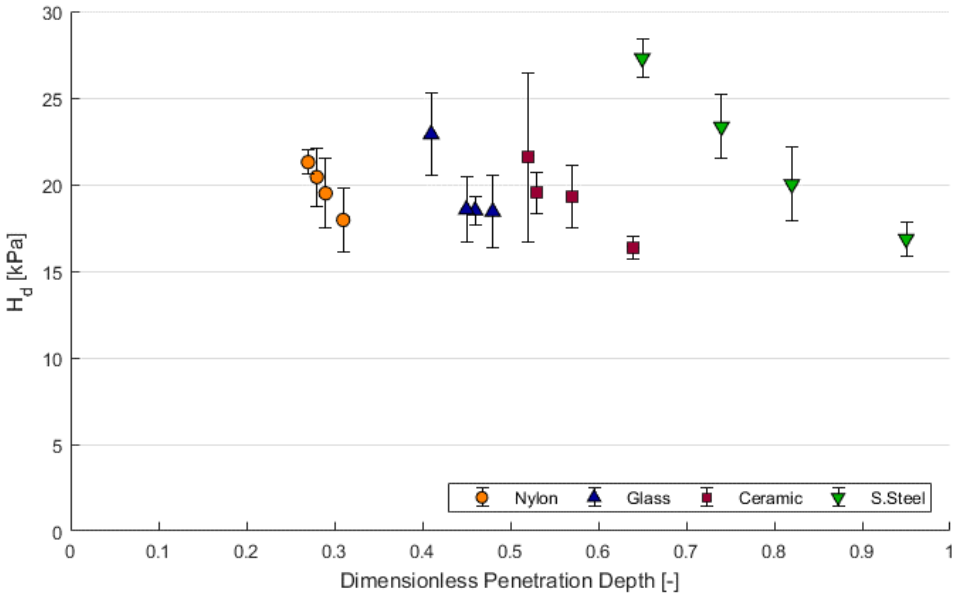

Figure 4.13. *Hardness versus dimensionless penetration depth. The hardness values are obtained dropping all the 16 available indenters onto 12.12 kPa compacted powder beds at 1.40 m/s (±0.02).*

Successively, in order to investigate higher values of dimensionless strain rates, a wide range of indentation speeds have been experimentally tested using the two Nylon indenters with diameters equal to 4.77 and 3.17 mm onto 17.78 kPa pre-consolidated powder beds. In detail, the impact velocities tested are: 1.31 (±0.02) m/s, 1.94 (±0.03) m/s, 3.05 (±0.06) m/s, 3.81 (±0.14) m/s and 4.08 (±0.12) m/s.

The hardness results are drawn in Figures 4.14 and 4.15 as a function of dimensionless shear rate, γ^*, and dimensionless penetration depth, *h/Ri*, respectively. Also in these cases, the error bars indicate the standard deviation of three measurements. The outcome suggests that the hardness is sensitive to the strain rate, indeed the stress increase with γ^*. In particular it seems that, this relations is rather linear, as in the case of Newtonian liquids. However it is not clear why there are some discrepancies in the results obtained with the two ball sizes: the hardness increases faster when BIM is performed with the smaller indenter. The problem is not due to the different penetration depth, because, as Figure 4.15 shows, both are investigating the same range of penetration. Likely, the reason is related to the difference in proportion of the indenters. Indeed, as Table 2.2 displays, the measured density has a standard deviation, indicating

that the indenters are not perfect spheres and, because the mass appears in the hardness equation, this may affect the results.

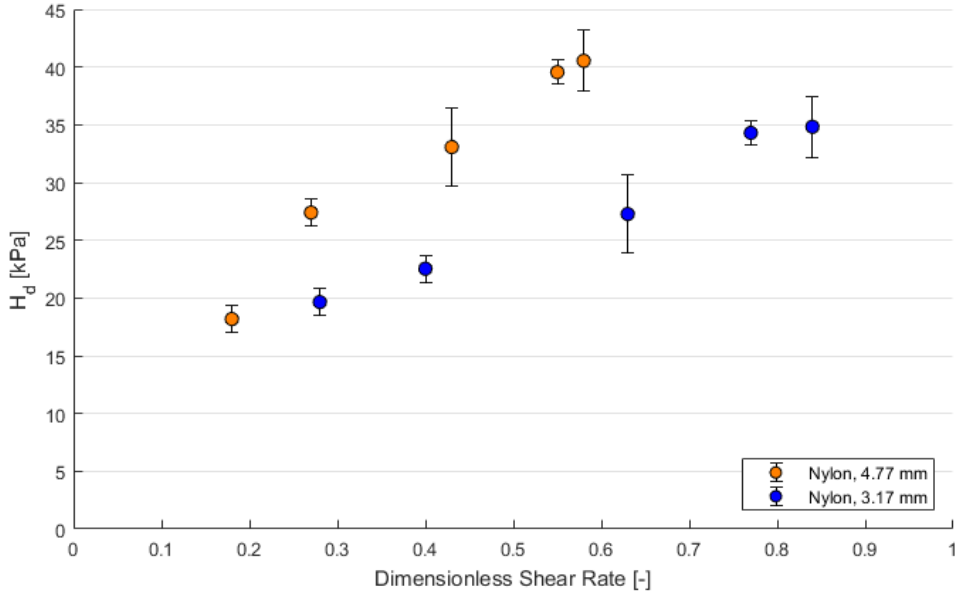

Figure 4.14. *Hardness versus dimensionless shear rate at different impact velocities. The hardness values are obtained dropping Nylon indenters (4.77 and 3.17 mm) onto 17.78 kPa compacted powder beds. The impact velocity ranges from 1.31 to 4.08 mm/s.*

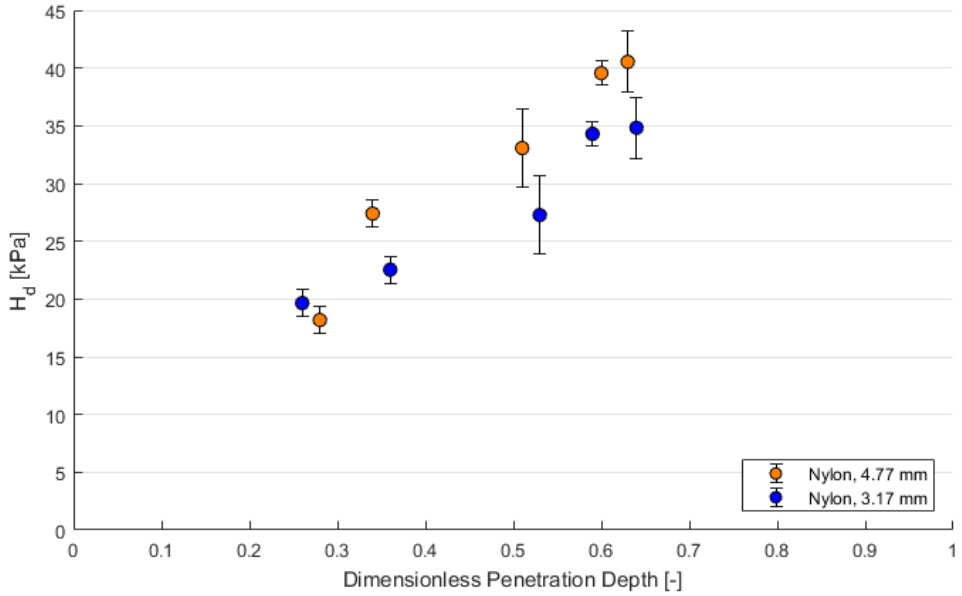

Figure 4.15. *Hardness versus dimensionless penetration depth at different impact velocities. The hardness values are obtained dropping Nylon indenters (4.77 and 3.17 mm) onto 17.78 kPa compacted powder beds. The impact velocity ranges from 1.31 to 4.14 mm/s.*

In conclusion, due to the particle dimension, and because the high range of impact velocities investigated, γ^* until unity has been evaluated with TiO_2 DT-51. Also in this case, it is demonstrated that in the uncertain boundary, as well as in the intermediate regime, hardness becomes shear rate dependent. Furthermore, the relation between shear stress and shear rate is rather linear for γ^*>0.30, meaning that in this condition the powder behaviour is liquid-like.

4.1.3.α-lactose monohydrate

The quasi-static hardness, evaluated with the FT4 powder rheometer, as a function of the consolidation state of the powder bed, is reported, for GranuLac, in Figure 4.16-a. It was found that hardness increases with powder compaction. However, the slope of the interpolating line is smaller than the two previous cases. This powder indeed is less cohesive than the two grades of Titanium Dioxide and, due to the smaller amount of voids in the bed, hardness increases more slowly with compression.

The relationship between quasi-static hardness and dimensionless penetration depth, which is evaluated for samples of GranuLac compacted at 5.75 kPa, is instead represented in Figure 4.16-b. Despite the fluctuation, hardness can be considered rather constant when dimensionless penetration depth ranges from 0.1 to 0.9. Therefore, every time the height of the penetration is in between 0.1 and 0.9 times the indenter radius, the hardness measurement is reliable.

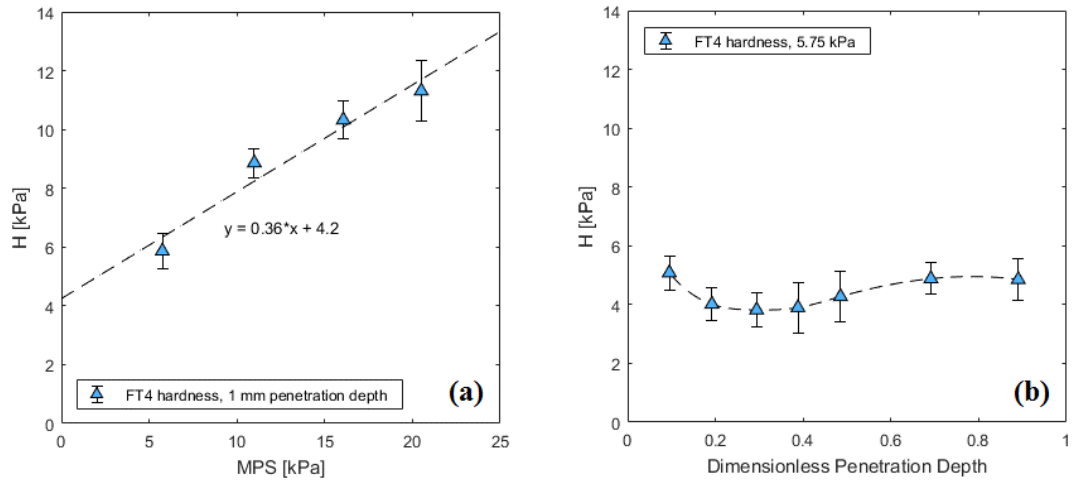

Figure 4.16. *Hardness measurements with the FT4 powder rheometer (a) considering 0.5 dimensionless penetration depth at different powder bed compactions and (b) for a range of dimensionless penetration depth when the powder is compacted at 5.75 kPa.*

The velocity range for all the available indenters and the test planning are represented in Table 4.3, for four Major Principal Stresses. Because the poor hardness of GranuLac in these conditions, indenters can never be dropped from the top of 0.5, 0.8 and 1.0 m height glass tubes. Furthermore, if samples are compacted at 5.75 kPa, Stainless Steel indenters cannot be used: they would penetrate too further in the powder bed.

Table 4.3. *Velocity range for all the indenter materials and height of the tubes suitable with GranuLac.*

		5.75 kPa	**10.99 kPa**	**16.06 kPa**	**20.50 kPa**
Nylon	$v_{i,min}$ [m/s]	0.28±0.00	0.33±0.01	0.36±0.01	0.37±0.01
	$v_{i,max}$ [m/s]	2.13±0.03	2.54±0.04	2.74±0.04	2.87±0.05
	H_{tube} [m]	0.05, 0.1, 0.2	0.05, 0.1, 0.2	0.05, 0.1, 0.2	0.05, 0.1, 0.2
Glass	$v_{i,min}$ [m/s]	0.19±0.00	0.22±0.00	0.24±0.00	0.25±0.00
	$v_{i,max}$ [m/s]	1.44±0.01	1.71±0.01	1.85±0.01	1.94±0.02
	H_{tube} [m]	0.05, 0.1	0.05, 0.1	0.05, 0.1	0.05, 0.1, 0.2
Ceramic	$v_{i,min}$ [m/s]	0.16±0.00	0.19±0.00	0.2±0.01	0.21±0.01
	$v_{i,max}$ [m/s]	1.20±0.03	1.43±0.04	1.54±0.04	1.61±0.04
	H_{tube} [m]	0.05	0.05, 0.1	0.05, 0.1	0.05, 0.1
S. steel	$v_{i,min}$ [m/s]	0.11±0.00	0.13±0.00	0.14±0.00	0.15±0.00
	$v_{i,max}$ [m/s]	0.84±0.02	1.01±0.03	1.09±0.03	1.14±0.03
	H_{tube} [m]	---	0.05	0.05	0.05

Despite in this case a wide range of speed cannot be experimented because the modest powder hardness, GranuLac has the largest particle dimension of all the other tested materials, with a median diameter equals to $d_{50,3}$=82.80 μm. Therefore, it is however possible to investigate the flow behaviour for shear rates characteristic of the intermediate regime.

Firstly, the BIM has been evaluated on 20.5 kPa compacted powder beds and dropping all the indenters from 0.05 m height. The impact velocity measured with post image analysis has resulted to be equals to 1.07 m/s (±0.07).

Although the large error bars, it can be seen in Figure 4.17 that all indenters lead approximately to the same results. However, in order to allow further observation, the same hardness values are reported in Figure 4.18 as a function of γ^*.

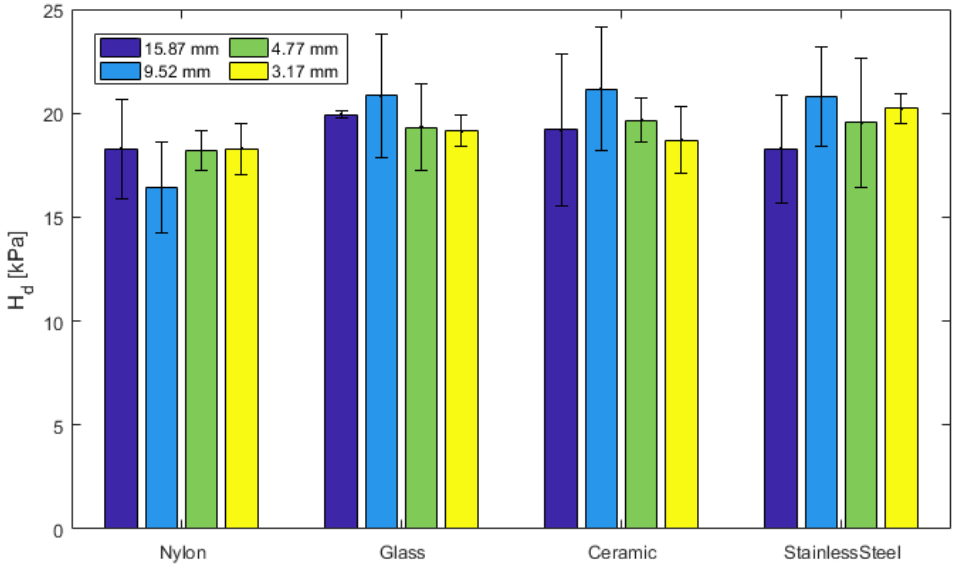

Figure 4.17. *Hardness measurements with the BIM. The hardness values are obtained dropping all the 16 available indenters onto 20.5 kPa compacted powder beds at 1.07 m/s (±0.07).*

As Figure 4.18 shows, the hardness is constant for all the entire range of dimensionless penetration depth investigated. This disagrees with the theoretical explanation of Tardos *et al.* (2003) that demonstrated that in the intermediate regime shear stress is dependent on shear rate. Despite the reason of this discrepancy is not clear, it could likely be because at 20.5 kPa compaction, GranuLac flows easily (see Figure 3.17). To lend credence to this statement, a similar set of experiments has been carried out on samples compacted at 5.75 kPa, condition where GranuLac is instead cohesive (*ff*=3.90). The results obtained are reported in Figure 4.19.

In Figure 4.19 the dimensionless shear rate ranges from about 0.5 to 2.0, thus the intermediate regime is the one investigated. It can be seen that hardness increases rather linearly for the investigated $\dot{\gamma}^*$. It is noteworthy that the error bars increases with the shear rate, indicating that there is an increase of fluctuations. The same behaviour was found also by Pasha *et al.* (2015) in their numeric simulation.

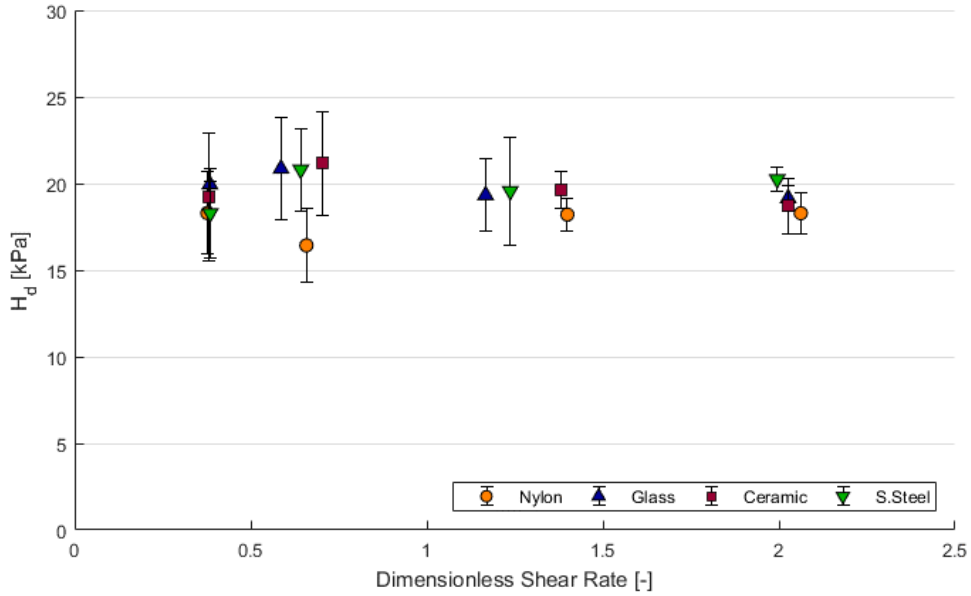

Figure 4.18. *Hardness versus dimensionless shear rates. The hardness values are obtained dropping all the 16 available indenters onto 20.5 kPa compacted powder beds at 1.07 m/s (±0.07).*

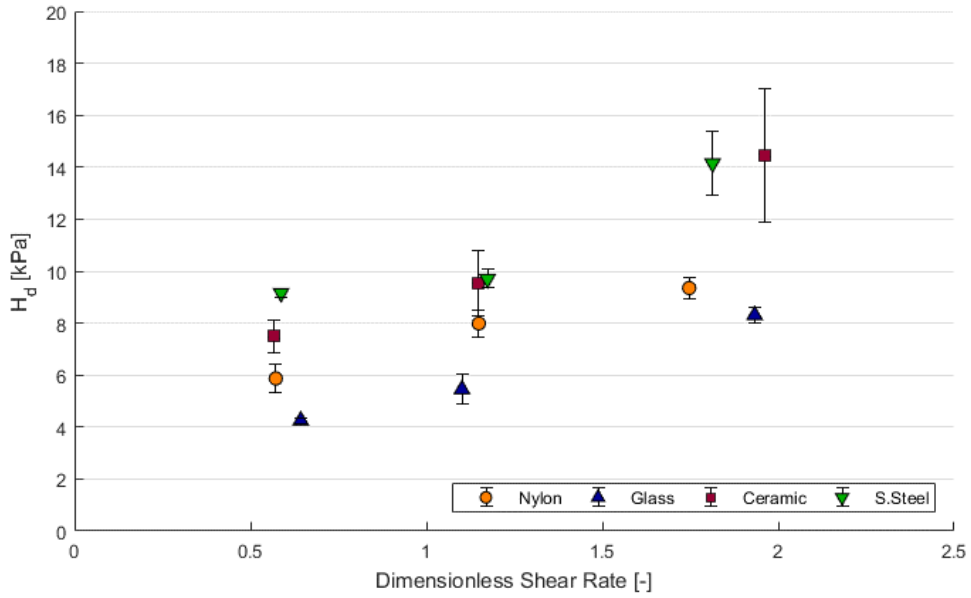

Figure 4.19. *Hardness versus dimensionless shear rates. The values are obtained dropping all the available indenters, except the biggest, onto 5.75 kPa compacted powder beds at v_i=0.97 m/s (±0.06).*

It can be observed that Ceramic and Stainless Steel indenters lead to higher variation in hardness measurement because, as it can be explained from Figure 4.20, higher is the variation in penetration depth. However, because hardness has been demonstrated to be constant when h/R_i ranges from 0.1 to 0.9, in this case all the measurements are reliable.

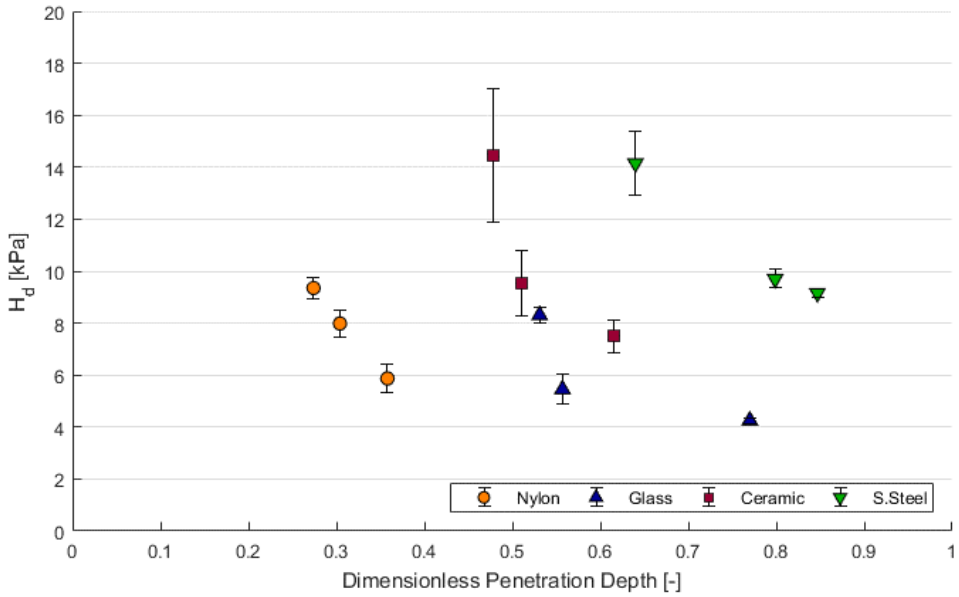

Figure 4.20. *Hardness versus dimensionless penetration depth. The hardness values are obtained dropping all the available indenters, except the bigger ones, onto 5.75 kPa compacted powder beds at 0.97 m/s (±0.06) impact velocity.*

For more in-depth investigation of the shear rate dependency of hardness at 5.75 kPa compaction, the same test as before has been carried out at the following drop height: 0.10 m. However, as it can be seen in Table 4.3, in this condition only Nylon and Glass balls can be used.

The results of hardness measurements, when nylon and glass indenters impact on 5.75 kPa compacted beds of GranuLac at 1.37 m/s (±0.02), are reported in Figure 4.21. Based on those measurements, there is a steady increase of hardness throughout the intermediate regime. Hence here, the rheological behaviour of cohesive powders is comparable to the behaviour of Newtonian liquids.

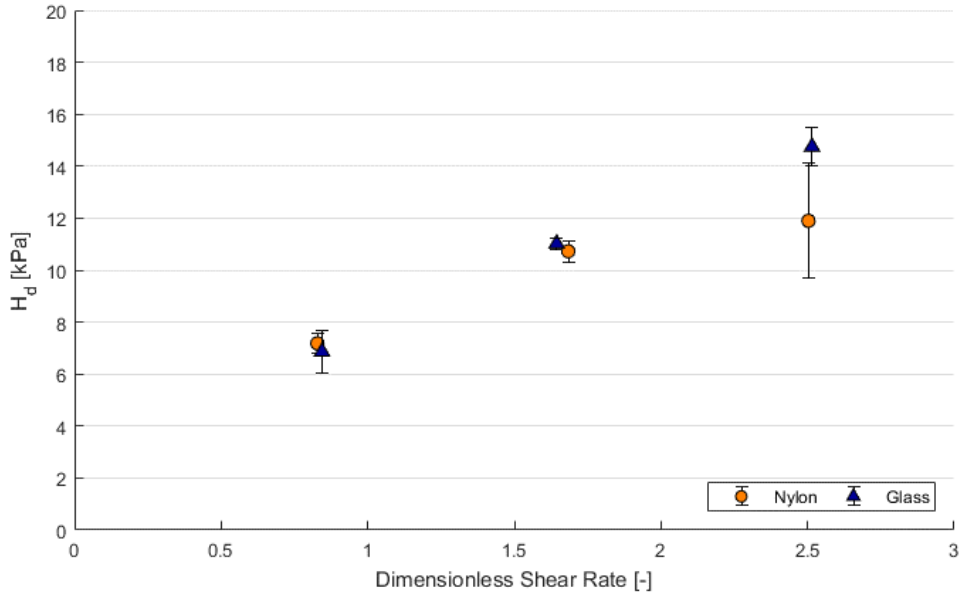

Figure 4.21. *Hardness versus dimensionless shear rates. The hardness values are obtained dropping Nylon and Glass indenters, except the bigger ones, onto 5.75 kPa compacted powder beds at 1.37 m/s (±0.02) impact velocity.*

In conclusion, despite the intermediate regime of flow has been investigated in all the tests performed on GranuLac, hardness increases with the strain rate only at lower values of compaction, namely when the powder behaves cohesively. In this case, as expected for cohesive materials, the hardness rises with the shear rate in the intermediate regime of flow. In detail, in the earlier part of the regime, $H_d \sim (\gamma^*)^n$, with n<1; then the dependency becomes linear ($H_d \sim \gamma^*$). On the other hand, when the power flows easily, the hardness measurements are independent of the strain rate, whatever the flow regime is.

4.1.4. Waxy Corn Starch

To further investigate the flow behaviour of easy flowing powders through indentation techniques, Waxy Corn Starch has been chosen as the last tested materials.

In Figure 4.22-a is reported the hardness values obtained performing the quasi-static indentation with the FT4 powder rheometer at different values of powder compaction. Because Waxy Corn Starch is always more free flowing of the other tested powders, hardness increases slower with the increase of the Major Principal Stress.

The dependency of hardness on the dimensionless penetration depth is instead represented in Figure 4.22-b. Note that the points have been obtained performing

indentation on samples compacted at 14.39 kPa. From this graph it can be seen that there is a limit of penetration depths below which the hardness measurements are considered unreliable. Higher values of hardness are measured at lower indentation load likely because at small penetration depths, only a small number of particles are displaced and the indenter comes in contact with only few particles. However, the hardness decreases to a constant stable value for dimensionless penetration depth greater than 0.5. Thus, at a given consolidation pressure, the height of the penetration must be at least half the indenter radius to give reliable measurement of hardness.

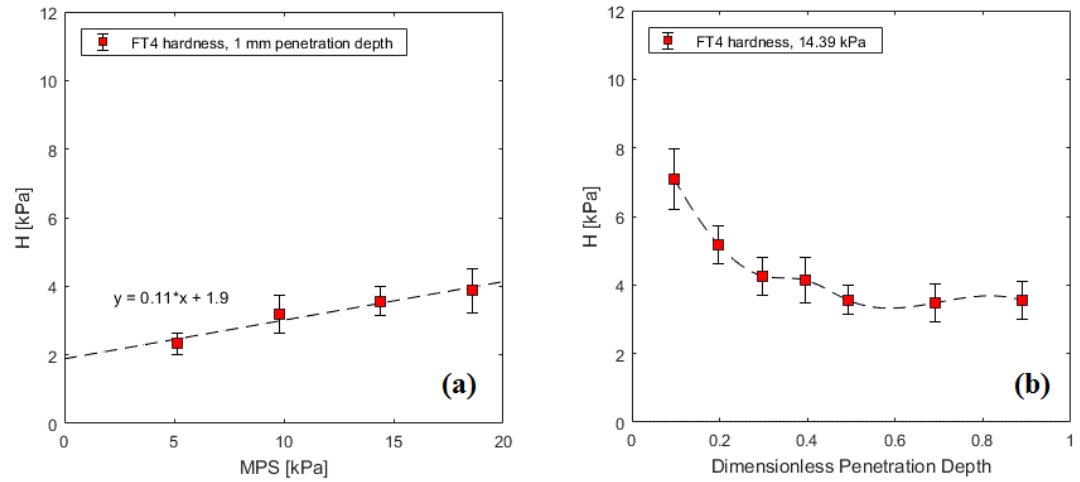

Figure 4.22. *Hardness measurements with the FT4 powder rheometer (a) considering 0.5 dimensionless penetration depth at different powder bed compactions and (b) for a range of dimensionless penetration depth when the powder is compacted at 14.39 kPa.*

From Table 4.4, where the minimum and the maximum velocities correspond to 0.5 and 0.9 dimensionless penetration depth respectively, it appears that the velocity range investigable with the available spherical indenters is very limited. Ceramic and stainless steel indenters can never be used at those values of compaction; glass ball can be dropped only from 0.05 m height and not in the case of 4.83 kPa compacted beds; instead for Nylon, only 0.05 or 0.10 m height tubes can be used. However, it should be reminded that the velocity ranges in table are calculated considering hardness at 0.5 penetration depth. Because the hardness is overestimated for smaller penetrations, probably in some conditions also ceramic indenters could be used.

Because the smaller number of tests performable with the Ball Indentation Method than in the previous cases, more impact velocities cannot be used to investigate higher shear rates. However, the median diameter of Waxy Corn Starch is big enough ($d_{50,3}$=30.60 μm), and it is possible to reach $\gamma^* \cong 1.5$.

Table 4.4. *Velocity range for all the indenter materials and height of the tubes suitable with Corn Starch.*

		4.83 kPa	9.82 kPa	14.89 kPa	18.59 kPa
Nylon	$v_{i,min}$ [m/s]	0.80±0.01	0.91±0.01	0.98±0.02	1.02±0.02
	$v_{i,max}$ [m/s]	1.31±0.02	1.50±0.02	1.61±0.03	1.68±0.03
	H_{tube} [m]	0.05	0.05, 0.1	0.05, 0.1	0.1
Glass	$v_{i,min}$ [m/s]	0.54±0.00	0.61±0.00	0.66±0.01	0.69±0.01
	$v_{i,max}$ [m/s]	0.89±0.01	1.01±0.01	1.09±0.01	1.13±0.01
	H_{tube} [m]	--	0.05	0.05	0.05
Ceramic	$v_{i,min}$ [m/s]	0.45±0.01	0.51±0.01	0.55±0.01	0.57±0.02
	$v_{i,max}$ [m/s]	0.74±0.02	0.84±0.02	0.90±0.02	0.94±0.02
	H_{tube} [m]	--	--	--	--
S. steel	$v_{i,min}$ [m/s]	0.32±0.01	0.36±0.01	0.39±0.01	0.40±0.01
	$v_{i,max}$ [m/s]	0.52±0.01	0.59±0.02	0.64±0.02	0.66±0.02
	H_{tube} [m]	--	--	--	--

All the hardness measurements performed with the Ball Indentation Method on Waxy Corn Starch are represented in Figure 4.23. Particularly Nylon, Glass and Ceramic indenter have been used from 0.05 m height; moreover Nylon indenters have also been dropped from 0.10 m height. In all cases samples have been previously compacted at 14.89 kPa.

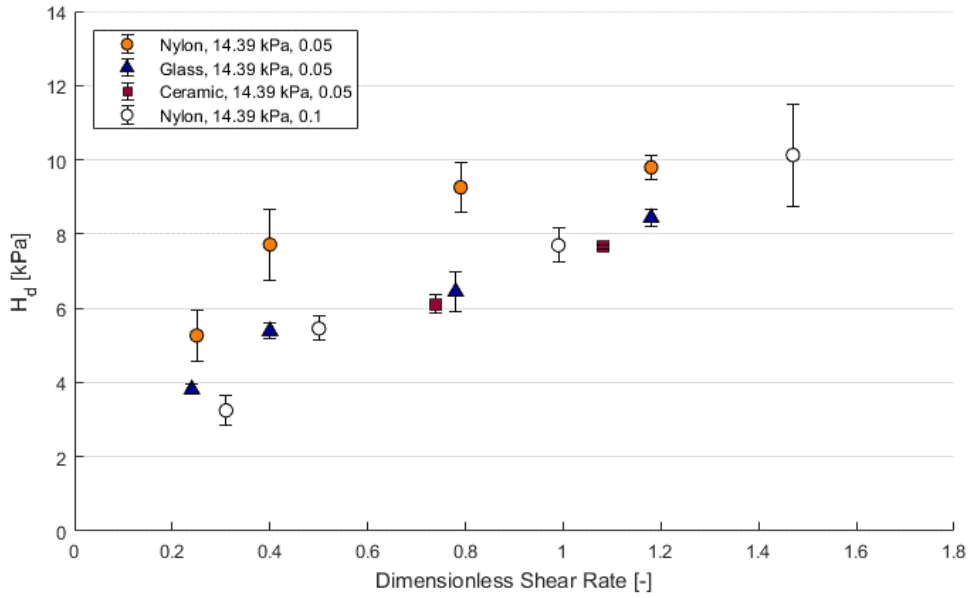

Figure 4.23. *Hardness versus dimensionless shear rates. The hardness values are obtained dropping the indenters onto 14.89 kPa compacted powder beds. The impact velocity used is 1.06 m/s (±0.04) for the coloured data, and 1.35 m/s (±0.03) for the colourless points.*

Except the results obtained with Nylon at 0.05 m drop height, all the other hardness measurements lie on the same line. Hardness increases rather linearly for shear rates characteristic of the intermediate range, also if the powder can be classified as an easy flowing material. It is not clear why the behaviour of Waxy Corn Starch differs from the easy flow behaviour of GranuLac.

According to what represented in Figure 4.22-b, measurements are reliable if the dimensionless penetration depth exceeds 0.5. So, from the hardness measurements as a function of dimensionless penetration depth graph represented in Figure 4.24, it can be seen that all the Nylon indenters, when dropped with 1.06 m/s (±0.04) impact velocity, overestimate hardness. Note that the data points obtained with Glass and Ceramic can be trusted everywhere.

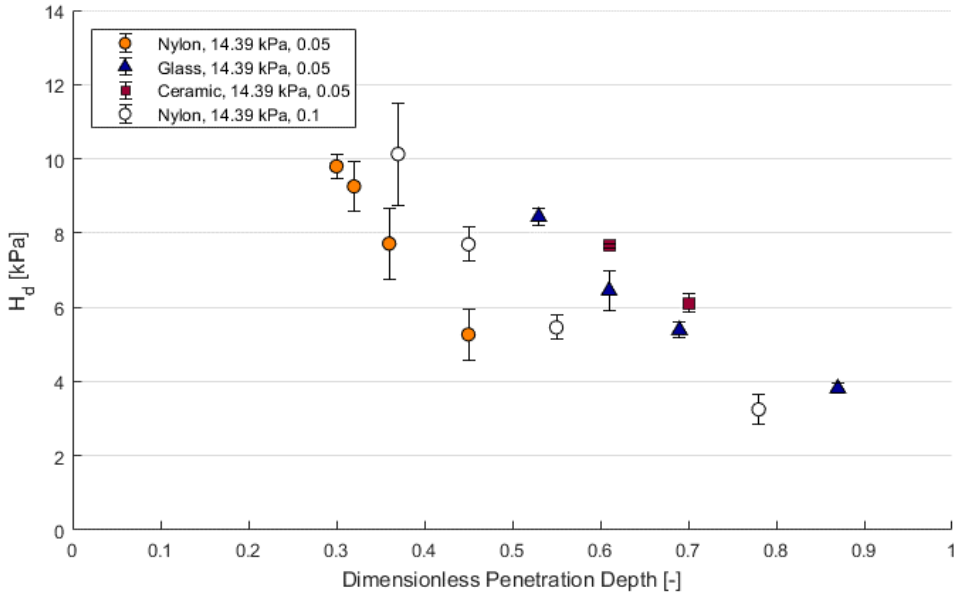

Figure 4.24. *Hardness versus dimensionless penetration depth. The hardness values are obtained dropping the indenters onto 14.89 kPa compacted powder bed. The impact velocity used is 1.06 m/s (±0.04) for the coloured data, and 1.35 m/s (±0.03) for the colourless points.*

In conclusion, also if Waxy Corn Starch is an easy flowing powder in the tested conditions, hardness increases with the shear rate rather linearly in the intermediate regime of flow, as far as the dimensionless penetration depth lies in the constant hardness range. Therefore, Ball Indentation Method is suitable also for assessing the flow behaviour of certain easy flowing powder but, because the limited number of tests applicable, it could not be useful enough.

4.1.5.Constraint factor

The unconfined yield stress determined from shear cell measurements can be compared with the hardness values obtained from the FT4 quasi-static indentation test if indentation is performed on samples compacted at the same Major Principal Stresses. In particular, hardness and Unconfined yield Stress are related through the Constraint Factor, from which it is possible to deduce the role of inter-particle adhesion on the flow behaviour.

In Figure 4.25 is reported the constraint factor for all the materials tested. The constraint factor of GranuLac and TiO_2 R-104 is around 3; whilst *C* is almost 2 for Waxy Corn Starch. This confirms that, the constraint factor of bulk solids depends on single particle properties. It is worthwhile noticing that *C* seems to dependent on the Major Principal Stress in the case of TiO_2 DT-51. The reason is that the Unconfined Yield Strength is estimated by a linear approximation of the Yield Loci, although they curve downward. Due to the error from extrapolating the Yield Locus, and because Hardness increases with penetration depth, the constraint factor for Titanium Dioxide DT-51 cannot be determined with reasonable accuracy.

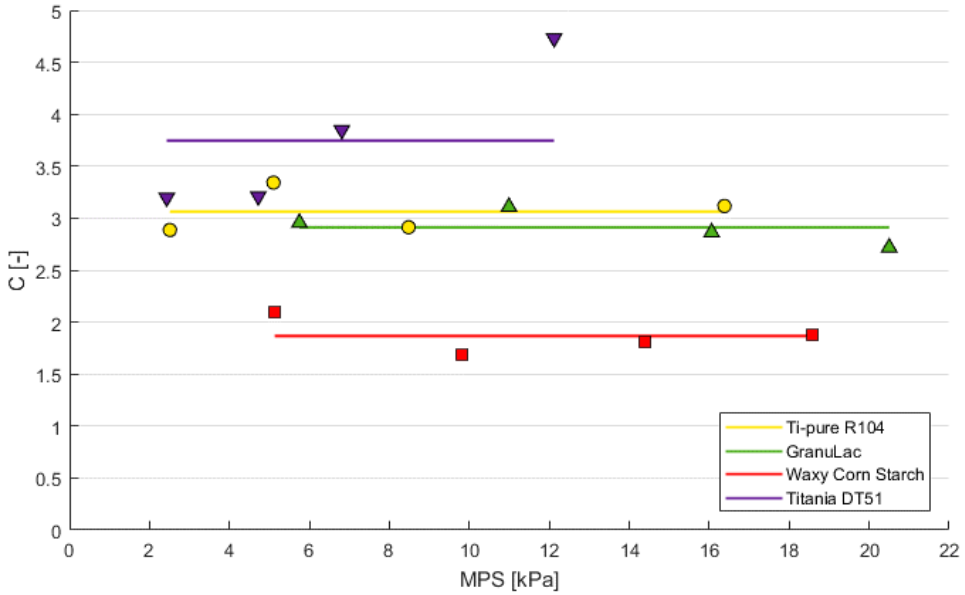

Figure 4.25. *Constraint factor of each tested material.*

If constant, knowing the constraint factor is useful because allows predicting the Unconfined Yield Strength from a hardness measurement. Indeed, by simply assessing the hardness with indentation tests, and applying Equation 1.24, it is possible to predict

σ_c also in such conditions that cannot be carried out with shear cell measurements: low stress environments and high strain rates.

Because in the previous paragraphs it has been demonstrated that the hardness increases for shear rates characteristic of the intermediate regime, and due to the proportionality between hardness and yield strength through the constraint factor, it can be deduced that also the yield strength increases with strain rate in the intermediate regime of flow. At high shear rates, when not only friction but also collisions between particles are present, powder is fluidized and its rheological behaviour is liquid-like.

4.2. Variable Flow Energy

In order to asses the flow rate sensitivity of the tested materials, the 48 mm diameter blade is driven downwards and rotated in an anticlockwise direction into the bed using tip speeds ranging from 10 to 300 mm/s and an helix angle equals to 5º to the horizontal plane. Furthermore, to evaluate if the flow rate sensitivity is affected by the initial powder compaction, the evaluation is done both on non-compacted samples and on previously compressed powder beds.

The flow energy is calculated considering the area under the energy gradient curve always for the first 20 mm of penetration, although the blade penetrates deeper in the powder bed. Indeed, because the flow energy does not take into account differences in mass, consider the same penetration depth is useful for making comparable the results. The sensitivity to blade speed is then assessed by the flow rate index, as defined in Equation 1.27. It is worth remembering that for cohesive materials, the energy is higher at low tip speeds because more voids are able to escape from the sample and, at least locally, the material is stiffer and more resistant to flow. On the other hand, free flowing materials are insensitive to change in tip speeds because the voids are unaffected by the shear rate (Leturia *et al.*, 2014).

Because it has been seen in other cases that the flow energy correlates well with other flowability measurement techniques (Hare *et al.*, 2015), the test is performed here with the purpose to find a relationship with the Ball Indentation Method.

4.2.1.Titanium Dioxide R-104

The variable flow rate method have been carried out three times in order to evaluate the standard deviation, both on non-compacted and on 5 kPa compacted powder beds of

TiO_2 R-104. In Figure 4.26-a, and 4.26-b, an example of energy gradient curves is represented for each case. In the former it is rather clear that, the area under the curves is higher for lower tip speeds, situation that is characteristic of cohesive powders. In the latter it looks like there are not differences in the flow energy so, for compacted samples, the flow energy required to make the powder flow is independent of tip speed.

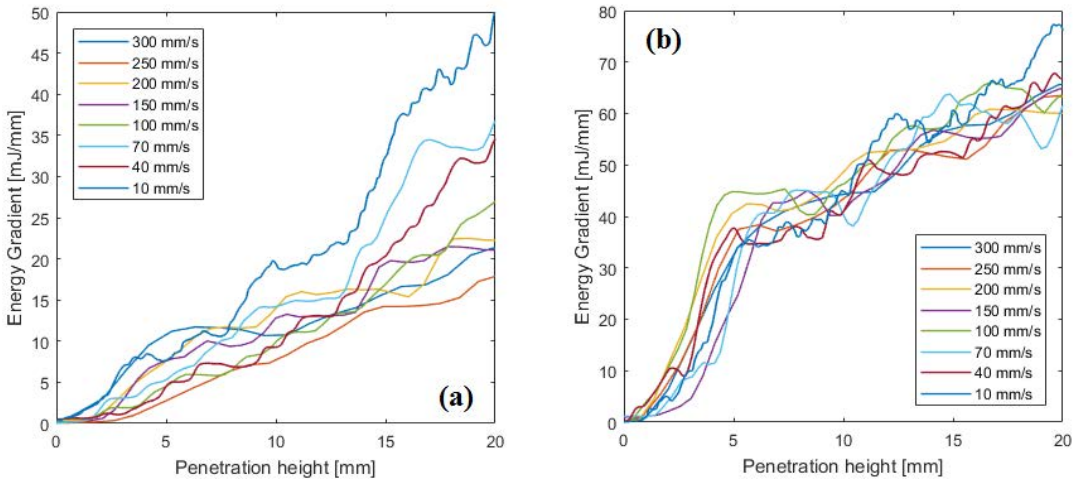

Figure 4.26. *Example of energy gradient Vs height at different tip speed considering samples of Titanium Dioxide R-104 (a) non compacted and (b) compacted at 5kPa.*

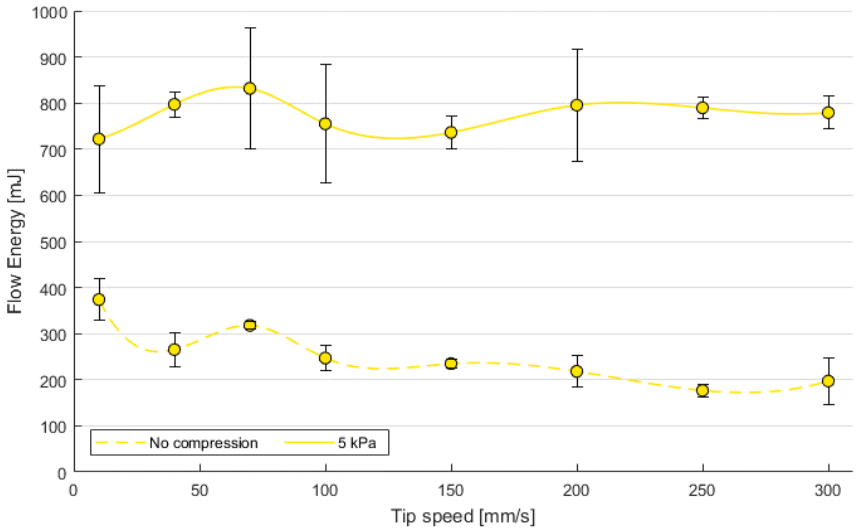

Figure 4.27. *Flow energy at different tip speed both on a free surface and on a compacted powder bed.*

Figure 4.27 illustrates instead the measured flow energy as a function of the tip speed. It is clear that the flow resistance is lower if samples are in free surface conditions because smaller is the hardness of the material. Furthermore, for non-compressed samples, the

energy needed to make the powder flow is lower at 100 mm/s than at 10 mm/s (*FRI*=1.5). At low tip speed indeed, the amount of air entrained is lower; at least locally, the blade consolidate more the powder; and the particle interlocking is higher (Freeman Technology, W7012, 2007). After 200 mm/s the flow energy becomes rather constant and TiO_2 R-104 is not sensitive anymore to changes in flow rates.

For compacted samples, the situation is not clear enough due to the fluctuating trend of the curve. The FRI_{comp}=0.96 indicates that the powder is not cohesive, but this departs from what found from the shear cell measurements. This could mean that the method does not give reliable results for compacted powder bed of TiO_2 R-104; or more likely that the FRI cannot be used to state if something is cohesive or not.

4.2.2. Titanium Dioxide DT-51

Figures 4.28-a and 4.28-b show the energy gradient curves at different tip speeds for a sample of TiO_2 DT-51 non-compacted and compacted at 4.72 kPa respectively. In the former case the energy measured for each millimetre blade travel increases constantly with the penetration; whilst in the latter it increases faster in the first 5 mm of travel and then rather slowly. This indicates that after compaction, the packing state is not uniform for all the full height of the powder bed, but it is higher in the upper part.

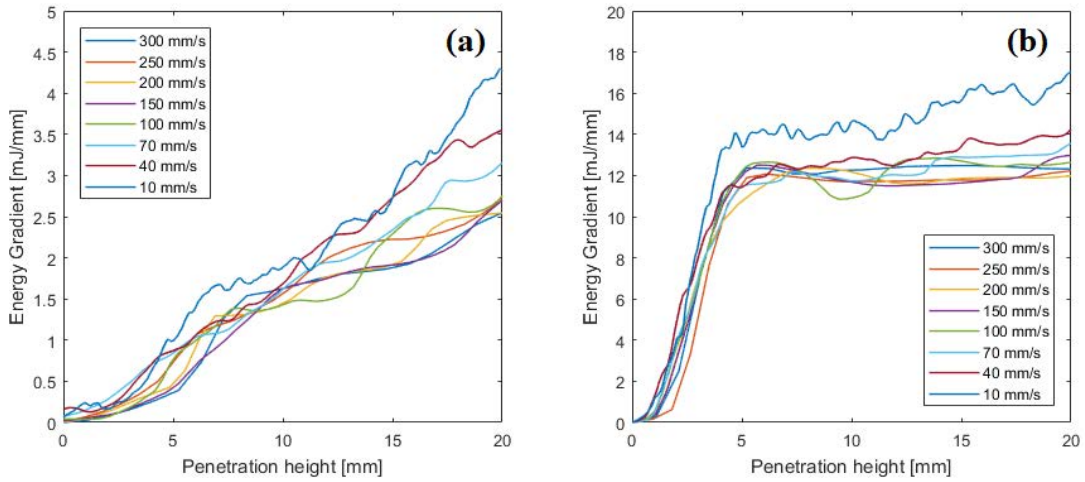

Figure 4.28. *Example of energy gradient Vs height at different tip speed considering samples of Titanium Dioxide DT-51 (a) non compacted and (b) compacted at 4.72 kPa.*

Representing the flow energy as a function of tip speeds leads to the curves reported in Figure 4.29, where the error bars indicate the standard deviation of three measurements. The good repeatability of the test and the stability of this material are confirmed by the

small errors. The flow rate indices equal to *FRI*=1.32 and $FRI_{comp.}$=1.21 reveal that the powder has a somewhat flow rate sensitivity. In particular the flow rate sensitivity increases as the pre-consolidation stress is increased.

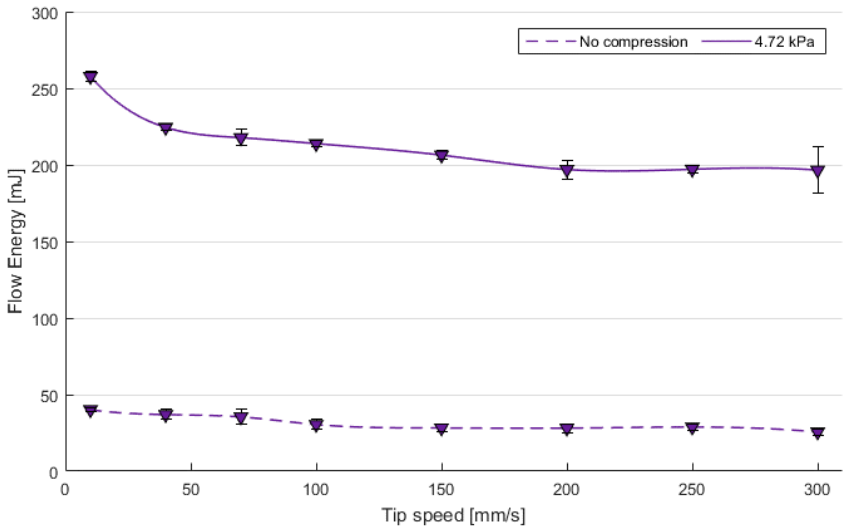

Figure 4.29. *Flow energy at different tip speed both on a free surface and on a compacted powder bed.*

Finally it is noteworthy saying that, for the same tip speed, the flow energy required at 4.72 kPa is at least 5 times the energy required by materials that have been subjected only to conditioning. The reason is the high variability of powder packing state with compaction.

4.2.3.α-lactose monohydrate

Examples of energy gradient curves for samples of GranuLac in free surface conditions and compacted at 5.75 kPa are reported in Figures 4.30-a and 4.30-b. Also in this case, when the powder is compacted, there is a change in the slope of the energy gradient curves at about 5 mm depth; however this change is not so relevant as in the case of Titanium grades, likely because the less cohesiveness of GranuLac.

Representing the flow energy as a function of the impeller tip speed (see Figure 4.31) allows doing interesting considerations. On free surface samples, the flow energy decreases with the tip speed, meaning that the powder has average flow rate sensitivity (*FRI*=1.56). However, when the powder is compacted at 5.75 kPa, the flow energy begins to increase with increasing the tip speed ($FRI_{comp.}$=0.97). This behaviour is characteristic of pseudo-plastic or Newtonian flow rate.

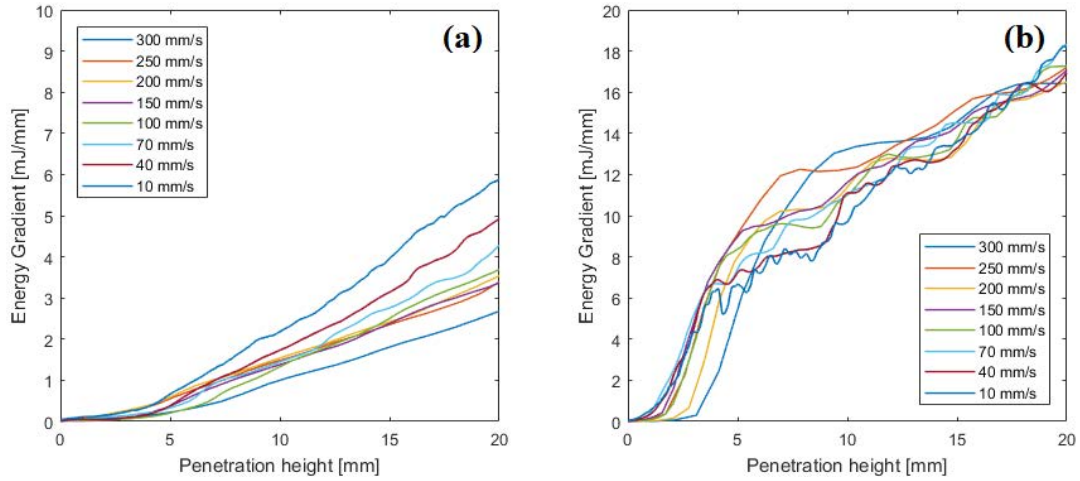

Figure 4.30. *Example of energy gradient Vs height at different tip speed considering samples of GranuLac (a) non compacted and (b) compacted at 5.75 kPa.*

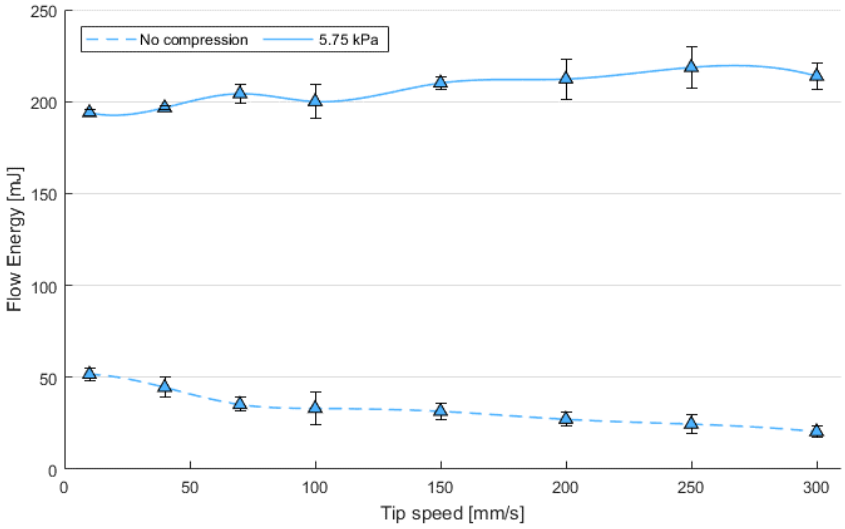

Figure 4.31. *Flow energy at different tip speed both on a free surface and on a compacted powder bed.*

In conclusion, the rheological behaviour of GranuLac depends on the initial state of powder compaction: by compacting the powder, its cohesiveness diminishes and it starts behaving like a liquid. This may explain why, at different compressions, hardness measurements by ball indentation are not always shear rate dependent, although the intermediate regime of flow is always the one studied.

4.2.4.Waxy Corn Starch

As it can be seen from Figure 4.32, the area under the energy gradient curves is always smaller than all the previous cases. This because Waxy Corn Starch is the less cohesive material tested here, with more spherical shaped particles that reduce interlocking.

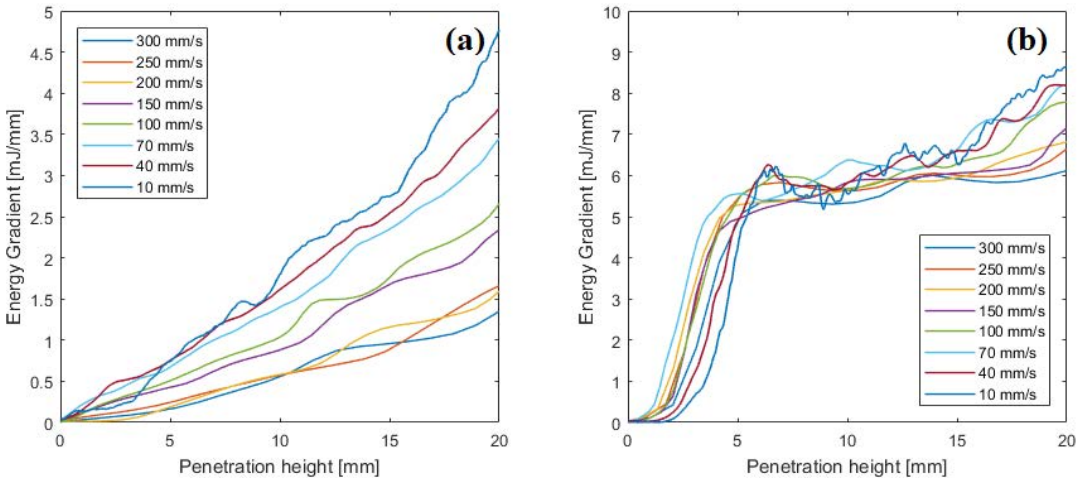

Figure 4.32. *Example of energy gradient Vs height at different tip speed considering samples of Waxy Corn Starch (a) non compacted and (b) compacted at 4.72 kPa.*

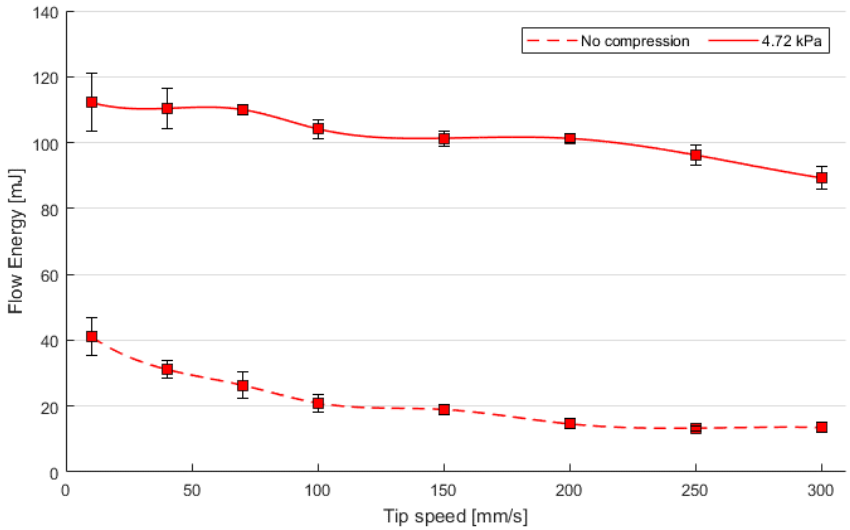

Figure 4.33. *Flow energy at different tip speed both on a free surface and on a compacted powder bed.*

The variation of the flow energy with the tip speed, which is represented in Figure 4.33, follows a similar trend in both powder conditions: at very low tip speed, flow energy is higher and then, as the tip speed increases, the flow energy reduces. However the flow

rate sensitivity is higher when the powder is not compacted (*FRI*=1.97) with respect to a 4.72 kPa compacted powder bed (FRI_{comp}=1.08).

4.2.5.Discussion

The variable flow rate method represents a quick way to evaluate flow properties of powders through their flow resistance. For some materials the flow rate sensitivity changes at different powder compaction. For instance the flow energy decreases slightly with increasing tip speed on free surface conditions samples of GranuLac, indicating an average flow rate sensitivity; whereas Granulac shows a Newtonian behaviour if compressed to 5.75 kPa. Furthermore, it has been found that the maximum flow energy is demanded by more cohesive powders, which have the higher shear strength. Finally the largest standard deviation is the one of TiO_2 R-104, because its lower stability.

To compare the results obtained with the variable flow rate method and with the ball Indentation technique, it is necessary to estimate the shear rate for the former case. In particular it should be represented the flow energy required to make the powder flow as a function of the dimensionless shear rate for any tip speed investigated.

In this case the strain rate, γ, might be calculated as given by Equation 4.1:

$$\gamma = \frac{dv}{n_{band} * d_p} \ , \tag{4.1}$$

where dv is the velocity differential across the shear band (0.9 v_{tip}), n_{band} is the number of particles in the shear band and d_p is the average particle diameter (Hare and Ghadiri, 2017). The dimensionless shear rate, γ^*, is still calculated as introduced by Tardos *et al.* (2003) (see Equation 1.16).

The width of the shear band, needed for evaluating n_{band}, is the only unknown variable. It could be estimated by DEM (Discrete Method Simulation), or using PIVlab. Here, during the tests, the system has been recorded with the high speed camera with the purpose of using a velocimetry tool for assessing the length of the shear band. However, because the materials tested adhere to the die wall, turned out that the shear band cannot be clearly determined. It is suggested, for future works, to use silanised glass beads such that the cohesiveness is enough to perform ball indentation technique, but it would also be possible to see clearly the blade during the its traverse into the bed. Alternatively, the

use of cohesive particles, more spherical in shape, is recommended, so the system could be easily simulated by DEM.

Concluding remarks and future work

The overall aim of this study was to further investigate Ball Indentation Method as a technique for assessing powder flowability at high shear rates.

Four different powders, which differ for size and shape, have been chosen in order to investigate different flow regimes. Firstly the flowability of powders has been characterised through qualitative method and rotational shear cell; instead thanks to SEM it has been possible to make some comments about powder morphology. For evaluating quasi-static powder hardness, the FT4 indentation technique has been applied at different powders compactions. Moreover it has been assess the range of penetration depth within which hardness can be considered constant. There, hardness represents a reliable measure of the powder resistance to plastic deformation. Successively, the hardness within a bed exposed to ball indentation have been analysed as a function of the indentation strain rate. The obtained hardness measurements corroborate the quantitative simulations reported in literature (Tardos *et al.*, 2003; Pasha *et al.*, 2015).

In detail, from the investigation done, it results that in the quasi-static flow regime, hardness does not significantly vary with the shear rate since inter-particles collisions are relatively weak and friction between particles is predominant. What happens in the uncertain boundary cannot be exactly defined, likely because this boundary was established considering perfect mono-modal particles, spherical in shape. However, generally, the hardness starts increasing prior to the intermediate regime.

In the intermediate regime ($0.25<\gamma^*<3$), where inter-particles collisions become energetic, the measured hardness is shear rate dependent: hardness increases with increasing shear rate. At a certain point, individual particles are sufficiently energised so the powder behaves in a fluidized manner. This is the reason why, in the earlier part of this regime, hardness increases as $H_d \sim (\gamma^*)^n$ with $n < 1$; and then the dependency becomes linear ($H_d \sim \gamma^*$). However, hardness is not shear rate dependent in intermediate regime for some powders if compacted at high pressure, as it has been seen for lactose monohydrate. Despite the reason is not clear, it likely concerns the free flowing behaviour that these powders exhibit at higher values of compression.

Although the dynamic flow regime ($\gamma^*>3$) has not been directly investigated due to the too small dimensions of the tested materials, the method looks suitable also for characterising flowability in dynamic conditions.

It can be said that ball indentation method can be successfully used to establish an engineering estimate of the powder flowability for a wide range of strain rates. Furthermore, it is quick, easy to perform, and leads to reproducible results. If the constraint factor of the material is known, it is also possible to use the hardness such obtained for estimating the unconfined yield strength and hence predicting the flow behaviour in a wide range of operative conditions, from low stress environments to high shear rates.

On the other hand, the technique has proved to have some limitations. Firstly, it has to be considered the variability of the method with the tested material. Indeed, a stable hardness range does not exist for all the powders. Another difficulty with the approach is that it is possible to control only the velocity of the indenters, whilst it is not possible knowing accurately and in advance how far the indenter will penetrate and whether it will remain in the stable hardness range, thus it is not possible predicting the strain rate. Finally, the method can be performed only on powders with a certain degree of cohesiveness, very free flowing material cannot be subjected to indentation. Because all of these give rise to many question marks and uncertainties, more studies are required.

One aspect that might be investigated concerns the automation of the method. Maybe, if it is possible to measure the force during dynamic indentation, the hardness would be calculated using the expression proposed by Hassanpour and Ghadiri (2007).

Future work should be done also in order to investigate directly the dynamic regime of flow. Because an increase in particle size leads to a rise in dimensionless shear rates, it is suggested to use bigger particles; however it is known that usually cohesiveness diminishes by increasing the particle size. The advice is to use treated powder, such as glass beads made cohesive by silanisation; or to increase the moisture content of big particles. Because the shear rate is directly proportional to the velocity of penetration and inversely proportional to the indenter radius, another way for characterising higher shear rates is using smaller size indenters of lower density. Lower density indeed allows expanding the velocity range.

The dynamic Ball Indentation Method might also be simulated by DEM and the results could be compared with the experimentally observed trends. Furthermore, a challenge may be to better define the boundaries between regimes of flows, which are still uncertain.

Finally, Ball Indentation Method might be compared to the dynamic methodology provided by the rheometers. Correlate the shear rate sensitivity with the hardness

measurements, as a function of the shear rate, could be done with DEM or, if the powder tested is transparent enough and does not stick to the die wall, using velocimetry tools such as PIVLab.

Appendix 1

A Matlab code has been developed to calculate the area beneath the energy gradient curves, and hence estimating the energy required to make the powder flows. Firstly the program reads the Excel spread sheet collecting the Energy Gradient versus penetration depth. Each file is composed of eight sheets, one for any tip speeds, and in each sheet the results achieved with three measurements are reported.

Then the program solves the area under the curves by applying, for each small travelled interval, the mean value theorem (as given in Eq. A.1). The total Energy is the sum of all the N interval areas (Eq. A.2).

$$f(c) = \frac{1}{a-b}\int_a^b f(x)\,dx \ , \tag{A.1}$$

$$E_{tot} = \sum_1^N f(c). \tag{A.2}$$

The program has been written in such a way to give as output a subplot, which contains the energy gradient curves of the three repetitions; and a second figure, which represents the average flow energy as a function of tip speed, also with error bars. Furthermore, the average values with their standard deviations, as well as the Flow Rate Index, appear in the command window. The code is reported below.

```
function VFR

%% Importing the Excel Spreadsheet

for ID=1:8
  res(ID).name = ['Test ' num2str(ID)];
  [num,txt] = xlsread('GRANULAC_5.75.xlsx', res(ID).name);
  res(ID).x1  = num(:,1);
  res(ID).y1 = num(:,2);
  res(ID).x2  = num(:,3);
  res(ID).xn1 = num(:,7);
  res(ID).xn2  = num(:,9);
  res(ID).xn3 = num(:,11);
end

%% Integral calculation

matrix=zeros(8,3); % 8 tip speeds, 3 repetitions
for ID=1:8 % means tip speed=[300, 250, 200, 150, 100,70,40,10] mm/s
  res(ID);
  hold on;
```

```
  NS=length(res(ID).x1);
  w=zeros(NS,3);

    for i = 1:NS-1 % to calculate the area of the n-th interval
      w(i,1) =abs((res(ID).x1(i+1)-res(ID).x1(i))*(res(ID).y1(i+1) ...
         + res(ID).y1(i)) / 2 );
      w(i,2) =abs((res(ID).x2(i+1)-res(ID).x2(i))*(res(ID).y2(i+1) ...
         + res(ID).y2(i)) / 2 );
      w(i,3) =abs((res(ID).x3(i+1)-res(ID).x3(i))*(res(ID).y3(i+1) ...
         + res(ID).y3(i)) / 2 );
    end
  matrix(ID,:)=sum(w); % Equation A.2
 end

%% Sub-plotting the energy gradient curves of the three repetitions

fig1=figure(1);
for i=1:8
    hold on
    subplot(1,3,1);
    plot(res(i).xn1,res(i).y1);
    hold on
    subplot(1,3,2);
    plot(res(i).xn2,res(i).y2);
    hold on
    subplot(1,3,3);
    plot(res(i).xn3,res(i).y3);
end
ylabel('Energy Gradient [mJ/mm]');
xlabel('Penetration height [mm]');
title('Energy Gradient Curves');
set(fig1, 'Position', [100 100 1600 450]);
legend('300 mm/s','250 mm/s','200 mm/s','150 mm/s',...
'100 mm/s','70 mm/s','40 mm/s','10 mm/s','location', 'northwest');


%% Plotting the Flow Energy Versus tip speed with error bars

M=mean(matrix'); % Average of the three repetitions
S=std(matrix'); % Standard deviation
tipspeed=[300 250 200 150 100 70 40 10];

fig2=figure(2);
lengthX = length(tipspeed);
samplingRateIncrease = 200;
newXSamplePoints = linspace(min(tipspeed), max(tipspeed), lengthX *
samplingRateIncrease);
smoothedY = spline(tipspeed, M', newXSamplePoints);
ySmooth = newXSamplePoints;
xSmooth = smoothedY;
hold on;
ax = gca;
ax.XGrid = 'off';
ax.YGrid = 'on';

plot(newXSamplePoints, smoothedY,'--','Color', ...
  [1,0.9,0],'LineWidth',1)
e=errorbar(tipspeed,M,S,'o', 'MarkerSize', 7,'MarkerFaceColor', ...
  [1, 0.9, 0], 'Color', 'k'),
xlabel('Tip speed [mm/s]');
```

```
ylabel('Flow Energy [mJ]');
set(fig2, 'Position', [100 100 800 450]);

% Printing in the command windows the flow energy at different tip
speed, their standard deviation and the FRI

FRI=M(8)/M(5); % (flow energy at 10 mm/s)/(flow enrgy at 100 mm/s)
  for i=1:8
    X = ['Tip speed: ',num2str(tipspeed(i)),' mm/s -> Flow ...
          Energy ', num2str(M(i)),' +/- ',num2str(S(i)), ' mJ'];
    disp(X);
  end
  disp(['FRI: ',num2str(FRI)]);
end
```

Appendix 2

Here some of the flow parameters obtained performing shear cell measurements at different value of pre-shear are reported, for each material tested.

Table A.1. *Flow parameters of Titanium Dioxide R-104.*

Pre-shear [kPa]	**1**	**2**	**3**	**6**	**9**	**15**
Cohesion	0.79	1.48	2.11	3.64	5.53	7.40
UYS [kPa]	2.78	5.65	8.94	16.91	24.19	34.21
MPS [kPa]	2.51	5.10	8.48	16.38	24.47	37.62
MCS [kPa]	-0.09	-0.15	-0.11	-0.10	0.05	0.64
ff	0.90	0.90	0.95	0.97	1.01	1.10
AIF [°]	30.97	34.81	39.41	43.50	40.88	43.21

Table A.2. *Flow parameters of Titanium Dioxide DT-51.*

Pre-shear [kPa]	**1**	**2**	**3**	**6**	**9**	**12**
Cohesion	0.52	0.76	1.02	1.44	2.01	1.84
UYS [kPa]	2.00	3.10	4.17	5.97	7.87	7.67
MPS [kPa]	2.43	4.72	6.81	12.12	17.78	23.16
MCS [kPa]	0.12	0.38	0.64	1.42	2.57	3.57
ff	1.22	1.53	1.64	2.03	2.27	3.05
AIF [°]	34.67	38.05	37.69	38.59	35.97	38.69

Table A.3. *Flow parameters of GranuLac 140.*

Pre-shear [kPa]	**3**	**6**	**9**	**12**	**15**
Cohesion	0.52	0.74	0.96	1.14	1.03
UYS [kPa]	1.98	2.85	3.60	4.16	3.86
MPS [kPa]	5.75	10.99	16.06	20.50	25.58
MCS [kPa]	1.03	2.20	3.56	4.93	6.17
ff	2.90	3.86	4.48	4.93	6.65
AIF [°]	34.80	35.08	33.76	32.44	33.90

Table A.4. *Flow parameters of Waxy Corn Starch.*

Pre-shear [kPa]	**3**	**6**	**9**	**12**	**15**
Cohesion	0.31	0.54	0.55	0.58	0.78
UYS [kPa]	1.11	1.88	1.97	2.06	2.77
MPS [kPa]	5.13	9.82	14.39	18.59	23.18
MCS [kPa]	1.24	2.61	3.86	5.17	6.50
ff	4.64	5.28	7.31	9.08	8.46
AIF [°]	31.88	30.32	31.75	31.57	31.14

Nomenclature

Latin Characters

Symbol	*Units*	*Description*
a	[J m^3 mol^{-2}]	Van der Waals constant. Effect of dipoles
A	[m^2]	Projected area of the impression
b	[m^3 mol^{-2}]	Van der Waals constant. Sterical effect
C	[–]	Constraint factor
C_w	[Pa]	Wall cohesive shear stress
d	[m]	Orefice diameter
$d_{50,3}$	[m]	Volumetric median diameter
d_p	[m]	Particle diameter
d_v	[m/s]	Velocity differential
D_a	[m]	Diameter of the penetration
D_i	[m]	Indenter diameter
E	[J]	Energy
E_{flow}	[J]	Resistance to flow
ff	[–]	Flow factor
F	[N]	Force
F_{max}	[N]	Maximum indentation load
g	[m/s^2]	Gravitational force
h	[m]	Penetration depth
h_d	[–]	Dimensionless penetration depth
H	[Pa]	Hardness
H_d	[Pa]	Dynamic hardness
I	[–]	Inertial number
M	[kg]	Indenter mass
n	[–]	Dimensionless curvature index
n_{band}	[–]	N. of particles in the shear band
P	[Pa]	Pressure
q_i	[atoms/cm^3]	Atomic density
R	[m]	Impeller radius
R_i	[m]	Indenter radius
T	[Nm]	Torque
U	[m^3]	Unrelaxed volume
v_i	[m/s]	Impact velocity
V	[m^3]	Volume

V_0	[m^3]	Unsettled volume
V_f	[m^3]	Tapped volume
V_m	[m^3/mol]	Molar volume
x	[m]	Reduced diameter

Greek Characters

Symbol	***Units***	***Description***
α	[°]	Helix angle
α_r	[°]	Angle of repose
γ	[s^{-1}]	Shear rate
γ^*	[–]	Dimensionless shear rate
δ	[°]	Angle of friction
ε	[-]	Strain coefficient
μ	[-]	Coefficient of friction
μ_w	[-]	Wall frictional coefficient
π	[–]	Pi greco
ρ_b	[kg/m^3]	Bulk density
ρ_s	[kg/m^3]	Solid density
ρ_t	[kg/m^3]	Tapped density
σ	[Pa]	Normal stress
σ_1	[Pa]	Major Principal Stress
σ_2	[Pa]	Minor Consolidation Stress
σ_c	[Pa]	Unconfined Yield Strength
σ_H	[Pa]	Hydrostatic stress
σ_{sf}	[Pa]	Pre-shear
τ	[Pa]	Shear stress
τ_c	[Pa]	Cohesion strength
φ_{lin}	[°]	Angle of Internal friction
φ_{sf}	[°]	Angle of Internal friction, Steady state flow
φ_c	[°]	Effective angle of Internal friction

Acronyms

Symbol	***Units***	***Description***
AIF	[°]	Angle of Internal friction
AIF(S)	[°]	Angle of Internal friction, Steady state flow
AIF(E)	[°]	Effective angle of Internal friction
BIM	[–]	Ball Indentation Method

BFE	[J]	Basic Flow Energy
CI	[–]	Compressibility index
FRI	[–]	Flow Rate Index
HR	[–]	Hausner Ratio
MCS	[Pa]	Minor Consolidation Stress
MPS	[Pa]	Major Principal Stress
SEM	[–]	Scanning Electron Microscope
SMD	[m]	Surface Mean Diameter
UYS	[Pa]	Unconfined Yield Strength
VFR	[–]	Variable Flow Rate
VMD	[m]	Volume Mean Diameter

References

Ai, Y. and J. l. Jane (2016). Starch: Structure, Property, and Determination. *Encyclopedia of food and healt*, 165-174.

Allen, T. (1990). *Particle size measurement*, 4th edition, Chapman & Hall.

Amidon, G. E., P. J. Meyer and D. M. Mudie (2017). Particle, Powder, and Compact Characterization. *Developing Solid Oral Dosage Forms*, 271-293.

Boschini, F., V. Delaval, K. Traina, N. Vandewalle and G. Lumay (2015). Linking flowability and granulometry of lactose powders. *Int. J. Pharm.*, **494**, 312-320.

Clifton, P. and J. Keogh (2016). Starch. *Encyclopedia of food and healt*, 146-151.

DuPont (2007). *Titanium Dioxide. Polymers, light and the science of* TiO_2.

Freeman, R. (2005). Measuring the flow properties of consolidated, conditioned and aerated powders – a comparative study using a powder rheometer and a rotational shear cell. Particulate Systems Analysis, Stratford.

Freeman, R. (2007). Measuring the flow properties of consolidated, conditioned and aerated powders — A comparative study using a powder rheometer and a rotational shear cell. *Powder Technology*, **174**, 25-33.

Freeman, R. E., J. R. Cooke and L. C. R. Schneider (2009). Measuring shear properties and normal stresses generated within a rotational shear cell for consolidated and non-consolidated powders. *Powder Technology,* **190,** 65-69.

Freeman technology. Dynamic Energy Calculation. INF21.

Freeman Technology (2006). The Conditioning Process. W7006.

Freeman Technology (2007). Variable Flow Rate Method. W7012.

Freeman Technology (2010). Shear cell. W7018.

Freeman Technology (2013). Additional Parameters Derived from Shear Cell Data. W7108.

Freeman Technology (2013). Compressibility. W7008.

Freeman Technology (2013). Experience. Hints & Tips n. 3.

Freeman Technology (2013). Obtaining reproducible data. Hints & Tips n. 2.

Freeman Technology (2013). The Basic Flowability Energy. W7030.

Hare, C. and M. Ghadiri (2017). Stress and strain rate analysis of the FT4 Powder Rheometer.

Hare, C., U. Zafar, M. Ghadiri, T. Freeman, J. Clayton and M. J. Murtagh (2015). Analysis of the dynamics of the FT4 powder rheometer. *Powder Technology,* **285**, 123-127.

Harnby, N. (2001). The mixing of cohesive powders. *Mixing in the process Industries*, Ch. 5, Butterworth-Heinemann, Oxford.

Hassanpour, A. and M. Ghadiri (2007). Characterisation of Flowability of Loosely Compacted Cohesive Powders by Indentation. *Particle & Particle Systems Characterization*, **24**, 117-123.

Herbert, E. G., G.M. Pharr, W.C. Oliver, B.N. Lucas and J.L. Hay (2001). On the measurement of stress–strain curves by spherical indentation. *Thin Solid Films***, 398–399**, 331–335.

Israelachvili, J. N. (2011). Van der Waals Forces between Particles and Surfaces. *Intermolecular and Surface Forces,* 3rd edition, 253-289.

Jee, A.-Y. and M. Lee (2010). Comparative analysis on the nanoindentation of polymers using atomic force microscopy. *Polymer Testing*, **29**, 95-99.

Jenike, A. W. (1964). Storage and flow of solids. *Engng. Exp. Station*, Bull. No. **123**, Univ. Utah, Salt Lake City.

Jin, T. and M. Berlin (2015). Titanium. *Handbook on the Toxicology of Metals,* 4th edition, 1287-1296.

Klausner, J. F., D. Chen and R. Mei (2000). Experimental investigation of cohesive powder rheology. *Powder Technology*, **112**, 94–101.

Lee-Desautels, R. (2005). Theory of van der Waals Forces as Applied to Particulate Materials. *Educ. Reso. for Part. Techn.*

Leturia, M., M. Benali, S. Lagarde, I. Ronga and K. Saleh (2014). Characterization of flow properties of cohesive powders: A comparative study of traditional and new testing methods. *Powder Technology,* **253,** 406-423.

Leuenberger, H. and M. Lanz (2005). Pharmaceutical powder technology — from art to science: the challenge of the FDA's Process Analytical Technology initiative. *Advanced Powder Technol.,* **16**, 3-25.

Li, Q., V. Rudolph, B.Weigl and A. Earl, (2004). Interparticle van der Waals force in powder flowability and compactibility. *Int. J. Pharm.,* **280**, 77-93.

Lumay, G., F. Boschini, K. Traina, S. Bontempi, J. C. Remy, R. Cloots and N. Vandewalle (2012). Measuring the flowing properties of powders and grains. *Powder Technology*, **224**, 19-27.

Malvern Instruments Ltd. (2013). *Zetasizer Nano User Manual.*

Manthey, F. A. (2016). Starch: Sources and Processing. *Encyclopedia of food and healt,* 160-164.

MEGGLE Excipient & Technology (2014). *Technical brochure Milled and sieved lactose.*

Mo, S.-D. and W. Y. Ching (1995). Electronic and optical properties of three phases of titanium dioxide: Rutile, anatase, and brookite. *Physical Review B.*, **51**, 13023-13032.

Moreno-Atanasio, R., S. J. Antony and M. Ghadiri (2005). Analysis of flowability of cohesive powders using Distinct Element Method. *Powder Technology*, **158**, 51-57.

Pasha, M. (2013). Modelling of Flowability Measurement of Cohesive Powders Using Small Quantities, *Ph.D. Thesis*, University of Leeds (UK).

Pasha, M., C. Hare, A. Hassanpour and M. Ghadiri (2013). Analysis of ball indentation on cohesive powder beds using distinct element modelling. *Powder Technology*, **233**, 80-90.

Pasha, M., C. Hare, A. Hassanpour and M. Ghadiri (2015). Numerical analysis of strain rate sensitivity in ball indentation on cohesive powder Beds. *Chemical Engineering Science*, **123**, 92-98.

Peleg, M., M. D. Normand and M. G. Corradini (2010). Interactive software for calculating the principal stresses of compacted cohesive powders with the Warren-Spring equation. *Powder Technology*, **197**, 268-273.

Rhodes, M. J. (2008). *Introduction to Particle Technology*, 2nd Edition, Wiley.

Salehi, H., D. Barletta and M. Poletto (2017). A comparison between powder flow property testers. *Particuology*, **32**, 10-20.

Santomaso, A. C. (2017). Notes of the lessons.

Santomaso, A., P. Lazzaro and P. Canu (2003). Powder flowability and density ratios: the impact of granules packing. *Chemical Engineering Science*, **58**, 2857-2874.

Schaeffer, D. G. (1987). Instability in the evolution equations describing incompressible granular flow. *Journal of differential equations*, **66**, 19-50

Schulze, D. (2011). *Flow Properties of Powders and Bulk Solids.*

Schulze, D. (2008). *Powders and Bulk Solids - Behavior, Characterization, Storage and Flow*, 1st edition, Springer Berlin Heidelberg.

Schüssele, A. and A. Bauer-Brandl (2003). Note on the measurement of flowability according to the European Pharmacopoeia. *International Journal of Pharmaceutics*, **257**, 301-304.

Schwedes, J. (2002). Consolidation and flow of cohesive bulk solids. *Chemical Engineering Science*, **57**, 287-294.

Schwedes, J. (2003). Review on testers for measuring flow properties of bulk solids. *Granular Matter*, **5**, 1-43.

Serna Saldivar, S. O. and E. Perez-Carrillo (2016). Maize. *Encyclopedia of food and healt*, 601-609.

Seville, J. and C.-Y. Wu (2016). *Particle Technology and Engineering - An Engineer's Guide to Particles and Powders: Fundamentals and Computational Approaches.*

Stasiak, M., M. Molenda, I. Opalinski and W. Blaszczak (2013). Mechanical Properties of Native Maize, Wheat, and Potato Starches. *Czech J. Food Sci*., **31**, 347–354.

Tardos, G. I., S. McNamara and I. Talu (2003). Slow and intermediate flow of a frictional bulk powder in the Couette geometry. *Powder Technology*, **131**, 23-39.

The European Pharmacopoeia, 6th edition (2007). Powder flow. 320-323.

The European Pharmacopoeia, 7th edition (2010). Bulk density and tapped density of powders. 305-308.

The European Pharmacopoeia, 7th edition (2010). Titanium dioxide. 3101-3103.

The European Pharmacopoeia, 8th edition (2013). Particle size analysis by laser light diffraction, 333-336.

Tirupataiah, Y. and G. Sundararajan (1990). The volume of the crater formed by the impact of a ball against flat target materials-the effect of ball hardness and density. *Int. J. Impact En.*, **9**, 237-246.

Valverde, J. M., A. Ramos, A. Castellanos and P. K. Watson (1998). The tensile strength of cohesive powders and its relationship to consolidation, free volume and cohesivity. *Powder Technology*, **97**, 237-245.

Vasilenko, A., B. J. Glasser and F. J. Muzzio (2011). Shear and flow behavior of pharmaceutical blends — Method comparison study. *Powder Technology*, **208**, 628-636.

Vasilenko, A., S. Koynov, B. J. Glasser and F. J. Muzzio (2013). Role of consolidation state in the measurement of bulk density and cohesion. *Powder Technology*, **239**, 366-373.

Wang, C., A. Hassanpour and M. Ghadiri (2008). Characterisation of flowability of cohesive powders by testing small quantities of weak compacts. *Particuology*, **6**, 282-285.

Wypych, G. (2016). Fillers − Origin, Chemical Composition, Properties, and Morphology. *Handbook of Fillers*, 4th edition, **13-266.**

Zafar, U. (2013). Assessing Flowability of Cohesive Powders by Ball Indentation. *Ph.D. Thesis*, University of Leeds (UK).

Zafar, U., C. Hare, A. Hassanpour and M. Ghadiri (2014). Drop test: A new method to measure the particle adhesion force. *Powder Technology*, **264**, 236-241.

Zafar, U., C. Hare, A. Hassanpour and M. Ghadiri (2017). Ball indentation on powder beds for assessing powder flowability: Analysis of operation window. *Powder Technology*, **310**, 300-306.

Zafar, U., C. Hare, G. Calvert, M. Ghadiri, R. Girimonte, B. Formisani, M. A. S. Quintanilla and J. M. Valverde (2015). Comparison of cohesive powder flowability measured by Schulze Shear Cell, Raining Bed Method, Sevilla Powder Tester and new Ball Indentation Method. *Powder Technology*, **286**, 807-816.

Web sites

https://www.malvernpanalytical.com

https://www.sympatec.com/en/particle-measurement/sensors/dynamic-image-analysis/qicpic/

https://www.phantomhighspeed.com/

http://www.freemantech.co.uk/

https://www.anton-paar.com/corp-en/products/group/rheometer/

https://www.stablemicrosystems.com